Hydration of acids: Towards molecular level understanding

By
Parvathi K.
CHEM01201204022

Bhabha Atomic Research Centre, Mumbai

A thesis submitted to the
Board of Studies in Chemical Sciences

In partial fulfillment of requirements
for the Degree of
DOCTOR OF PHILOSOPHY
of
HOMI BHABHA NATIONAL INSTITUTE

August, 2017

Hydration of acids: Towards molecular level understanding

By
Parvathi K.
CHEM01201204022

Bhabha Atomic Research Centre, Mumbai

A thesis submitted to the
Board of Studies in Chemical Sciences

In partial fulfillment of requirements
for the Degree of
DOCTOR OF PHILOSOPHY
of
HOMI BHABHA NATIONAL INSTITUTE

August, 2017

Homi Bhabha National Institute

Recommendations of the Viva Voce Committee

As members of the Viva Voce Committee, we certify that we have read the dissertation prepared by Ms. Parvathi K. entitled "Hydration of acids: Towards understanding at molecular level" and recommend that it may be accepted as fulfilling the thesis requirement for the award of Degree of Doctor of Philosophy.

Chairman - Prof. A. K. Arya Date: 01/11/2017

Guide / Convener - Prof. D. K. Maity Date: 01/11/2017

R. B. Sunoj

Examiner - Prof. R. B. Sunoj, IIT Bombay Date: 1/11/17

01/11/2017

Member 1- Prof. T. K. Ghanty Date:

01/11/2017

Member 2- Prof. H. P. Upadhyaya Date:

Member 3- Prof. C. Majumder Date:

Final approval and acceptance of this thesis is contingent upon the candidate's submission of the final copies of the thesis to HBNI.

I/~~We~~ hereby certify that I/~~we~~ have read this thesis prepared under my/our direction and recommend that it may be accepted as fulfilling the thesis requirement.

Date: 01/11/17

Place: Mumbai

Guide: Prof. D. K. Maity

STATEMENT BY AUTHOR

This dissertation has been submitted in partial fulfillment of requirements for an advanced degree at Homi Bhabha National Institute (HBNI) and is deposited in the Library to be made available to borrowers under rules of the HBNI.

Brief quotations from this dissertation are allowable without special permission, provided that accurate acknowledgement of source is made. Requests for permission for extended quotation from or reproduction of this manuscript in whole or in part may be granted by the Competent Authority of HBNI when in his or her judgment the proposed use of the material is in the interests of scholarship. In all other instances, however, permission must be obtained from the author.

Parvathi K

Parvathi K.

DECLARATION

I, hereby declare that the investigation presented in the thesis has been carried out by me. The work is original and has not been submitted earlier as a whole or in part for a degree / diploma at this or any other Institution / University.

Parvathi K

Parvathi K.

List of Publications arising from the thesis

Journal

1. "Microhydration of Oxalic Acid Leading to Dissociation", Parvathi Krishnakumar, Dilip Kumar Maity, *Molecular Physics*, **2017**, DOI: 10.1080/00268976.2017.1359346.

2. "Microhydration of a benzoic acid molecule and its dissociation", Parvathi Krishnakumar, Dilip Kumar Maity, *New Journal of Chemistry*, **2017**, *41*, 7195-7202.

3. "Microhydration of Neutral and Charged Acetic Acid", Parvathi Krishnakumar, Dilip Kumar Maity, *Journal of Physical Chemistry A*, **2017**, *121*, 493-504.

4. "Theoretical studies on dimerization vs. microhydration of carboxylic acids", Parvathi Krishnakumar, Dilip Kumar Maity, *Computational and Theoretical Chemistry*, **2017**, *1099*, 185–194.

5. "Effect of Microhydration on Dissociation of Trifluoroacetic Acid", Parvathi Krishnakumar, Dilip Kumar Maity, *Journal of Physical Chemistry A*, **2014**, *118*, 5443–5453.

Conferences

1. Parvathi Krishnakumar, Dilip Kumar Maity, "Microhydration of Acids", *13th Discussion Meeting on the Structure and Dynamics of Molecular Clusters (SDMC)-2016*, February 18-21, 2016, Mahabaleswar, India.

2. Parvathi Krishnakumar, Dilip Kumar Maity, 'Dimerization v/s Microhydration of Carboxylic acids", *13th Trombay Symposium on Radiation and Photochemistry (TSRP)-2016*, January 5-9, 2016, Mumbai, India.

3. Parvathi Krishnakumar, Dilip Kumar Maity, "Microhydration of Oxalic Acid", *13th National Symposium on Radiation and Photochemistry (NSRP)-2015*, March 9-11, 2015, Kanpur, India. Received best poster award.

4. Parvathi Krishnakumar, Dilip Kumar Maity, "Effect of microhydration on dissociation of trifluoroacetic acid", 11th *Discussion Meeting on the Structure and Dynamics of Molecular Clusters (SDMC)-2014*, February 20-23, 2014, Puri, India.

5. Parvathi Krishnakumar, Dilip Kumar Maity, "How much water is needed to ionize trifluroacetic acid?", *International symposium on Current Trends in Theoretical Chemistry (CTTC)-2013*, September 26-28, 2013, Mumbai, India.

Other Journal Publications

1. "Enhanced fluorescence of aqueous BODIPY by interaction with cavitand cucurbit[7]uril", Monika Gupta, K. Parvathi, Soumyaditya Mula, Dilip K. Maity, Alok K. Ray, *Photochemical & Photobiological Sciences*, **2017**, *16*, 499-506.
2. "Supramolecularly Assisted Modulation of Optical Properties of BODIPY–Benzimidazole Conjugates" Shrikant S. Thakare, Goutam Chakraborty, Parvathi Krishnakumar, Alok K. Ray, Dilip K. Maity, Haridas Pal, Nagayan Sekar, *Journal of Physical Chemistry B*, **2016**, *120*, 11266-11278.

3. "Steric effects in complexes of diphenyl (2-pyridyl) phosphine oxide with the uranyl ion. Synthetic, structural and theoretical studies" Bal Govind Vats, S. Kannan, K. Parvathi, D.K. Maity, M.G.B. Drew, *Polyhedron*, **2015**, *89*, 116-121.
4. "An insight into the electrocatalysis of uranyl sulphate on gold nanoparticles modified glassy carbon electrode" Saurav K. Guin, Parvathi K., Arvind S. Ambolikar, Jisha S. Pillai, Dilip K. Maity, S. Kannan, Suresh K. Aggarwal, *Electrochimica Acta*, **2015**, *154*, 413–420.

Parvathi K

Parvathi K.

ACKNOWLEDGEMENT

I would like to thank all the people, who in some way, contributed to the completion of this thesis. Foremost, I would like to express my sincere gratitude to my advisor Prof. Dilip K. Maity, for his patience, motivation, enthusiasm and immense knowledge. He contributed to a rewarding research experience by giving me intellectual freedom in my work, supporting my attendance at various conferences, engaging me in new ideas, and demanding a high quality of work in all my endeavors. Additionally, I would like to thank my doctoral committee members Professor A. K. Arya, Professor T. K. Ghanty, Professor C. Majumdar and Professor H. P. Upadhyaya, for their interest in my work and for giving me helpful suggestions. The availability of ANUPAM parallel computing facility in BARC is also highly acknowledged. Special thanks to Shri Vaibhav Kumar for his spontaneous software related help. I would also like to thank HBNI and DAE, for my fellowship.

I thank Uma, my fellow colleagues Rahul Kumar, Vinod Balwanshi and Ashish Shelke, for the stimulating discussions and technical help. Also I thank my dear friends for making these five years memorable.

I thank my parents, Apputan, chechi and Neenus for being my pillars of strength.

CONTENTS

SYNOPSIS

Water plays a crucial role in many biological, chemical and environmental phenomena by facilitating proton transfer between molecules. Acidic solutions are ubiquitous in nature and hence microscopic description of hydrated acids would help in understanding a broad spectrum of topics ranging from proton transport to acid rain. Hydration of an acid molecule involves formation of stabilizing interactions between the solute acid molecule and the solvent water molecules. Macroscopic hydration models describe the effect of bulk hydration on a solute molecule. In these models, the solute molecule is placed in a cavity within a continuous dielectric medium imitating the solvent. Studies on the effect of macroscopic hydration on various properties of different molecules are numerous. Several macroscopic solvation models have been developed as well.[1,2] These implicit solvation models consider solvent effect as a perturbation to the electronic cloud of the solute. Though this leads to a reduction in the number of degrees of freedom of the system studied, it only gives an average effect of the solvent on the solute molecule. Explicit solute-solvent interactions are not included in the calculations. Such an approximation cannot accurately describe the process of hydration, especially when non-covalent interactions are involved.

When a solute acid molecule is placed in solvent water pool, the water molecules reorient to accommodate the solute into their hydrogen bonded network. This leads to weakening of the acidic bond and a contact ion pair is formed. Further, the cation and the anion parts of the acid molecule are hydrated separately and we get solvent separated ion pair. This can be depicted by the schematic diagram shown in Figure 1. Understanding the molecular level interactions between the acid molecule and solvent water molecules will help in having a better insight about several biological and environmental processes.

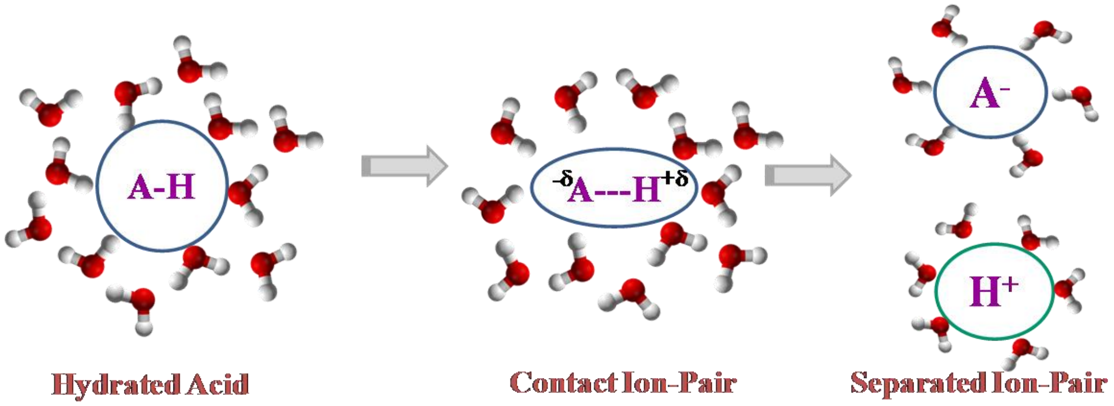

Figure 1 Schematic representation of hydration of acids. A-H represents the acid molecule and the red and grey balls represent oxygen and hydrogen atoms of the water molecule respectively. The reorientation of the water molecules around the acid molecule, the weakening of the A-H bond and formation of solvent separated ion pair is shown.

With the advent of fast spectroscopic techniques, the structure and dynamics of proton in the presence of a few water molecules have been analyzed extensively.[3–8] The proton-water systems are probed, using size selective spectroscopic techniques, at low temperature and pressure. This has led to the emerging of a new field: the microhydration of acid molecules, leading to their dissociation. The microhydration of an acid molecule implies controlled addition of water molecules to the acid molecule to form acid-water molecular clusters that are stabilized by hydrogen bonding. A few studies have been reported in the literature discussing microhydration of acid molecules. Most of them report the microhydration of strong inorganic acids.9–14 However, microhydration of weak organic acids and its dissociation are not well characterized.

This thesis is devoted to the study of hydrated clusters of several acid molecules leading to dissociation by the transfer of its acidic proton to the solvent water molecules. The hydrogen bonding between the acid molecule and the solvent water molecules causes weakening of the acidic hydroxyl bond making acid ionization possible. A stronger acid molecule needs a lesser number of solvent water molecules to form dissociated products. This implies that at molecular level, the strength of an acid is related to the number of solvent water molecules needed to ionize the acid molecule. In the present study, the molecular interactions between weak organic acid molecules and solvent water molecules are studied to get a better understanding of the hydration of acid molecules. Equilibrium geometries of different size hydrated clusters of selected acid molecules are calculated. The minimum number of water molecules needed for the dissociation of an acid molecule is determined. Microhydration of a photo acid is also considered. Photo acids have different pKa values at ground and excited states. Often excited state pKa values of photo acids are much lower compared to the ground state. It is reported that in case of 2-naphthol, the excited singlet state has a low pKa value compared to its ground state and excited triplet state.[15] Analysis of the microhydrated clusters of both ground state and first excited singlet and triplet states of 2-naphthol is carried out. At macroscopic level, strength of an acid is described by its pKa value, while at molecular level the acidic strength can be expressed in terms of the number of water molecules needed for its dissociation. A linear relation is observed between the two quantities. Thus, this study also presents a non-thermodynamic route to calculate the pKa value of an acid molecule, if the number of water molecules needed for its dissociation is known and vice-versa. The thesis is organized in 7 chapters. A brief description of each chapter is given below:

Chapter 1: It is the introductory chapter of the thesis. It gives a general description about microhydration of acid molecules and its relevance. The experimental and theoretical studies on microhydrated clusters reported in the literature are discussed. A summary of the contents of each chapter is also given.

Chapter 2: This chapter gives an overview of the important computational methods including *ab initio*, electron correlation and DFT methods, along with a brief account on basis sets and geometry optimization. Applying these methods, the present study aims to understand at molecular level, the hydration of an acid.

Chapter 3: This chapter deals with the determination of minimum energy conformers of different size hydrated clusters of selected acid molecules, namely: trifluoroacetic acid, acetic acid, benzoic acid and oxalic acid. The selection is made so as to understand the electronic effects on the ionization of an acid molecule. These acids also play a significant role in many atmospheric processes. The bench-marking done to decide upon a suitable level of theory is provided in this chapter. The effect of bulk solvation models and their inability to accurately describe the hydrogen bonded acid-water clusters is mentioned. The evolution from acid dimer to microhydrated acid cluster is also discussed. The minimum number of water molecules needed for the dissociation of the selected acid molecules is determined. Geometrical parameters and microwave spectra generated is compared with available experimental data.

Chapter 4: The interaction between the acid molecule and solvent water molecules are analyzed in this chapter. The free energy of formation of the hydrated acid clusters is calculated at room temperature and atmospheric pressure as well as at low temperature and pressure, to determine the temperature-pressure dependence on their thermodynamic stability. The solvent stabilization energy and interaction energy are also determined to understand the molecular interactions present in the acid-water clusters. The solvent stabilization energy considers all types of interactions, both solute-solvent and solvent-

solvent. Hence, the interaction energy is defined to exclude all solvent-solvent interactions and exclusively gives solute-solvent interactions. The variation of solvent stabilization energy and interaction energy with increase in size of the hydrated cluster is studied.

Chapter 5: The formation of contact ion-pair should be reflected in some of the properties of the hydrated acid clusters. This chapter describes the variation in various properties of the hydrated acid clusters, with increase in cluster size. The variations in net dipole moment, acidic O-H bond dipole moment, isotropic polarizability and hydrogen bond energy of the selected acid-water clusters have been studied. Intermolecular interactions in a solvated system can be understood by the system’s response to an external electric field, which is given by its electronic polarizability. The variation of static polarizability of the hydrated acid clusters, with increase in the size of the cluster, is studied. The addition of water molecules to the acid molecule causes a weakening of the acidic O-H bond. The elongation of the hydroxyl bond of the acid molecule due to hydrogen bonding with solvent water molecules causes a change in the dipole moment of the hydrated acid clusters. Hence, dipole moment can be a property which can be monitored to determine the proton transfer in carboxylic acid-water cluster. Two bonds crucial in the study of dissociation of the acid molecule are: the acidic O-H bond and the hydrogen bond between the acidic H atom and the O atom of the neighboring water molecule. The breaking of the former and the formation of the latter bonds can be studied from their hydrogen bond energy. The dissociation energy curve of the hydrated acid clusters is useful in obtaining information about the proton transfer barrier of the cluster. The dissociation energy curve is obtained by carrying out a rigid potential energy scan of the acidic hydroxyl bond of the hydrated acid cluster. Marked differences in some of these properties are observed upon ionization of the acid molecules. The simulated infrared spectra of the hydrated acid clusters are also discussed here and are compared to available experimental data. The IR spectrum is generated by calculating the hessian matrix of the system. As this calculation is done considering a harmonic approximation, a scaling factor is included to account for the anharmonicity. The weakening of the acidic O-H bond, with increase in size of the hydrated cluster, is manifested as a red shift in its IR stretching frequency. Large red shifts in acidic O-H stretching frequency, with respect to free acid, are observed in case of ionized acid-water clusters. Formation of new peaks corresponding to vibrational frequencies of hydrated proton is also noticed in case of hydrated clusters of ionized acid molecule.

Chapter 6: This chapter is dedicated to the microhydration of photo acid. Photo acids have different pKa values at ground and excited state. 2-naphthol is taken up as a case study. The minimum energy geometries of 2-naphthol and its hydrated clusters, at both ground state and first excited singlet and triplet states, are reported. It is noted that the minimum number of water molecules needed to dissociate 2-naphthol at first excited singlet state is different from that of ground and excited triplet state.

Chapter 7: It is the concluding chapter. It gives a summary of the study on microhydration of weak organic acids. Based on the present study, an interesting relationship is observed between the number of water molecules needed to dissociate an acid molecule and its pKa. A non-thermodynamic route for determining the pKa of an acid is reported.

The future direction of the current work would be to study the microhydration of other systems such as alcohols, amines and photo acids. This would help in expanding the database to verify the correlation observed between the pKa and number of water molecules needed by the system for proton transfer. Moreover, a microscopic theory based approach may be considered to predict number of water molecules needed to dissociate an acid in the ground state.

LIST OF FIGURES AND PAGE No.

LIST OF TABLES

Chapter 1

How Many Water Molecules are Needed to Ionize an Acid Molecule?

> *If we were to name the most powerful assumption of all, which leads one on and on in an attempt to understand life, it is that all things are made of atoms, and that everything that living things do can be understood in terms of the jigglings and wigglings of atoms.*

-Richard Feynman, The Feynman Lectures on Physics, 1970

Carboxylic acids are known to ionize in water to form carboxylate anion and proton. The extent of ionization of an acid is defined in terms of the pKa value of the acid. Observing from a microscopic point of view, the degree of ionization depends on the strength of the O-H bond of the acid molecule, which is reflected in the number of water molecules needed for its dissociation. Understanding the microscopic description of hydration is essential for the fundamental understanding of acid dissociation as well as for understanding and modeling several atmospheric as well as biological phenomena. This thesis deals with the dissociation of acid molecule in the presence of water molecules. Molecular level acid dissociation can be studied using acid-water clusters.

1.1 Clusters

Clusters are defined as finite aggregates of particles (atoms or molecules). They bridge the gap between molecules and bulk materials. Although cluster science is an emerging area of research, clusters have been in use for ages, for example, the beautiful colors imparted to the glass artifacts by the Romans, and AgBr clusters used in photography. Most of the elements of the periodic table form clusters. The size of a cluster varies from a few to several thousand atoms or molecules. The properties of clusters are very different from that of its individual constituents and that of the bulk. The electronic, optic, magnetic and chemical properties of a cluster depend on its size. The evolution of properties with the variation in size of the cluster is of great fundamental interest. The physical and chemical properties can be tuned by varying the size and constituent particles of the cluster. Cluster science tries to find answers to fundamental questions such as ‘how large should the cluster be for its properties to resemble that of the bulk material’.[16] Depending on the composition and nature of bonding in the clusters, they can be broadly classified as metallic, ionic and weakly bound clusters. In metallic clusters, like Al_{77}, Pd_{145} etc., the atoms are held together by long range forces originating from valence electron sharing over many adjacent atoms.[17] The binding force in ionic clusters is the electrostatic interaction between oppositely charged species.[18] In weakly bound molecular clusters inter-molecular interactions are non-covalent in nature.[19–23]

The size-dependent evolution of properties in a cluster is a popular field of theoretical and experimental research. The development of molecular beam techniques has helped in better understanding of cluster geometries and properties in an interaction-free environment. Cluster generation begins with vaporization, where the atoms/molecules constituting the cluster are produced in gas phase. The atoms/molecules then condense to form the cluster nucleus. The cluster grows with the addition of more atoms/molecules to the nucleus. The merging of small clusters to form larger clusters is known as coalescence. The structure and properties of the cluster are studied using molecular beam techniques, inert matrices, supporting surfaces or in solid state. Theoretical chemistry has also been playing a crucial role to understand the structure and properties of atomic and molecular clusters.

1.2 Experimental techniques to study clusters

A few of the experimental techniques used to study clusters are described here briefly. Gas phase clusters can be generated by pulsed supersonic jet expansion techniques, where a dilute mixture, of the sample to be studied and an inert gas, is allowed to expand through a slit-jet source.[24,25] The expansion can be coupled with experimental techniques such as IR spectroscopy, microwave spectroscopy, photo electron spectroscopy etc to study the properties of the clusters generated. Mass spectrometry is used along with other experimental techniques to determine the size of the cluster. Direct absorption spectroscopy employs FTIR to obtain accurate information over a broad spectral coverage.[26,27] In IR cavity ring down spectroscopy, a laser is used to illuminate a high finesse optical cavity formed by two highly reflective mirrors.[28–30] Intensity builds up in the cavity when the laser is in resonance with a cavity mode. The ring down pulse intersects a pulsed slit jet expansion in a vacuum chamber. The sample is seeded in to the expansion by bubbling an inert carrier gas through the room temperature liquid. The ability to provide quantitative absorption intensity information and to probe gaseous samples with high sensitivity makes this technique very popular. Matrix isolation IR spectroscopy is also used to study cluster properties.[31] In this method, the sample is trapped in an inert gas matrix, like Ar or N_2 at low temperature. The sample concentration is kept very low to ensure molecular isolation; the sample is surrounded only by the inert gas molecules. This method can be applied to study van der Waals complexes, polycyclic aromatic hydrocarbons and hydrogen bonded clusters due to its small line-width and spectral sharpening features. In supersonic jet expansion, the vibrational-rotational energy levels of the sample are separated by the expansion of the gas at high pressure.[25,32] Microwave spectrum of such a system can then be studied thoroughly.[33] The rotational spectra of weakly bound clusters have been widely investigated using Fourier Transform microwave spectroscopy. Other important tools for studying clusters are electron attachment and photo electron spectroscopies.[34,35] They are valuable in determining the electron affinity and ionization energy of the clusters as well as for obtaining information about the production and identification of ions in mass spectrometry. Photo electron spectroscopy has been used to determine the size of CO_2 clusters.[36] The free neutral CO_2 clusters are generated in a free jet condensation source and are expanded from a stagnation chamber. The cluster-rich part of the beam consisting of molecules and clusters is extracted by a skimmer. The recorded C_{1s}

photoelectron spectrum shows two distinct peaks corresponding to the clusters of various size and uncondensed monomers.

1.3 Theoretical investigation of clusters

Theoretical methods play an important role in the development and application of cluster science. Many cluster properties, like geometry, binding energy etc. cannot be easily measured from experiments directly. Computational models also help in interpreting the experimental results. Early ab initio level calculations of small water clusters were reported by Clementi and co-workers in 1974.[37] Due to limited computational resources, HF calculations were the only options available until the end of 1980s. During the 1990s, ab initio calculations at MP2 levels became feasible for dimers and trimers of small molecules. With advancement in computational resources, larger clusters of larger molecules can be studied using ab initio as well as DFT calculations.[38–43] The inherent $O(N^5)$ (N is the number of electrons) scaling of MP2 level calculations limits its use in geometry optimization to less than 100 first row atoms. DFT based methods have become increasingly popular for the computational study of molecular clusters. It is observed that the geometry and energy of water clusters up to size four, obtained from DFT functionals like BLYP and BP86 coupled with correlation consistent basis sets, are comparable to those obtained from MP2 calculations.[44] However, these functionals are not suitable for larger water clusters, where hydrogen bonding plays a major role in shaping geometry. Introduction of long range dispersion corrected density functionals have helped in the modeling of large weakly bound clusters.[45–50] HF, DFT and MP2 are the most popular levels of theory for geometry optimization for large clusters. The energy of the clusters so obtained can then further be improved using higher levels of theory like MP4, coupled cluster method etc. It may be noted that coupled cluster method with single and double excitations including triplet correction (CCSD(T)) is regarded as the contemporary gold standard of quantum chemistry.

1.4 Microhydrated Clusters

Water clusters as well as microhydrated clusters are among the most extensively investigated clusters, because of their role in a wide range of phenomena from solution chemistry to large number of biochemical processes. Microhydrated clusters are formed by the step-wise addition of water molecules to a chemical species. These clusters are stabilized by hydrogen bonding. Hydrogen bonds play a key role in determining the three dimensional structure of the cluster. Microhydration of chemical species has been a subject of intense research, to understand the structural, energetic, spectroscopic, and dynamic aspects of hydration at molecular level.[51–55] The size-dependent variation in the properties of hydrated systems can be studied from molecular level to the bulk solution. Explicit hydration studies are also important in understanding the correlation between solubility and acidity of the solute. The importance of including specific interactions between solute and solvent molecules in the condensed phase has been reported previously.[56] A large part of the experimental and theoretical microhydration studies reported, are on acid molecules.[9–14,57–68]

1.5 Hydrated Acids

Acids (A-H) are ubiquitous in nature. Acidic solutions play a major role in a wide range of fields. A plethora of chemical, physical and biological phenomena involves acid–water interactions. Be it many enzyme catalyzed reactions in biological systems or the formation of cloud condensation nuclei in the atmosphere, it all depends on the proton transfer process between the acid and water molecules, that is, acidity of the acid. With the advent of ultra-fast spectroscopic techniques and high level computational facilities, the nature and characterization of the excess proton in water, shifting between Eigen and Zundel forms, has been a field of extensive study, which is summarized in the review by Hassanali et al.[3] The understanding of spectral signatures of hydrated proton has led to the progress of the study of microhydration of acids.

An accurate description of hydration of acids, at molecular level, can deepen our understanding of a broad spectrum of phenomena, from proton transfer to acid rain. Further, acid-water molecular clusters provide an ideal system to study the relation between solvation and reactivity, as ionization of the acid molecule occurs during the progress from molecular clusters to aqueous solution. Studying the structure and properties of acid-water clusters provides basic understanding of the fundamental interactions responsible for the phenomenon of hydration, which is important not just to chemists, but also to physicists, biologists and material scientists. The intermolecular interactions determine the stability and geometry of the molecular clusters.

In macroscopic description, a strong acid signifies an acid that ionizes completely in an aqueous solution whereas a weak acid does not ionize fully in such an environment. Thus, the ability to transfer a proton to a water molecule is the answer to differentiate an acid based on its strength. In the context of the microscopic or molecular level description of the strength of an acid, one may ask a fundamental question: how much water is required to ionize an acid? The answer to this question involves a microscopic study of the hydration of acids. In acid-water clusters ($A\text{-}H.nH_2O$), solute acid molecule forms hydrogen bonds with the solvent water molecules present in the immediate neighborhood. As a result of intermolecular interactions between the acid molecule and solvent water molecules, the A-H bond of the acid molecule weakens and proton transfer from the acid molecule to solvent water molecules occurs, leading to dissociation of the acid molecule, as depicted in Figure 1.1.

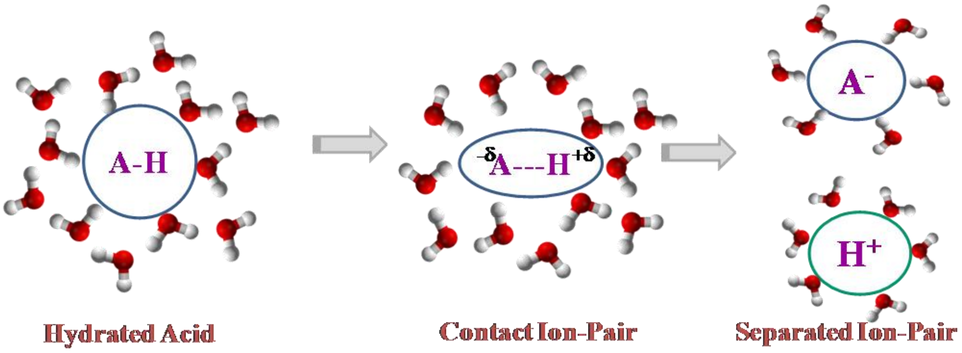

Figure 1.1 Schematic representation of hydration of acids. A-H represents the acid molecule and the red and grey balls represent oxygen and hydrogen atoms of the water molecule respectively. The reorientation of the water molecules around the acid molecule, the weakening of the A-H bond and formation of solvent separated ion pair is shown.

The process of hydration of an acid molecule involves formation of contact ion pair followed by solvent separated ion pair, and yields hydrated protons in either Eigen ($H_3O^+\cdot 3H_2O$) or Zundel ($H_3O^+\cdot H_2O$) forms.[7,69–71] Thus, determining the number of water molecules needed to stabilize the hydrated ion pair will tell us the number of water molecules that are needed to ionize an acid.

A few recent theoretical studies report the number of water molecules needed to ionize H_2SO_4, HCl, HNO_3 and $HClO_4$.[61],[9],[67],[14] When a solute is added to a solvent water pool, the water molecules in the immediate neighborhood of the solute get rearranged to form a hydrogen-bonded cluster of solute and solvent water molecules. The electron distribution pattern of the added solute molecule plays a key role in forming stable hydrogen-bonded water network around the solute. Spectroscopy and first principle based quantum chemical studies have been successfully applied to determine the detailed structure of hydration shell around the solute molecule.

In experimental front, Matrix isolation studies, Helium nano-droplet spectroscopy and thin film IR studies have been employed to analyze acid-water molecular clusters.[11,59,61,64] From experimental and theoretical studies, a general trend noted in the geometry of mono-hydrates of acid molecules is that a linear or near linear hydrogen bond is formed between the acidic proton of the acid and the oxygen atom of the water molecule. The covalent O-H bond of the acid molecule increases only slightly from that of the free acid molecule and the O..H hydrogen bond distance range between 1.6 to 2.2 Å. A red-shift in the O-H stretching frequency of the acidic proton is also noted, due to the formation of H bond between the acid molecule and the water molecule. Number of possible geometries increases with increase in size of the acid-water cluster as the number of H bond donors and acceptors increases. However the relative stability of the isomers becomes very small. As the size of the cluster increases, the potential energy surface of the hydrated acid clusters become complex due to the availability of multiple H bond acceptors. Characterization of such a potential energy surface which has several low lying minima is essential for studying the hydrated acid clusters. The possibility for proton transfer from the acid molecule to the water molecules also increases with increase in size of the acid-water cluster. Low concentrations, absence of size selectivity etc makes it difficult to obtain experimental insights about higher hydrated acid clusters and majority of the reported studies on higher hydrates are based on theoretical studies.[9,10,12–14,52,54,57,59,61,63,66–68] However a few IR and microwave studies for higher hydrates have also been reported. [3,14,46,50,54,57,64,68] A dominant structural motif consistent in higher hydrates of acid-water clusters is the hydrogen bonded closed rings. The water molecule added either forms part of a new ring or expands an existing ring. This introduces conformational variety. The hydrated acid clusters prefer closed ring conformers, even when the size of the cluster is very small. This observation is very different from that of hydrated proton systems, where closed ring conformers are first observed only for the hepta-hydrated cluster.[8] Unlike smaller clusters of hydrated proton clusters, conformers with dangling O-H bonds have higher energy in case of hydrated acid clusters.

Experimental reports of proton transfer in hydrated acid molecules are mainly based on matrix isolation and thin-film IR studies. Based on the study of amorphous thin films of HNO_3 and water, Ritzhaupt and Devlin reported that three waters of hydration are required to stabilize ionized HNO_3.[76] Gas-phase ultra-fast pump-probe experiments on HBr-water clusters by Castleman et al led to the conclusion that five water molecules are needed to induce ionization of HBr.[77] High resolution mass-selective infrared laser spectroscopy was employed by Gutberlet et al to observe the formation of hydronium ion in the tetra-hydrated cluster of HCl, within superfluid He cluster, at a temperature of 0.37 K.[62] Ab initio molecular dynamics was used to explore the free energy surface of the HCl-water system and explain how the proton transfer barrier was surmounted under the cryogenic conditions of the experiment. The addition of a fourth water molecule to the unionized tri-hydrate was predicted to yield a “partially aggregated” complex which then transforms into the structure containing Cl^- and $H_3O^+(H_2O)_3$. HF undergoes significant ionization in aqueous solution and results combining matrix IR spectroscopy and molecular dynamics simulations conclude that ionization of HF depend on the local hydration environment.[65,78]

As of yet majority of studies on hydrated acid clusters come from computational calculations. In a few of the acid-water systems studied, local minima on the potential energy surface show contact ion pair formation. With increase in number of water molecules, the global minimum of these clusters also show acid dissociation. Though variation in level of theory used may cause a slight difference in the results, in general it can be concluded that inorganic acid molecules dissociate in the presence of 3-5 water molecules, which is consistent with available experimental results. The formation of ion pairs in smaller hydrated clusters is observed to cause a structural transformation from the closed ring conformers to conformers with dangling O-H bonds. The ionized conformers of hydrated acid clusters resemble Eigen cation interacting with the corresponding counter anions.[11,52,60,62,63] Zundel-like structures are not so commonly observed.

The A-H bond length is an indicator for ionization of acid molecules in hydrated acid clusters. Upon hydration, due to hydrogen bonding between the proton of the acid molecule and O atom of the nearest water molecule, weakening of the A-H bond occurs. This leads to elongation of A-H bond. With increase in size of the hydrated acid cluster, the A-H bond also increases and finally after dissociation of the acid, the A-H bond distance would be in the range of H-Bond lengths. There is a corresponding decrease in the H..O H-bond distance, which finally reduces to O-H covalent bond length of the hydronium ion, upon acid dissociation. These distances are usually determined computationally, as their experimental measurement is difficult because the increase is usually a few hundredths of an angstrom. Another manifestation of acid dissociation lies in the vibrational stretching frequency of the A-H bond of the hydrated acid cluster, which can indicate the weakening of the A-H bond. A red-shift of the IR stretching frequency of the A-H bond is expected for the hydrated acid cluster, relative to free A-H, due to weakening of the A-H covalent bond upon hydration. The red-shift in vibrational stretching frequency of hydrated acids and H-bonded systems in general has been widely studied computationally incorporating anharmonic effects.[79–81]

Atmospheric impacts of the hydrated acids have certainly been one of the motivations to study these systems. Nitric acid, sulfuric acid and a number of carboxylic acids and their hydrates play a major role in many environmental phenomena and have been thus studied.[82,83] They are involved in the formation of cloud condensation nuclei, aerosol formation, acid rain etc. Smaller clusters are intermediate in the formation of micron-sized particles, from gas phase species, and they can affect particle formation rate. Molecular interactions of acid molecules and water are also important in understanding many surface and interfacial phenomena.

The importance of microhydration studies of acids is cited in a review by Leopold.[84] It gives an overview of the acids that have been studied and goes on to mention the lack of systematic theoretical studies on weak carboxylic acids, which are important in the modeling of many environmental as well as biological systems. The scarcity in microhydration studies of weak acids could probably be due to their higher pK_a values and the associated complexity of calculations.

1.6 Microhydration of Carboxylic Acids (RCOOH)

Carboxylic acids are one of the dominant classes of organic species found in the troposphere up to the lower stratosphere.[85] Low molecular weight carboxylic acids, in particular, formic acid, acetic acid, and oxalic acid, play a significant role in cloud formation due to their polarity and characteristic hygroscopicity.[86] They are the prevalent carboxylic acids found in rain, fog, and snow samples from both urban and rural sites.[87] These pollutants significantly contribute to important environmental concerns, such as rain acidification and aerosol formation. In this context, the study of microhydration of carboxylic acids is environmentally relevant as the acid molecules are present along with water vapor in the upper atmosphere. Thus, understanding the interactions of these weak organic acid molecules with water molecules can shed light on various atmospheric phenomena. The present study deals with the microhydration of selected acids, namely, trifluoroacetic acid, acetic acid, benzoic acid and oxalic acid. The acids are chosen to understand the electronic effect on the hydrated acid cluster as well as for their atmospheric impact. A comparison between these acids and previously reported formic acid is made. The structures of different size hydrated clusters of these acids are determined and their properties are studied. A brief summary of the studies done so far on the selected acid-water clusters is mentioned below.

1.6.1 Trifluoroacetic acid (tfa)

Trifluoroacetic acid is the most abundant halogenated acid in the atmosphere, produced mainly from the degradation of hydrochlorofluorocarbons (HCFCs). Because of the presence of water vapor in the atmosphere, the formation of its water cluster is inevitable. Its removal in the gas phase proceeds mainly in the wet deposition because it is inert toward reaction with hydroxyl radical (•OH), the major chlorofluorocarbon scavenger from atmosphere. Infrared spectra and first principle-based theoretical reports are available in the literature on stable structures of $\text{tfa}\cdot n\text{H}_2\text{O}$ ($n \leq 5$) clusters.[72,88,89] Experimental studies on clusters of tfa and water, $\text{tfa}\cdot n\text{H}_2\text{O}$ ($n \leq 3$) have been reported based on pulsed nozzle Fourier transform microwave spectroscopy.[73] Assignments of the observed microwave emission lines have also been made to H-bonded ring structures of tfa and water molecules with the support from ab initio quantum-chemical results. However, no report is available in the literature on the hydrated cluster of trifluoroacetic acid (pKa =0.52), where contact ion pair is the most stable structure, leading to the dissociation of acidic proton.

1.6.2 Acetic acid (acoh)

Acetic acid is highly soluble in water and this is due to strong interaction of acetic acid molecules with solvent water molecules through hydrogen bonding. IR and Raman spectroscopic studies in the condensed phase have suggested that in dilute aqueous solution of acetic acid, major components are hydrates of acetic acids.[90,91] Under atmospheric conditions, formation of hydrates of acetic acid is expected due to strong H-bonding interaction between the acid and water. Microwave spectroscopic studies have been carried out on acetic acid and its small size hydrates, $CH_3COOH.nH_2O$ (n =1, 2) to extract rotational constants and geometrical information.[74] Recently, a combined experimental and theoretical study has been reported on two isomers of acetic acid and water complex (1:1) trapped in an argon matrix at 11 K.[75] The most stable isomer has a six-member ring structure involving two hydrogen bonds: one between the hydroxyl hydrogen atom of the acid molecule and the oxygen atom of the water molecule and the other between the hydrogen atom of the water molecule and carbonyl oxygen atom of the acid molecule. Non-covalent interaction of only 1:1 acetic acid and water cluster ($CH_3COOH.1H_2O$) has been studied experimentally by IR spectroscopy in a nitrogen matrix and theoretically at MP2 and CCSD(T) level.[92] Only a few theoretical studies have been reported in the literature on small size (n =1, 2) hydrated clusters of acetic acid, elucidating mainly hydrogen bonding interactions.[93,94] Gao and Leung reported DFT results on equilibrium structures and binding energies of mono and di-hydrated clusters of acetic acid applying B3LYP functional.[93] Structure, energy parameters, and infrared vibrational frequencies of $CH_3COOH{\cdot}nH_2O$ (n = 1, 2) clusters have also been calculated at the MP2 level of theory. This thesis reports the sequential addition of water molecules to acetic acid molecule to study the dissociation of acetic acid molecule.

1.6.3 Benzoic acid (bza)

Benzoic acid is a pollutant present in the atmosphere, from engine exhaust[95] and from the photo-oxidation of toluene etc forming secondary organic aerosols.[96] Apart from its environmental impact, it is the smallest aromatic acid, making it the standard on which Hammett rules are based upon. Its derivatives are used as templates for many drug syntheses[97] as well as precursors in many organic syntheses. Its interaction with water would help shed light on various atmospheric and biological processes. An attempt has been made earlier to calculate the pKa of benzoic acid using MD simulations, based on free energy of ionized and unionized conformers of benzoic acid-water clusters.[98] Microwave spectrum of mono-hydrate of benzoic acid has been reported.[99] No reports of higher hydrates of benzoic acid are reported. Microhydration leading to dissociation of benzoic acid molecule is reported here.

1.6.4 Oxalic acid (oxa)

Though a few studies have been reported on oxalic acid-water systems,[100–102] a systematic comprehensive study of sequential addition of water molecules, leading to dissociation of the oxalic acid molecule, is missing. Theoretical studies have shown that oxalic acid can enhance the stability of ionic clusters.[103] Hence determining the number of water molecules needed to ionize an oxalic acid molecule could help in environmental modeling. The dissociation of one of the protons of oxalic acid molecule, following sequential addition of water molecules is reported in this thesis.

1.7 Motivation of the thesis

Macroscopic or bulk strength of an acid (A-H) is determined by the pKa value of the acid. At molecular level, the acidic strength may be correlated with the ease of proton transfer from the acid to the neighboring solvent water molecules. Proton transfer in an acid-water hydrated cluster depends on the bond strength of the A-H bond. The proton-transfer process involves polarization of A-H bond induced by solvent water molecules, followed by contact ion pair ($A^{\delta-}\cdots H^{\delta+}\cdots{}^{\delta-}OH_2$) formation. Depending on the strength of an acid, several molecules of water are needed to form stable contact ion pair in an acid molecule and make proton transfer possible. A weak acid molecule needs more number of solvent water molecules whereas a strong acid needs less number of water molecules. It is interesting to investigate if any relation exists between these two parameters, the bulk parameter: pKa and the molecular parameter: number (n) of solvent water molecules needed to form contact ion-pair. The aim of this thesis is to determine the correlation that exists between the acid strength at molecular and bulk level. This could help in determining the pKa of an acid through a non-thermodynamic route.

1.8 Brief overview of the thesis

This thesis aims to understand hydration of carboxylic acids at molecular level. Hydrated acid clusters represent embryonic form of their aqueous solutions, illuminating the transition between molecular to bulk behavior. The study of microhydration of acids is relevant not only from a fundamental point of view but also for modeling reliable atmospheric processes. The strength of an acid in microscopic context is defined by the ease of transfer of proton from the acid molecule to the neighboring solvent water molecules. This in turn is reflected in the minimum number of water molecules needed to break the hydroxyl bond of the acid molecule or in other words, the minimum number of water molecules needed to stabilize the charge separated ion pair. Structure of microhydrated clusters of weak organic acids are studied in the present work and their properties are determined. The thesis is divided into seven chapters. The second chapter gives an overview of the theoretical methods used in the thesis. The third chapter is ‘Structures of Hydrated Carboxylic acid Clusters’. The determination of geometry of acid-water cluster is the crucial step in discerning the number of water molecules needed for dissociation of an acid molecule. The delicate balance between proton transfer energy, coulombic attraction and stabilization due to H bond energy determines the structure of a hydrated cluster. A systematic study on step-wise microhydration of selected the acid molecules following first-principle-based electronic structure calculations are discussed in this chapter. The acid-water molecular clusters are stabilized by H bonds. These hydrogen bonds help in shaping the molecular cluster. Understanding the geometry of the clusters is also important in determining the properties of the clusters. In this chapter, geometry of each size cluster of tfa, acoh, bza and oxa are determined. Several initial input structures of each size cluster are optimized to obtain equilibrium geometries. The geometry optimization follows Newton-Raphson algorithm which is infamous for its initial value problem, i.e., the geometry converges to the local minimum nearest to the initial geometry. Hence the initial guess structures must be chosen with care and is explained in this chapter. To obtain initial input geometries, ab initio Molecular Dynamic simulations have been carried out in a few cases. All the structures within a cut-off energy range are then re-optimized at present level of theory. The minimum energy conformer is then selected. The most stable hydrated cluster showing contact ion pair formation is selected for each acid. The electronic effect on the minimum number of water molecules needed for contact ion pair formation is also mentioned in this chapter. Geometrical parameters like bond length and microwave rotational constants are compared with available experimental data.

The fourth chapter reports variation in energy parameters of the hydrated acid clusters. The stability of hydrated clusters is determined by their free energy of formation. In this chapter, the free energy of formation of the minimum energy structures of each size cluster of the selected acids is determined at different temperatures and pressure. The solvent stabilization energy is defined to understand the molecular interactions between the acid and water molecules. The variation of the energy parameter of each acid system with increase in size of the cluster is discussed. As the solvent stabilization energy fails to show any characteristic feature representing the ionization of the acid molecule, a new energy parameter, interaction energy, is defined. Its variation with respect to increase in size of the cluster is also monitored.

The Fifth chapter attempts to decipher the correlation between the structure and properties of the different hydrated acid clusters. The addition of water molecules to the acid molecules weakens the hydroxyl bond of the acid molecule. This is reflected in some of the properties of the hydrated acid. The polarizability, dipole moment, hydrogen bond energy, O-H bond dissociation curve and IR spectra of the most stable structure of different size hydrated clusters are presented. The isotropic polarizability, which shows the response of the hydrated cluster to an external electric field, is calculated. The variation of net dipole moments and selected bond dipole moments with increase in size of the hydrated cluster, for the selected acid molecules, are reported. The IR spectra of the hydrated clusters of the selected acid molecules are simulated to monitor the weakening of the hydroxyl bond, which manifests as a red-shift in the O-H stretching frequency. The potential energy scan for the acidic hydroxyl bond shows the potential energy barrier for proton transfer in the hydrated acid cluster. The hydrogen bond energy of the dissociating hydroxyl bond of the acid molecule and the bond forming between the hydroxyl H atom of the acid molecule and the O atom of the nearest water molecule are also calculated.

Chemists have been fascinated by the stark difference in dissociation characteristics of photo acids in the ground and excited state. Photo acids have different pKa values at ground and excited state. It has been reported that the pKa of ground state and excited singlet and triplet state of 2-naphthol are different. The sixth chapter deals with systematic studies carried out to elucidate the structure of the most stable conformers of hydrated 2-naphthol in the ground and excited states. The number of water molecules needed to ionize the ground state and first excited singlet and triplet states of 2-naphthol is examined in this chapter.

The final chapter of the thesis is 'Prediction of pKa: From Molecule to Bulk'. Depending on the extent of dissociation in aqueous medium, the strength of an acid (A-H) is defined in terms of pK_a value, at macroscopic level.

$$pK_a = -\log K_a \qquad 1.1$$

where, K_a is the acid dissociation constant. At molecular level, the acid strength depends on the strength of the A-H bond, which in turn is reflected in the number of water molecules need to dissociate the acid molecule. An empirical linear relation is observed between the number of water molecules needed to dissociate a number of acid molecules and their pKa. In this chapter, a novel non-thermodynamic route is presented to predict pKa of an acid based on the studies of its hydrated clusters. This can be used to determine the pKa of an acid if number of water molecules needed for its dissociation is known and vice-versa.

The summary and future prospects of the thesis are also provided.

Chapter 2

Theoretical Background

An atom consists of a nucleus and electrons. The motion of the electrons is described by the laws of quantum mechanics. When these laws were formulated more than 70 years ago, researchers realized immediately that in them was contained the explanation of the chemical bond. It was realized that if the quantum mechanical equations could be solved, one would be able to explain how atoms are bound together to form molecules. It would be possible to explain why molecules look as they do, what their properties are, and how they react with each other to form new molecules. A theoretical description of all of chemistry was within reach.

-Presentation Speech for the 1998 Nobel Prize in Chemistry for John Pople, by Professor Björn Roos of the Swedish Academy of Sciences, December 10, 1998.

This thesis deals with the microhydration of acid molecules leading to its dissociation. It involves determining the most stable structures of hydrated clusters of selected carboxylic acid molecules. Before going into details about the actual work, this chapter will provide a theoretical background for the calculations carried out.

Time-independent Schrödinger equation, $\hat{H}\Psi = E\Psi$ is the theoretical foundation of quantum chemistry. $\hat{H}$ is the Hamiltonian operator, which is associated with the observable energy. Ψ is the wave function and E is the energy of the system. A wave function or the state function is a complex valued mathematical function of the coordinates of the system, which contains all possible information about the system. The Hamiltonian operator for a system of M nuclei and N electrons is written as (in atomic units):

$$\hat{H} = -\frac{1}{2}\sum_{i=1}^{N}\nabla_i^2 - \frac{1}{2}\sum_{A=1}^{M}\frac{1}{M_A}\nabla_A^2 - \sum_{i=1}^{N}\sum_{A=1}^{M}\frac{Z_A}{r_{iA}} + \sum_{i=1}^{N}\sum_{j>i}^{N}\frac{1}{r_{ij}} + \sum_{A=1}^{M}\sum_{B>A}^{M}\frac{Z_A Z_B}{R_{AB}} \qquad 2.1$$

Z_A is the charge and M_A is the mass of the A^{th} nucleus and r_{iA}, r_{ij} and R_{AB} are the distance between the i^{th} electron and A^{th} nucleus, i^{th} electron and j^{th} electron and A^{th} nucleus and B^{th} nucleus, respectively. The kinetic energy of the electrons and the nuclei are described by the first two terms respectively. The last three potential energy terms give electron-nucleus, electron-electron and nucleus-nucleus interactions respectively. The negative sign indicates attractive interaction while the positive sign shows repulsive interactions. For a system of M nuclei and N electrons, the wave function, Ψ, depends on 3M+4N variables, including the spin of the electrons, making it very difficult to solve. Hence several approximations are required to simplify the problem.

2.1 Born-Oppenheimer Approximation

The huge mass difference between the nuclei and the electrons enables the separation of motion of electrons from that of the nuclei. The Born-Oppenheimer approximation assumes that the nuclei are stationary during electronic motion. Thus, kinetic energy term of the nuclei becomes zero and nucleus-nucleus repulsion term becomes constant in the Hamiltonian. The Hamiltonian is now reduced to electronic Hamiltonian:

$$\hat{H}_{elec} = -\frac{1}{2}\sum_{i=1}^{N}\nabla_i^2 - \sum_{i=1}^{N}\sum_{A=1}^{M}\frac{Z_A}{r_{iA}} + \sum_{i=1}^{N}\sum_{j>i}^{N}\frac{1}{r_{ij}} \qquad 2.2$$

Total energy can then be defined as the sum of electronic and nuclear energy: $E_{tot}= E_{elec}+ E_{nuc}$. However, Schrödinger equation cannot be solved exactly for many-electron systems. As most of the practical problems involve systems with more than one electron, attempts were made to develop other theoretical models that could describe such systems and help in understanding as well as predicting chemical phenomena.

2.2 Theoretical model chemistry

A theoretical model is a well-defined mathematical procedure of simulation that can approximately describe a complex process. John Pople, in his Nobel lecture on quantum chemical models, described the features of theoretical models.[104] He mentioned five stages in the development and use of a model. These are (a) determining the level of accuracy of the systems predicted;(b) precisely formulating an approximate mathematical procedure to describe a system, while making the formulation as general and continuous as possible;(c) implementing the formulated method as efficient and easily used computer programs;(d) verifying the model against experimental data; and (e) using the model to predict unknown chemical problems. Models can be broadly classified as semi-empirical and *ab initio*, on the basis of the parameters used in the models.

Models which include empirical parameters, obtained from experiments, are classed as semi-empirical methods. The *ab initio* methods do not rely on any empirical values. Instead they use fundamental constants of physics to define a system. When applied to chemistry, a model describes the molecular behavior of a system. Electronic structure theory deals with the description of electrons in atoms or molecules. Hartree-Fock (HF) theory is the basic and fundamental method on which most of electronic structure theory is based on.

2.3 Hartree Fock (HF) model

The concept of orbital theory of many electron systems was popularized by Slater, Hartree and Fock. The many electron wave function for a molecule having n electrons can be written as a Slater determinant:

$$\psi = \frac{1}{\sqrt{n!}} \det[(\varphi_1\alpha)(\varphi_1\beta)(\varphi_2\alpha)\varphi_2\beta)...] \qquad 2.3$$

where φ_{i} is the orthonormal molecular orbital and α and β are spin functions.

The Hamiltonian operator applying on the Slater determinant gives the energy as[105]:

$$E = \sum_{i=1}^{Nelec} < \phi_i \,|\, h_i \,|\, \phi_i > + \frac{1}{2} \sum_{ij}^{Nelec} (< \phi_j \,|\, J_i \,|\, \phi_j > - < \phi_j \,|\, K_i \,|\, \phi_j >) + V_{nn} \qquad 2.4$$

where,

$$h_i = -\frac{1}{2}\nabla_i^2 - \sum_{a}^{Nnuclei} \frac{Z_a}{|\, R_a - r_i \,|} \qquad 2.5$$

$$J_i \,|\, \phi_j(2) > = < \phi_i(1) \,|\, \frac{1}{|\, r_1 - r_2 \,|} \,|\, \phi_i(1) > |\, \phi_j(2) > \qquad 2.6$$

$$K_i \mid \phi_j(2) > = < \phi_i(1) \mid \frac{1}{\mid r_1 - r_2 \mid} \mid \phi_j(1) > \mid \phi_j(2) > \qquad 2.7$$

J is the coulomb integral while K is the exchange integral. 1 and 2 represent electron coordinates while ϕ_i and ϕ_j are molecular orbitals. V_{nn} is the nuclear repulsion term, which is a constant.

As the actual wave functions are not known, trial wave functions are used to solve the Hartree Fock equation iteratively. This is done by Self Consistent Field (SCF) method. It involves solving Schrödinger equation iteratively, by choosing an approximate Hamiltonian to operate on the trial wave function to obtain more accurate wave functions, applying variation principle, until the results converge. The resulting energy is then consistent with the orbitals that generate it and hence the procedure is called Self Consistent Field. Variational principle states that the ground state energy is always less than or equal to the expectation value of $\hat{H}$:

$$\langle \Psi \mid \hat{H} \mid \Psi \rangle \geq E_0 \qquad 2.8$$

E_0 is the ground state energy.

In case of HF model, motion of each electron is described by a single particle function and it does not explicitly depend on the motion of other electrons.

2.4 Basis Sets

Molecular orbitals are approximated as the linear combination of basis functions, which are one particle functions. A complete basis set is not an approximation. However, for a complete basis set, infinite number of basis functions must be used, which is not practical. A finite basis set defines the components of molecular orbitals in the direction of the selected basis functions. As the computational cost for *ab initio* methods scales as M^4, where M is the number of basis functions, there is a trade-off between expense and accuracy. There are mainly two types of basis functions: the Slater Type Orbital and the Gaussian Type Orbital.[105] The STO is of the type:

$$\chi_{\varsigma,n,l,m}(r,\theta,\phi) = NY_{l,m}(\theta,\phi)r^{n-1}e^{-r\varsigma} \qquad 2.9$$

where, N is the normalization constant, $Y_{l,m}$ is the spherical harmonic function, r is the radial function and ζ controls the width of the orbital. STOs do not have radial nodes. Radial nodes are introduced by taking linear combination of STOs. But, analytical calculation of three and four-centre two-electron integrals cannot be done in case of STOs. Hence the much more popular GTOs are used which are easier to calculate. GTOs are represented as:

$$\chi_{\varsigma,n,l,m}(r,\theta,\phi) = NY_{l,m}(\theta,\phi)r^{2n-2-l}e^{-r^2\varsigma} \qquad 2.10$$

The r^2 in the exponential causes the GTO to poorly represent proper behavior near the nucleus and also at the tail of the wave function. Hence, a combination of GTOs, i.e., Contracted type GTOs (CGTO) are mostly used, which mimics the STOs but are easy to calculate.

Depending on the combination of the GTOs there are several classifications of basis sets like the minimal basis sets, which contain just one basis function for each atomic orbital in the atom; the split valence basis sets which treat the core and valence orbitals differently; Pople basis sets, Dunning's correlation-consistent basis sets, which are optimized using correlated wave functions, etc. There are also the plane wave basis sets, which are used to describe periodic systems.

The molecular orbitals, ϕ_i , are expanded in terms of linear combination of basis functions, χ.

$$\phi_i = \sum_{\alpha}^{M_{basis}} C_{\alpha i}\chi_\alpha \qquad 2.11$$

Applying the Fock operator the energy is obtained as:

$$\hat{F}_i \sum_{\alpha}^{M_{basis}} C_{\alpha i}\chi_{\alpha} = \varepsilon_i \sum_{\alpha}^{M_{basis}} C_{\alpha i}\chi_{\alpha} \qquad 2.12$$

The Roothan-Hall equations for closed shell systems are obtained by multiplying the LHS by a specific basis function followed by integration.

$$\sum_{\alpha}^{M_{basis}} C_{\alpha}\langle \chi_{\alpha} | \hat{F} | \chi_{\beta}\rangle = \varepsilon \sum_{\alpha}^{M_{basis}} C_{\alpha}\langle \chi_{\alpha} \ | \chi_{\beta}\rangle \qquad 2.13$$

This can be written in the matrix notation as:

FC=SCε 2.14

$F_{\alpha\beta} = \langle \chi_{\alpha} | \hat{F} | \chi_{\beta}\rangle$ and $S_{\alpha\beta} = \langle \chi_{\alpha} | \chi_{\beta}\rangle$ 2.15

F matrix contains the Fock matrix elements and S matrix contains the overlap elements between basis function. Roothan-Hall equation gives the Eigen values of the Fock matrix. The unknown molecular orbital coefficients are obtained by diagonalzing the Fock matrix. However, to determine the Fock matrix, the molecular orbital coefficients must be known. So a self consistent procedure is followed wherein, some guess values are taken as the MO coefficients to form a Fock matrix which is diagonalized to obtain new coefficients. This process is repeated till a self consistent field solution is obtained.

However, in case of HF theory, the trial wave function consists only of a single Slater determinant. Thus HF scheme does not take into account electron correlation completely, and is referred to as mean-field approximation, as the electron-electron repulsion is accounted for only in an average manner. HF accounts for correlation of electrons with same spin. However, electrons of opposite spins are uncorrelated. With sufficiently large basis set, HF method has an accuracy of 99%. Unfortunately, most of chemical phenomena belong to the 1% that is not accounted for by the HF method. Dispersion forces are a consequence of electron correlation and thus HF fails for systems with non-covalent interactions. Hence electron correlation methods are important.

2.5 Electron correlation methods

The exact representation of a wave function requires infinite number of determinants, while HF theory uses just one, which is a crude approximation. The difference between the HF and lowest possible energy for a given basis set is called the correlation energy. Addition of determinants, for a given set of molecular orbitals implies considering different electron configurations, which are essential for better description of the system. There are several methods to introduce electron correlation. The Configuration Interaction and Perturbation theory consider electron correlation, by including more Slater determinants to describe the system. As corrections are added to the HF method, these correlation techniques are called post HF methods.

2.5.1 Configuration Interaction (CI)

In CI, the wave function is expressed as a linear combination of Slater determinants. The coefficients are determined variationally, by minimizing the total energy. A complete CI, though accurate, is impractical as it involves arrangement of all electrons in all possible ways in a complete basis set. A full CI also considers all possible arrangements of all the electrons, but in a finite basis set. This becomes computationally very costly and impractical except for very small systems. CI singles and doubles (CISD) and CI singles, doubles and triples (CISDT) are much more popular. They truncate the expansion according to the excitation level. This is possible because the contribution of the determinants to the system drops off with higher excited states. In the CISD, single and double excitations of electrons are considered and in CISDT, single, double and triple excitations are considered.

2.5.2 Perturbation Theory

In Perturbation Theory, the correction to the HF energy is added as a Taylor expansion in powers of a perturbation parameter. Depending on the perturbations added, there is Møller-Plesset (MPn) theory, Coupled Cluster (CC) theory etc. As the computational cost as well as accuracy increases with increase in order of perturbation, there is a trade off and expansion is truncated after achieving suitable level of accuracy.

Post-HF methods are costly and in most cases they cannot be applied for geometry determination as the memory requirements will be very high. Therefore the use of Density Functional Theory (DFT) is very popular. The DFT is based on the electron density of the system. The electron correlation is incorporated into DFT as a function of electron density. For an N electron system, while the wave function depends on 4N variables (3N spatial and N spin variables), the electron density depends only on three spatial coordinates, irrespective of the number of electrons. DFT is computationally comparable to HF and provides better results. However, there is no systematic way of improving the results obtained through DFT, to get exact solution.

2.6 Density Functional Theory

The Hohenberg and Kohn theorems (HK theorems) form the basis of DFT. The first HK theorem states that the external potential applied on a system, in ground state, is defined as a unique functional of electron density. The external potential determines the Hamiltonian, $\hat{H}$, axiomatically making it a unique functional of density. The second HK theorem states that the approximate electron density associated with an external potential is always greater than or equal to the exact ground state energy.

Thus, the ground state energy of the system can be expressed as:

$$E_0 = T[\rho_0] + E_{ee}[\rho_0] + E_{Ne}[\rho_0] \qquad 2.16$$

T is the kinetic energy, E_{ee} is the electron-electron interaction energy and E_{Ne} is the nucleus-electron interaction energy. The first two terms are independent of number of electrons, electron-nucleus distance and nuclear charge and are universally valid while the E_{Ne} depends on those variables and is therefore system dependent. The independent parts of the above equation is the Hohenberg-Kohn functional, $F_{HK}[\rho]$. The exact HK functional is not known. The E_{ee} term can be written as the sum of coulomb term and a term containing all non-classical contributions to the electron-electron interaction. The energy is then determined using variational principle. To improve the results obtained, Kohn-Sham orbitals have been developed. Here, the hypothetical system consists of non-interacting electrons, having ρ equivalent to the real system, which experiences average repulsion field from other electrons. The total energy is then written as:

$$E[\rho] = \mathrm{T_s}[\rho] + \int [\hat{\mathrm{V}}_{\mathrm{ext}}(r) + \hat{J}(r)]\rho(r)dr + E_{XC}[\rho] \qquad 2.17$$

where, $T_s[\rho]$ is the electron kinetic energy of the hypothetical system, $\hat{J}(r)$ gives the classical coulomb interaction between electrons and $\hat{\mathrm{V}}_{ext}(r)$ is the potential due to the nuclei.

Kinetic energy is computed in terms of one electron function:

$$T_S[\rho] = \frac{1}{2}\sum_{i=1}^{N}\langle\varphi_i \,|\, \nabla^2 \,|\, \varphi_i\rangle \qquad 2.18$$

$$\hat{V}_{ext} = \sum_{A}\frac{Z_A}{|R_A - r|} \qquad 2.19$$

$$\hat{J}(r) = \int \frac{\rho(r')}{|r' - r|}dr' \qquad 2.20$$

r and are r' the coordinates of the two electrons and Z_A is the nuclear charge. E_{XC} contains all the other contributions to energy such as electron exchange, correlation energy, correction for self-interaction and the difference in kinetic energy between interacting and non-interacting system. The Hamiltonian for the non-interacting system is:

$$\hat{H}_s = -\frac{1}{2}\sum_i^N \nabla_i^2 + \sum_i^N V_{S(\bar{r}_i)} \qquad 2.21$$

The non-interaction fictitious system is represented by Kohn-Sham orbitals, φ_i. They are determined using one-electron Kohn-Sham operator, $\hat{f}^{KS}$.

$$\hat{f}^{KS} \quad \varphi_i = \varepsilon_i \varphi_i \qquad 2.22$$

$$\hat{f}^{KS} = -\frac{1}{2}\nabla^2 + V_{S(\bar{r})} \qquad 2.23$$

V_s is the effective potential of non-interacting system.

The major part of kinetic energy can thus be computed and the residual part is merged with non-classical E_{XC} term. E_{XC} is the unknown term and different approximations for its determination have led to the development of several density functionals.

2.7 Microhydration-Theoretical background

The correlation between electronic structure of a system and its properties forms the basis of chemistry. First principle calculations and experiments act complementary to each other in determining the structure and properties of chemical systems. Computational assistance is particularly helpful in cases were experimental determination of structure and properties are difficult. Microhydration refers to step-wise addition of water molecules to a solute molecule. The crucial step of in-silico studies of microhydration is the geometry determination of the microhydrated cluster. Each conformation of the molecular cluster is associated with a definite energy. The variation of the energy with respect to change in geometry of the molecule, within Born-

Oppenheimer approximation, is given by its potential energy surface. The minimum in the potential energy surface of a given system is obtained through geometry optimization.

Optimization in general refers to determining stationary points of a function, where the first derivative of energy with respect to the geometric coordinates of the system, is zero. Geometry optimization essentially predicts the equilibrium energy structure of a system. The minimum energy configuration of a system is determined iteratively, by minimizing the force on the comprising atoms in each step. Several procedures are available to locate minimum energy structures, like Steepest Descent (SD) method, Conjugate Gradient (CG) method, Newton-Raphson (NR) method etc.

In SD method, the search direction is defined along the negative gradient.

$$d_i = -g_i \qquad 2.24$$

Though there is a guarantee to approach a minimum, there is an oscillation around the minimum path. Also the rate of convergence drops as the minima is reached.

The CG method improves on this by performing the search along a line that is conjugate to the direction of the previous search.

$$d_i = -g_i + \beta_i d_{i-1} \qquad 2.25$$

β values can be chosen in several ways, depending on the method. CG method is not suitable for non-linear surfaces.

In the NR method, the function is approximated as a quadratic surface and minimum is determined. The true function is expanded about the current position, x_0 up to second order and its gradient is made zero.

$$\mathrm{f}(x) = \mathrm{f}(x_0) + g(x - x_0) + \frac{1}{2} H (x - x_0)^2 \qquad 2.26$$

$$(x - x_0) = -H^{-1} g \qquad 2.27$$

$$\Delta x' = \sum_i \Delta x'_i = -\frac{f_i}{\varepsilon_i} \qquad 2.28$$

where Hessian, *H*, is the diagonal in the coordinate system (x'). f_i is projection of gradient along Hessian Eigen vector with Eigen value ε_i. Since the real function may have terms beyond second order, the NR method iteratively approaches towards stationary point. NR method always converges to the nearest local minimum. Hence care should be taken in preparing the initial geometries to get the correct configuration. Many optimization algorithms in quantum chemical software packages use some variant of the NR method. One such is the "Berny" algorithm developed by Bernhard Schlegel[106], which is used in the present study.

In Berny optimization, the local minimum on the potential energy surface is located using the forces on the atoms as well as the Hessian matrix. Since explicit calculation of the Hessian is costly, an approximated Hessian is constructed at the beginning, applying valence force field and is updated during each iteration, using the energies and gradients calculated in each step.

The optimized geometry can be a local/global minimum or a saddle point on the potential energy surface. The first (gradient) and second (Hessian) derivatives of energy of the system with respect to geometrical parameters, provides information about the nature of the minima. The negative of the gradient gives the vector of forces on the atoms. The eigenvectors of the mass-weighted Hessian matrix gives the normal modes of vibration. A minimum in the potential energy surface has zero gradient and all positive vibrational frequencies. A first order saddle point (Transition State) has maximum in one direction and minimum in all other directions in the potential energy surface. Thus, it has zero gradient and one negative vibrational frequency. Similarly, nth order saddle point will have zero gradient and n imaginary frequencies.

All these methods can be implemented computationally. Manual calculations of even the simplest systems would be very time consuming and complicated. With the evolution of computers into easily accessible machines with large memory and computing powers, the field of computational chemistry has expanded and relied upon by many industries. Many modern chemistry softwares have graphical interfaces and most of them can be used without much training in theoretical chemistry.

Chapter 3

Structures of Hydrated Carboxylic acid Clusters

The underlying physical laws necessary for the mathematical theory of a large part of physics and the whole of chemistry are thus completely known, and the difficulty is only that exact application of these laws leads to equations much too complicated to be soluble.

-Paul A. M. Dirac (1929)

This chapter deals with structures of the different size hydrated clusters of trifluoroacetic acid (tfa), acetic acid (acoh), benzoic acid (bza) and oxalic acid (oxa) molecules. The addition of the solute acid molecule to solvent water pool causes a reorganization of the immediate neighboring water molecules to accommodate the solute molecule in their hydrogen bonded network. The electron distribution of the added acid molecule plays the key role in the formation of hydrogen bonded network of water molecules around the solute. The hydrogen bonding interactions between the acid molecule and the solvent water molecules determine the shape of the hydrated clusters, and hence their properties. Thus determining the geometry of the hydrated acid clusters is important in understanding their properties. Study on microhydration of formic acid has been previously reported.[107] In the present thesis, the electronic effect of the acid molecule on the geometry of the hydrated acid clusters is examined. The effect of electron donating and withdrawing groups is studied by considering trifluoroacetic acid and acetic acid hydrated clusters respectively. Benzoic acid-water system is investigated to determine the effect of an aromatic ring. Microhydrated clusters of the simplest dicarboxylic acid, namely, oxalic acid, are also studied.

The effect of bulk solvation on the acid molecule is examined. Carboxylic acids are known to form dimers in the vapor phase as well as in non-polar solvents. The transition of dimer to microhydrated clusters is also discussed. This chapter describes how the initial guess structures of the hydrated clusters are chosen, the different local minima obtained, the minimum energy structures obtained for each size acid cluster and the geometric parameters of the minimum energy structures. Comparison is made with available experimental data. The minimum number of water molecules needed to ionize each acid molecule studied is predicted and reported.

The task of obtaining the exact potential energy surface for system with weak interactions, like hydrogen-bonded systems, is a herculean, as there would be numerous local minima, and the potential energy surface is shallow, especially for large size clusters. Thus, choice of initial guess structures is very important. As the size of the hydrated acid clusters increase, number of possible initial guess structures becomes very large and the risk of missing out important structures becomes high. Hence, the studies are limited to hydrated clusters with maximum eight water molecules.

3.1 Theoretical method

As the geometry, and hence properties of hydrated clusters depend very much on hydrogen bonding, it is important to choose a level of theory that describes these interactions accurately. Hence, all optimization calculations are done using long range corrected hybrid density functional, ωB97X-D, including empirical atom-atom dispersion corrections.[108] Dunning's correlation consistent, augmented double zeta set of basis functions is used. The present level of theory is decided based on the bench-marking studies carried out on a few selected systems (described in detail in section 3.2.1) as well as from reported study on carboxylic acid.[107] The equilibrium structures for each size hydrated carboxylic acid clusters, RCOOH.nH2O, are obtained by geometry optimization of several possible initial guess structures, following Newton Raphson algorithm. The choice of guess structures is important as the geometry optimization following this algorithm does not ensure that the geometry corresponding to the global minimum is achieved. The input geometry converges to the nearest local minimum energy conformer. The objective is to determine the minimum number of water molecules needed for breaking the hydroxyl bond of the acid molecule. The initial geometries are prepared so as to facilitate the dissociation of the O-H bond of the acid molecule and maximize solute-solvent as well as solvent-solvent interactions. The water molecules are placed in such a way that they form hydrogen bonding with the carbonyl oxygen, hydroxyl oxygen as well as the hydroxyl hydrogen of the acid molecule. Optimization of the input geometries, without any symmetry restrictions, results in various equilibrium conformers of which, the zero-point energy corrected minimum energy conformer is chosen for each size hydrated cluster. To obtain initial guess structures, ab initio Molecular Dynamic simulations have been carried out in a few cases. All the MD calculations are performed using Quantum ESPRESSO software, a plane wave based implementation of density functional theory.[109] The electronic exchange and correlation potential are described by the generalized gradient approximation (GGA) as parameterized by Perdew-Burke-Ernzerhof (PBE).[110] Projector-Augmented Wave (PAW) methods are used for the elemental constituents.[111] The simulations are allowed to run for 2000 ionic steps with 1fs time step. The cut-off energy for the plane wave basis set was fixed at 600 eV. The molecule is placed in a unit cell of fixed volume, ensuring that the periodically repeating clusters do not interact with each other. The minimum energy structure and all the structures with relative energy within 200meV (~5 kcal/mol) of the minimum energy structure are selected and optimized at ω-B97XD/aug-cc-pVDZ level of theory. Hessian calculations are done to identify the nature of the optimized geometries, obtain thermodynamic parameters and to simulate the IR spectra of the microhydrated clusters. In cases where the optimized geometry has normal modes with imaginary frequency, they are optimized further to obtain only positive frequencies. The molecular electronic calculations are done on a Linux cluster platform, with general *ab initio* quantum package, GAMESS.[112] Structure and IR spectra of the microhydrated systems are visualized using MOLDEN.[113]

3.2 Results and Discussion

For easy identification, the hydroxyl oxygen of the acid molecule studied is referred as O1, the carbonyl oxygen of the acid molecule is referred as O2 and the oxygen of the water molecule, closest to the hydroxyl hydrogen of acid molecule, is referred as O3 in case of trifluoroacetic acid (tfa), acetic acid (acoh) and benzoic acid (bza).In case of oxalic acid (oxa), O1 and O2 are the two hydroxyl oxygen atoms of the acid molecule and Oa and Ob are the oxygen atoms on the water molecule closest to O1 and O2 respectively. In the following discussions, these conventions will be used.

3.2.1 Benchmark studies

To decide upon a suitable level of theory, geometrical parameters of isolated water molecule and trifluoroacetic acid molecule, calculated using different DFT functionals and MP2 method are compared with available experimental data. Trifluoroacetic acid is chosen for benchmark studies as experimental data of hydrated clusters (up to three water molecules) of trifluoroacetic acid are available from literature.

For benchmark studies, popular hybrid density functional, B3LYP; a functional including dispersion correction, ωB97X-D and a modern meta-hybrid GGA DFT functional that accounts for non-covalent interactions, M06-2X, are tried. Selected Geometrical parameters for minimum energy equilibrium structures of CF_3COOH and H_2O molecules calculated applying different DFT functional and MP2 method are supplied in Table 3.1 and are compared with reported experimental values. As the size of the hydrated clusters can be very large, Dunning's correlation consistent double zeta set of atomic basis functions, augmented with diffuse functions (aug-cc-pVDZ) is used as trade-off between accuracy and computational expense and is seen to serve well to describe these hydrated systems. From Table 3.1, it is seen that B3LYP performs well for trifluoroacetic acid as well as water molecule. But this functional does not involve dispersion corrections which is very important for systems with non-covalent interactions, and is hence known to fail for such systems. As the systems studied are hydrogen bonded systems, B3LYP is not chosen, because this functional cannot treat such systems accurately. The gross performance of the selected DFT functionals and MP2 method are similar in case of these two molecules. Calculated rotational constants, applying rigid rotor model, are compared to the available experimental data. The comparison of rotational constants is given in Table 3.2. For mono and di-hydrates of trifluoroacetic acid (tfa), rotational constants calculated using ωB97X-D are within 1% error with respect to experimental values, while for tri-hydrate the percentage-error is higher.

Table 3.1 Comparison of geometrical parameters and hydroxyl stretching frequency of isolated water and trifluoroacetic acid molecule, calculated at different levels of theory using aug-cc-pVDZ basis set, with available experimental data

Method	CF_3COOH								H_2O			
	r_{C-F} (Å)[a]	r_{C-C} (Å)	$r_{C=O}$ (Å)	r_{C-O} (Å)	r_{O-H} (Å)	ν_{C-F} (cm^{-1})	$\nu_{C=O}$ (cm^{-1})	ν_{O-H} (cm^{-1})	r_{O-H} (Å)	∠HOH (degree)	$^{sym}\nu_{O-H}$ (cm^{-1})	$^{asym}\nu_{O-H}$ (cm^{-1})
MP2	1.349	1.544	1.212	1.349	0.974	1182	1819	3736	0.966	103.8	3804	3937
ωB97X-D	1.337	1.547	1.197	1.333	0.967	1216	1898	3821	0.961	104.7	3881	3992
LC-wPBE	1.338	1.540	1.196	1.331	0.969	1208	1922	3813	0.962	105.1	3871	3982
M062X	1.334	1.542	1.194	1.333	0.969	1248	1928	3798	0.962	104.8	3867	3977
B3LYP	1.345	1.550	1.200	1.341	0.972	1162	1850	3735	0.965	104.8	3795	3905
Expt[b]	1.325	1.546	1.192	1.342	0.960	1240	1792	3587	0.957	104.5	3657	3756

[a]average of the three C-F bonds; [b]References [114], [115]

However, when compared to other DFT functionals and MP2 method, overall performance of ωB97X-D is better. Also, as mentioned earlier, previous study has shown that ωB97X-D works well for microhydrated formic acid clusters.[107]

Thus, ωB97X-D/aug-cc-pVDZ is chosen as the level of theory for geometry optimization of all systems presented in this thesis. The bond length and bond angle of free H_2O molecule at ωB97X-D/aug-cc-pVDZ level of theory is 0.961Å and 104.76°, which is very close to the experimentally determined values of 0.9575 Å and 104.51°, respectively.

Table 3.2 Comparison of rotational constants (A, B, and C in MHz) for hydrated clusters of trifluoroacetic acid, $CF_3COOH.nH_2O$ (n = 1−3) calculated at different levels of theory

Rotational constant	Method	CF_3COOH	$CF_3COOH.H_2O$	$CF_3COOH.2H_2O$	$CF_3COOH.3H_2O$
A/MHz	MP2	3771	3737	2506	1711
	wB97XD	3848	3811	2549	1905
	LC-wPBE	3849	3815	2559	1769
	M062X	3855	3821	2562	1910
	B3LYP	3805	3737	2530	1752
	Expt[a]	*3865.13*	*3835.11*	*2533.71*	*1733.35*
B/MHz	MP2	2471	1085	716	499
	wB97XD	2484	1090	724	497
	LC-wPBE	2495	1100	727	494
	M062X	2501	1103	730	504
	B3LYP	2463	1085	719	488
	Expt[a]	*2498.79*	*1082.58*	*718.46*	*493.41*
C/MHz	MP2	2044	993	621	428
	wB97XD	2063	1000	628	465
	LC-wPBE	2071	1009	631	416
	M062X	2073	1010	633	477
	B3LYP	2046	993	624	411
	Expt[a]	*2075.2*	*993.78*	*622.5*	*414.75*

[a] Reference[73]

3.2.2 Macroscopic Hydration of Carboxylic Acids

To determine the effect of macroscopic hydration of acid molecule, optimization of trifluoroacetic acid, acetic acid, benzoic acid and oxalic acid molecules are done using macroscopic solvation models. Macroscopic solvation models like Polarized Continuum Model (PCM) and Solute Density Model (SMD) are used applying ωB97X-D/aug-cc-pVDZ level of theory. In PCM model, a cavity is formed by the union of spheres which are centered on each atom and the electrostatic interaction, between the wave function of the solute and a dielectric model of the bulk solvent, is determined.[1] The solute electron density interacts with the solvent, taken into account as a dielectric continuum, in case of the SMD model.[2] Trifluoroacetic acid, acetic acid, benzoic acid and oxalic acid molecules are known to dissociate in water to form corresponding carboxylate anion. However, the O-H bond length of acetic acid molecule, calculated using PCM and SMD models are 0.968 and 0.970 Å respectively, indicating the acid is still undissociated. Similar results are observed in case of trifluoroacetic acid, benzoic acid and oxalic acid. The O-H bond length of trifluoroacetic acid, benzoic acid and oxalic acid calculated using SMD model is 0.972, 0.969 and 0.974 Å respectively, which is not correct. Hence for an accurate description of the hydration of carboxylic acids, explicit solvation models must be adopted at least for the primary shell of solvation. This is especially needed, as the systems studied are hydrogen bonded clusters and the implicit solvation models fail to take into account such kind of solute-solvent interactions.

3.2.3 Dimerization versus Microhydration of Carboxylic acid

Before going into details about the possible structures of acid-water molecular clusters, a brief note on the relative stability of carboxylic dimers and microhydrated acid clusters is interesting to know. It is well known that carboxylic acids form dimeric complexes in gas phase and non-polar solvents. Hence to fully understand the fundamental nature of acid dissociation, the breaking of the acid dimers, to form microhydrated acid clusters, needs to be studied. It has applications in biological as well as environmental modeling. The number of water molecules needed for the dimer to break and form micro-hydrated acid clusters is studied for the two cases: formic and acetic acid.

The free energy of formation calculated for formic and acetic acid systems shows that at room temperature and pressure, the microhydrated systems are not stable. However, at lower temperatures and pressures, all the systems studied are predicted to be stable. It may be noted that these systems will be stable in the upper atmosphere. It is observed that with four or more water molecules, the microhydrated clusters are formed predominantly over their dimer counterparts.[116] The calculated interaction energy also supports the above statement. Another engaging point noticed is that when a single water molecule is added to the dimers of formic or acetic acid, the most stable conformer is the one with the water molecule incorporated in between the two acid molecules of the dimer. In other words, the presence of a single water molecule can break the carboxylic acid dimer.

3.2.4 Structure

3.2.4.1 Trifluoroacetic Acid (tfa)

The electron withdrawing -CF_3 group makes the removal of proton of tfa easier, compared to formic acid. The minimum energy equilibrium geometry of tfa is given in Figure 3.1(a), with O-H bond length of 0.968Å. Computed geometrical parameters of free tfa in the gas phase are noted to be fairly close to the experimental data. The largest deviation in bond length is predicted for C−F bond, and it is 0.017 Å longer than the reported experimental data when the calculation is carried out without any symmetry restriction (see Table 3.1). It is to be noted that the present calculated O−H bond distance in free tfa at ωB97X-D/aug-cc-pVDZ level is the same as the earlier value calculated applying MP2/6-311++G(2df,2pd)level.[73] Minimum energy equilibrium structures of tfa and hydrated clusters of tfa (tfa.nH_2O, n=1-7) are given in Figure 3.1. Only one equilibrium structure is obtained for the mono-hydrated cluster, and is shown as Figure 3.1(b). Addition of the first solvent water molecule to tfa increases its C=O bond distance by 0.01 Å and O−H bond distance by 0.024 Å. The present calculated value of O-H bond length compares well with the previous reported value.[73] The calculated distance between the transferring H atom and O atom of the neighboring solvent H_2O molecule is 1.713 Å, which is less than that observed in case of formic acid.[107] The present calculated values are very close to previously reported values at B971 and MP2 levels of theory.[72] The C−O bond of tfa is also shortened significantly on addition of a water molecule to tfa. The most favored structure for di-hydrated cluster of tfa is displayed as Figure 3.1(c). The present calculated values of O1-H and H-O3 bond lengths are lesser than the earlier reported MP2 values.[72,73]

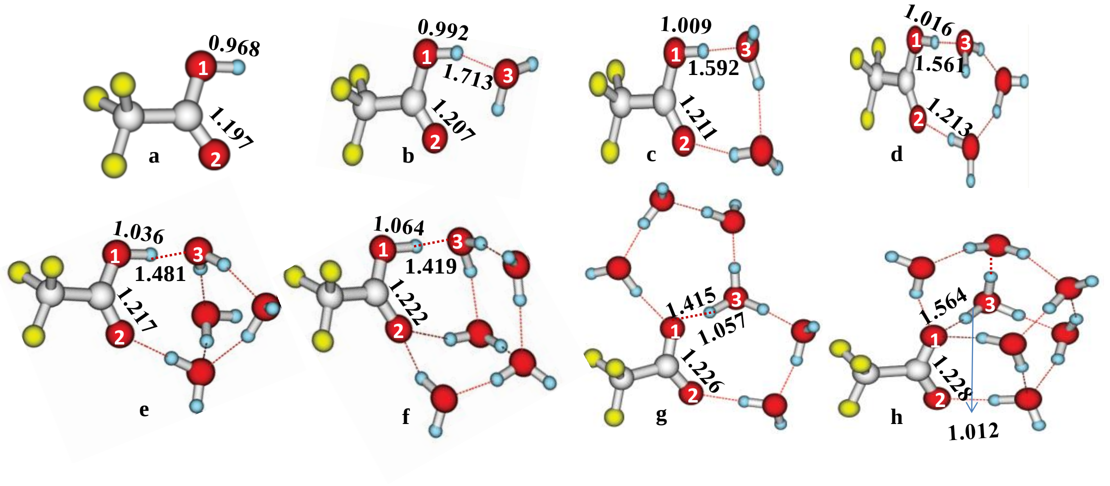

Figure 3.1 Minimum energy equilibrium structures of (a) CF_3COOH; (b) $CF_3COOH.1H_2O$; (c) $CF_3COOH.2H_2O$; (d) $CF_3COOH.3H_2O$; (e) $CF_3COOH.4H_2O$; (f) $CF_3COOH.5H_2O$; (g)

$CF_3COOH.6H_2O$ and (h) $CF_3COOH.7H_2O$ calculated at ωB97X-D/aug-cc-pVDZ level of theory. O1and O2 are hydroxyl and carbonyl oxygen atoms of acid molecule. O3 is the oxygen atom on the water molecule closest to hydroxyl hydrogen atom of acid molecule. Yellow balls represent fluorine, red balls represent oxygen, grey balls represent carbon and blue balls represent hydrogen atoms.

The minimum energy structure of the five equilibrium conformers obtained for tfa.3H_2O is shown in Figure 3.1(d). The three water molecules form a hydrogen bonded closed-ring motif, which is hydrogen bonded to the hydroxyl hydrogen and carbonyl oxygen of the acid molecule. The O-H bond length of the acid molecule increases to 1.016 Å and the H bond distance between the H atom of the acid molecule and O atom of the nearest water molecule is 1.561 Å. For the tetra-hydrate of tfa, tfa.4H_2O, the most stable conformer obtained has hydrogen bonded close ring structure, with hydrogen bonds between the acid molecule and the solvent water molecules as well as between the water molecules (see Figure 3.1(e)).

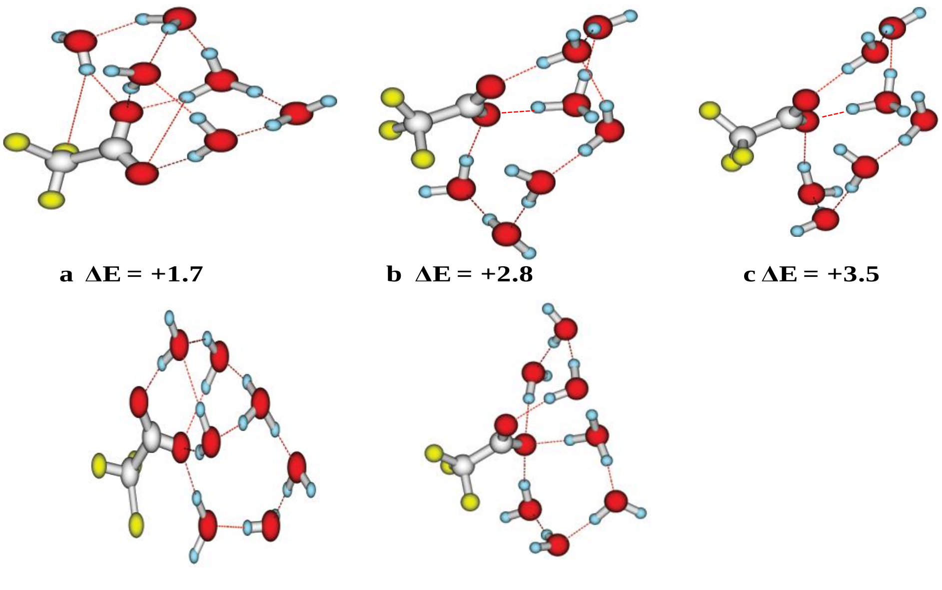

a **ΔE = +1.7** **b** **ΔE = +2.8** **c** **ΔE = +3.5**

d **ΔE = +4.0** **e** **ΔE = +4.6**

Figure 3.2 Higher energy equilibrium structures of (a)$CF_3COOH.6H_2O$ and (b)-(e) $CF_3COOH.7H_2O$ showing contact ion pair formation. Zero point energy corrected relative energy (in kcal/mol) of the conformers with respect to minimum energy conformer of that size cluster is also given. Yellow balls represent fluorine, red balls represent oxygen, grey balls represent carbon and blue balls represent hydrogen atoms.

There is 0.02 Å increase in O-H bond length and 0.08 Å decrease in H-O3 H-bond length, relative to the tfa.3H_2O. Of the eight equilibrium conformers obtained after optimization, the minimum energy structure of penta hydrate of tfa, tfa.5H_2O, is given in Figure 3.1(f), where the O-H and H-O3 H-bond distances are1.064 and 1.419 Å, respectively.

Table 3.3 Selected bond lengths of tfa.nH_2O, n=0-7, calculated at ωB97X-D/aug-cc-pVDZ level of theory. $r_{O1\text{-}H}$, $r_{C=O2}$ and $r_{H\text{-}O3}$ represent hydroxyl O-H and carbonyl C=O bond of the acid molecule and hydrogen bond between the hydroxyl hydrogen of acid molecule and oxygen of the nearest water molecule, respectively.

System	Bond Length (Å)		
	$r_{O1\text{-}H}$	$r_{C=O}$	$r_{H\text{-}O3}$
$CF_3COOH.1H_2O$	0.992	1.207	1.713
$CF_3COOH.2\ H_2O$	1.009	1.211	1.592
$CF_3COOH.3\ H_2O$	1.016	1.213	1.561
$CF_3COOH.4\ H_2O$	1.036	1.217	1.481
$CF_3COOH.5\ H_2O$	1.064	1.222	1.419
$CF_3COOH.6\ H_2O$	1.415	1.226	1.057
$CF_3COOH.7\ H_2O$	1.564	1.228	1.012

As is seen from Figure 3.1(g), the minimum energy equilibrium conformer of tfa.6H_2O shows dissociation of trifluoroacetic acid and formation of contact ion pair. The O-H bond length of the acid molecule increases significantly to 1.415 Å and there is a drastic reduction in the bond distance between the transferring H atom of the acid molecule and the O atom of the nearest water molecule, to 1.057 Å, indicating proton transfer from acid molecule to solvent water molecules. A higher energy equilibrium conformer of tfa.6H_2O containing contact ion pair is given in Figure 3.2(a). In case of tfa.7H_2O also, the most stable conformer shows the dissociation of the acid molecule, the O1-H and H-O3 bond distances being 1.564 and1.012 Å respectively (see Figure 3.1(h)). Higher energy ionized conformers (relative energy < 5 kcal/mol with respect to minimum energy structure) of tfa.7H_2O is given in Figure 3.2(b)-(e).

It is observed that at least six water molecules are needed for ionizing trifluoroacetic acid molecule while seven are needed in case of formic acid molecule. The hydrated clusters of tfa prefer hydrogen bonded close ring geometry. Selected bond distance parameters of tfa.nH_2O, n=0-7 are given in Table 3.3.[117] The calculated rotational constants are comparable to available experimental data (see Table 3.2).

Many higher energy conformers of each size hydrated clusters are obtained for trifluoroacetic acid molecule. The higher energy conformers of each size cluster of tfa and their relative energy with respect to the minimum energy conformer of that size is given in Figure 3.3.

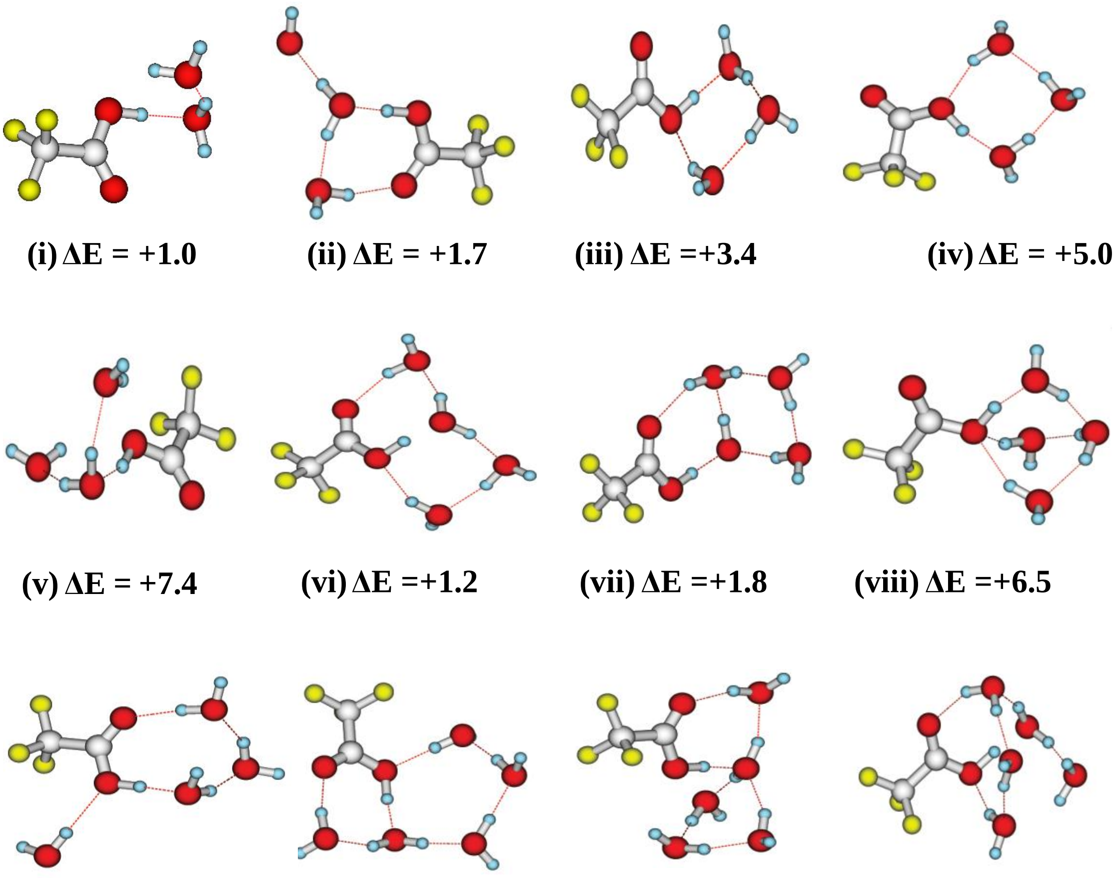

(i) ΔE = +1.0 **(ii) ΔE = +1.7** **(iii) ΔE =+3.4** **(iv) ΔE = +5.0**

(v) ΔE = +7.4 **(vi) ΔE =+1.2** **(vii) ΔE =+1.8** **(viii) ΔE =+6.5**

(ix) ΔE = +7.3 **(x) ΔE =+0.6** **(xi) ΔE =+1.9** **(xii) ΔE =+2.4**

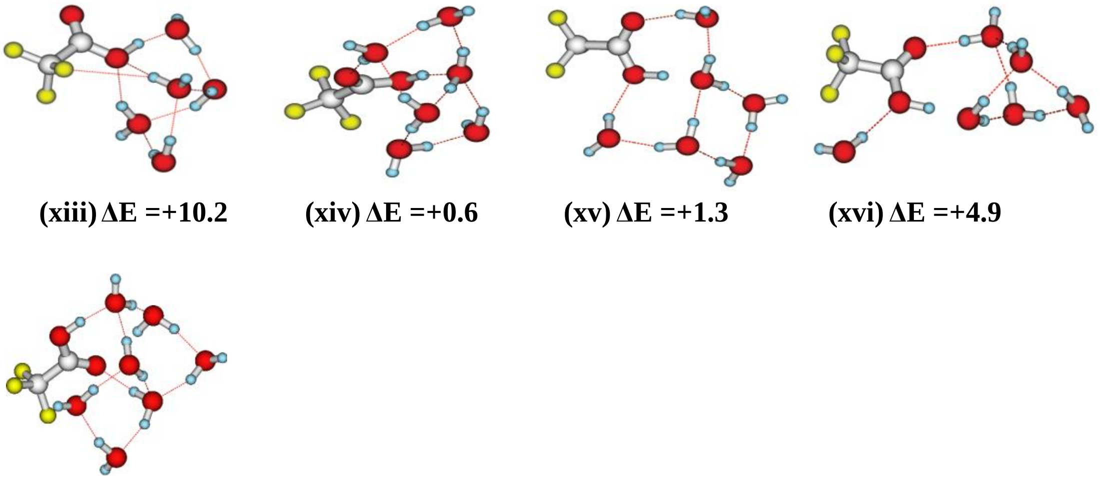

(xiii) ΔE =+10.2 **(xiv) ΔE =+0.6** **(xv) ΔE =+1.3** **(xvi) ΔE =+4.9**

(xvii) ΔE =+3.3

Figure 3.3 Higher energy equilibrium structures of (i)$CF_3COOH.2H_2O$ (ii-v)$CF_3COOH.3H_2O$, (vi-ix) $CF_3COOH.4H_2O$, (x-xiii) $CF_3COOH.5H_2O$, (xiv-xvi) $CF_3COOH.6H_2O$ and (xvii) $CF_3COOH.7H_2O$. Zero point energy corrected relative energy (in kcal/mol) of the conformers with respect to minimum energy conformer of that size cluster is also given. Yellow balls represent fluorine, red balls represent oxygen, grey balls represent carbon and blue balls represent hydrogen atoms.

3.2.4.2 Acetic Acid (acoh)

The +I effect of $-CH_3$ group in acetic acid makes the removal of proton from the acid molecule difficult compared to formic acid. This is reflected in its pKa value (4.75), which is greater than that of formic acid (3.75). Calculated O1-H bond length of acetic acid molecule at ωB97X-D/aug-cc-pVDZ level of theory is 0.967 Å, which is comparable to the reported experimental value of 0.97 Å.[118] C-O and C=O bond lengths determined are 1.352 and 1.207 Å respectively, compared to experimental values of 1.365 and 1.196 Å.[115] The minimum energy conformer of acoh is given in Figure 3.4(a). The values obtained presently are very close to previously reported values at B3LYP/6-311++G(3df,3pd) level of theory.[93] With the addition of a single water molecule, the minimum energy geometry obtained is similar to that of the mono-hydrates of formic and trifluoroacetic acids, as shown in Figure 3.4(b). The O1-H bond length of acoh.$1H_2O$ is 0.985 Å and the H-O3 bond distance is 1.789 Å. Of the four equilibrium conformers determined for acoh.2H_2O, the minimum energy structure has hydrogen bonded closed ring structure as shown in Figure 3.4(c). The O1-H bond length increases to 0.996 Å and H-O3 bond distance decreases to 1.675 Å. It must be noted that initial geometries with hydrogen bonded interactions between water molecules and -CH_3 group of the acid molecule are not considered for the present study as they are not directly relevant to acid dissociation.

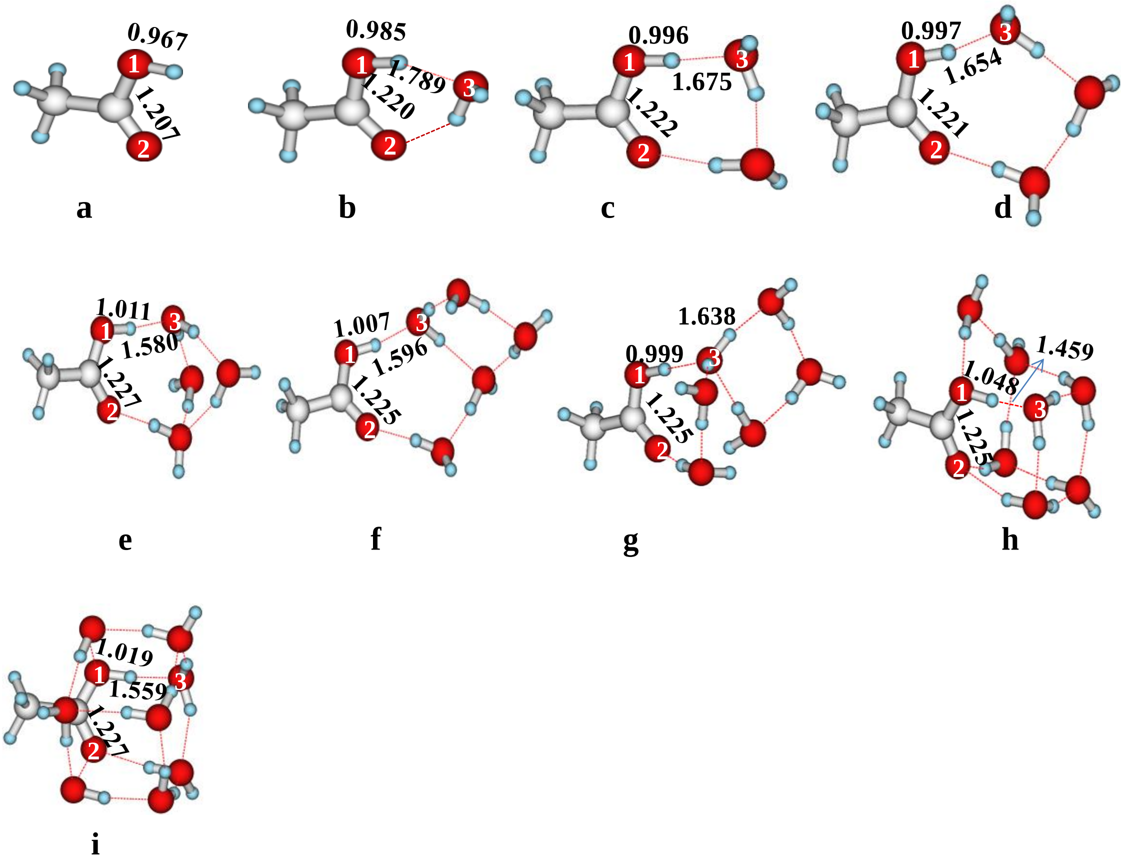

Figure 3.4 Minimum energy equilibrium structures of (a) CH_3COOH; (b) $CH_3COOH.1H_2O$; (c) $CH_3COOH.2H_2O$; (d) $CH_3COOH.3H_2O$; (e) $CH_3COOH.4H_2O$; (f) $CH_3COOH.5H_2O$; (g) $CH_3COOH.6H_2O$ (h) $CH_3COOH.7H_2O$; and (i) $CH_3COOH.8H_2O$. O1and O2 are hydroxyl and carbonyl oxygen atoms of acid molecule. O3 is the oxygen atom on the water molecule closest to hydroxyl hydrogen atom of acid molecule. Red balls represent oxygen, grey balls represent carbon and blue balls represent hydrogen atoms.

Also, optimization of a few such structures of lower hydrates showed that they are higher in energy compared to the other structures. The minimum energy structure, of the seven equilibrium conformers of acoh.3H_2O, has the three water molecules forming hydrogen bonded closed ring motif connected to the hydroxyl hydrogen and carbonyl oxygen of the acid molecule via hydrogen bonds (see Figure 3.4(d)).There is a marginal increase in O1-H bond length when compared to that of di-hydrate and a decrease in H-O3 bond distance. The geometry of the minimum energy conformer of acoh.4H_2O is similar to the tetra-hydrates of formic and trifluoroacetic acid molecules, as shown in Figure 3.4(e), with solute-solvent and solvent-solvent hydrogen bonds forming a closed ring motif. There is an elongation of the O1-H bond length to 1.011 Å and a reduction in H-O3 bond distance. In case of acoh.5H_2O, the minimum energy geometry consists of hydrogen bonded closed ring motif between the acid molecule and three of the water molecules. The remaining two water molecules forms a second hydration shell through inter-water hydrogen bonding as shown in Figure 3.4(f).

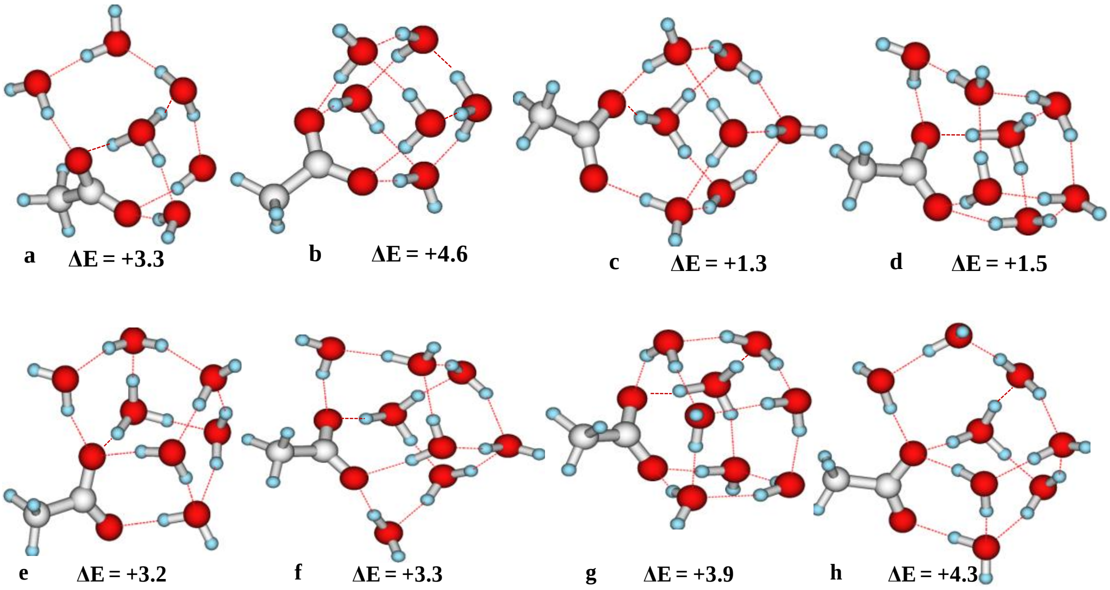

Figure 3.5 Higher energy equilibrium structures of (a)-(b)$CH_3COOH.6H_2O$, (c)-(e) $CH_3COOH.7H_2O$ and (f)-(h) $CH_3COOH.8H_2O$ showing contact ion pair formation. Zero point energy corrected relative energy (in kcal/mol) of the conformers with respect to minimum energy conformer of that size cluster is also given. Red balls represent oxygen, grey balls represent carbon and blue balls represent hydrogen atoms.

For the hexa-hydrate of acetic acid, acoh.6H_2O, though the minimum energy structure has the undissociated acid molecule in it, a few higher energy conformers are obtained which show contact ion pair formation. The minimum energy structure has O1-H and H-O3 bond distances of 0.999 and 1.638 Å respectively, as shown in Figure 3.4(g). Higher energy conformers of acoh.6H_2O (relative energy <5kcal/mol with respect to minimum energy structure) are given in Figure 3.5(a) and (b). The un-ionized minimum energy conformer of the hexa-hydrate is more stable than the most stable conformer, containing charge separated ion-pair formation, by 3.3 kcal/mol. Twenty minimum energy structures are predicted in the case of the hepta-hydrated cluster, acoh·7H_2O; out of which eight structures show formation of a charge-separated ion pair and hydronium ion, H_3O^+. The most stable conformer has a cage-like structure (Figure 3.4(h)), and it is more stable than the most stable ionized structure, shown in Figure 3.5(c), by 1.3 kcal/mol. The O1-H and H-O3 bond distances are 1.048 and 1.459 Å respectively. With eight water molecules, the minimum energy structure of acoh.8H_2O has an un-ionized cage like structure, consisting of four and five hydrogen bonded rings of water molecules. O1-H bond length of 1.019 Å and H-O3 bond distance of 1.559 Å indicate that the acid molecule still remains undissociated. However, higher energy conformers with charge separated ion-pairs are observed for the octa-hydrate (see Figure 3.5(f)-(h)).

A general trend observed is that hydrogen bonded closed ring structures are favored in case of smaller hydrates while cage-like motifs are prominent in higher hydrates of the acid molecule. The shaping of the structures of the hydrated clusters involves a delicate balance in the formation of solute-solvent and solvent-solvent hydrogen bonding. With seven water molecules, twenty equilibrium geometries were obtained for acoh.7H_2O, after optimization, while for octa-hydrate, it is twenty four. With nine water molecules, number of possible guess geometries becomes very large.

Applying the present strategy for determining the global minima is not suitable for larger size clusters. As the risk of missing out important structures increases with increase in size of the hydrated cluster, interaction of acetic acid molecule up to eight water molecules are only considered at present. The formation of ion pair does not occur in the most stable structure, even in case of acoh.8H_2O, though elongation of the O1-H bond is observed for the hydrates of acetic acid molecule. Selected bond distance parameters of acoh.nH_2O, n=0-8 are given in Table 3.4.[119]

Table 3.4. Selected bond lengths of $CH_3COOH.nH_2O$, n=0-8, calculated at ωB97X-D/aug-cc-pVDZ level of theory. r_{O1-H}, $r_{C=O2}$ and r_{H-O3} represent hydroxyl O-H and carbonyl C=O bond of the acid molecule and hydrogen bond between the hydroxyl hydrogen of acid molecule and oxygen of the nearest water molecule, respectively.

System	Bond distance (Å)		
	r_{O1-H}	$r_{C=O2}$	r_{H-O3}
CH_3COOH	0.967	1.207	-
$CH_3COOH.H_2O$	0.985	1.220	1.789
$CH_3COOH.2H_2O$	0.996	1.222	1.675
$CH_3COOH.3H_2O$	0.997	1.221	1.654
$CH_3COOH.4H_2O$	1.011	1.227	1.580
$CH_3COOH.5H_2O$	1.007	1.225	1.596
$CH_3COOH.6H_2O$	0.999	1.225	1.638
$CH_3COOH.7H_2O$	1.048	1.225	1.459
$CH_3COOH.8H_2O$	1.019	1.227	1.559

Experimental microwave rotational constants A, B and C of free acetic acid and its mono and di-hydrates have been reported previously.[74,120] The calculated rotational constants, applying rigid rotor approximation, are comparable with the available experimental data. For free acetic acid molecule the calculated rotational constants, A, B and C are 11380, 9462 and 5339 MHz respectively and they differ from the experimental values by +45,-17 and +14 MHz respectively. In case of acoh.1H_2O (with calculated A, B and C values of 11064, 2639 and 2169 MHz) the A, B and C rotational constants differ by +4, +55 and +42 MHz respectively. For acoh.$2H_2O$, A, B and C values observed experimentally are 4445, 1618 and 1200 MHz respectively. The variations in the calculated rotational constants, A, B and C, from the experimental values are +84, +28 and +23 MHz respectively.

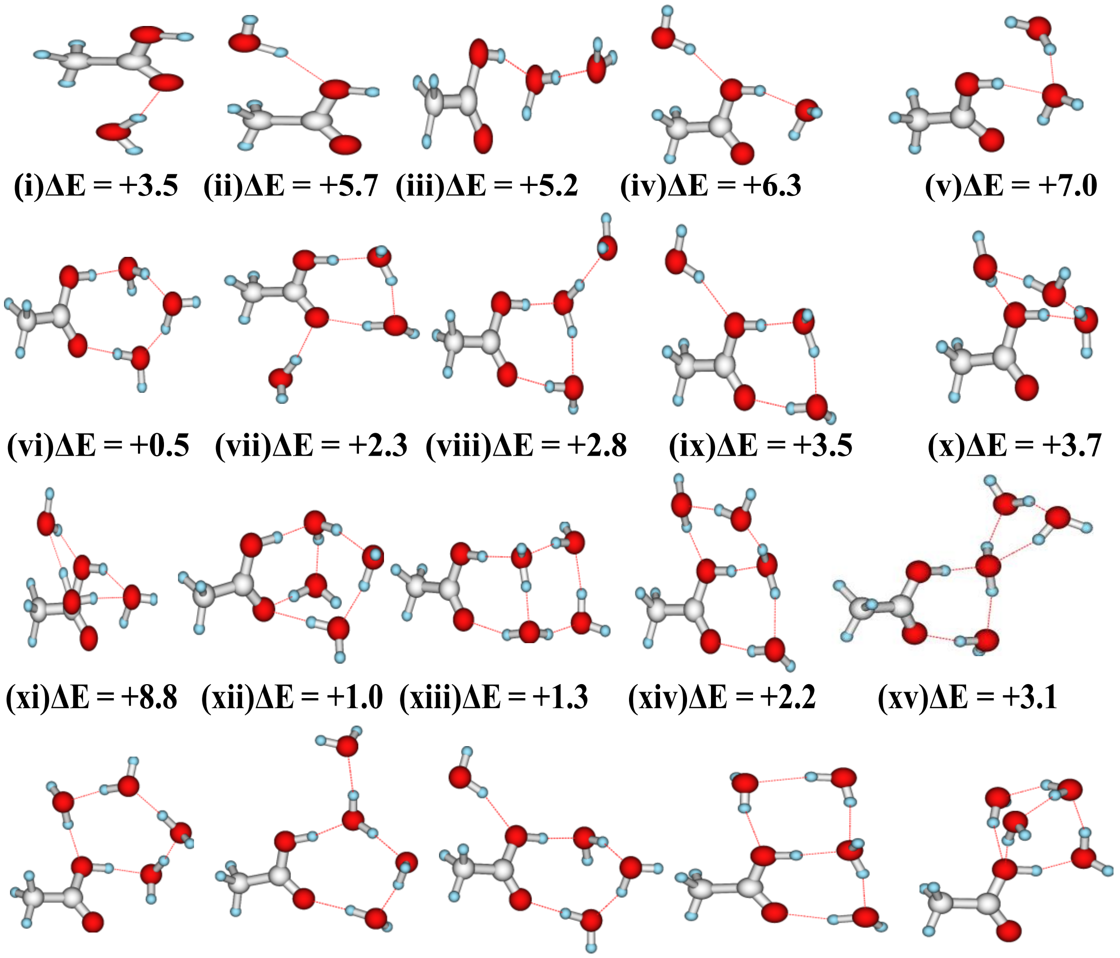

(i)ΔE = +3.5 (ii)ΔE = +5.7 (iii)ΔE = +5.2 (iv)ΔE = +6.3 (v)ΔE = +7.0

(vi)ΔE = +0.5 (vii)ΔE = +2.3 (viii)ΔE = +2.8 (ix)ΔE = +3.5 (x)ΔE = +3.7

(xi)ΔE = +8.8 (xii)ΔE = +1.0 (xiii)ΔE = +1.3 (xiv)ΔE = +2.2 (xv)ΔE = +3.1

(xvi)ΔE = +4.0 (xvii)ΔE = +4.3 (xviii)ΔE = +4.8 (xix)ΔE = +7.5 (xx)ΔE = +7.6

Figure 3.6 Higher energy equilibrium structures of (i-ii) $CH_3COOH.1H_2O$, (iii-v) $CH_3COOH.2H_2O$, (vi-xi)$CH_3COOH.3H_2O$ and(xii-xx) $CH_3COOH.4H_2O$. Zero point energy corrected relative energy (in kcal/mol) of the conformers with respect to minimum energy conformer of that size cluster is also given. Red balls represent oxygen, grey balls represent carbon and blue balls represent hydrogen atoms.

Similar to hydrated clusters of trifluoroacetic acid, several higher energy conformers for each size cluster are also obtained for acetic acid-water systems. The higher energy conformers of mono, di, tri and tetra-hydrated clusters and the relative energy of these conformers with respect to the minimum energy conformer of that size are given in Figure 3.6.

Fifteen higher energy conformers, along with their relative energy with respect to the minimum energy conformer, obtained for penta-hydrate of acetic acid are shown in Figure 3.7. Three of these conformers are less than 0.5 kcal/mol higher in energy than the most stable conformer, implying that the penta-hydrate can exist in those conformations as well.

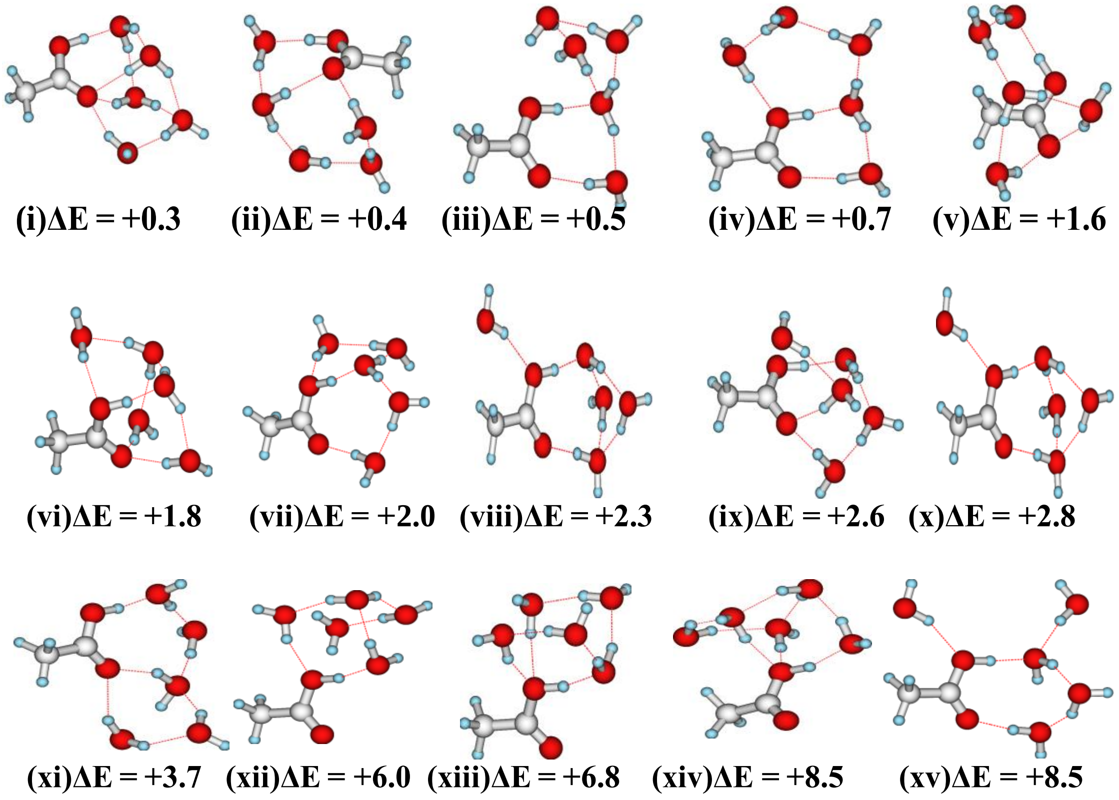
(i)ΔE = +0.3 **(ii)ΔE = +0.4** **(iii)ΔE = +0.5** **(iv)ΔE = +0.7** **(v)ΔE = +1.6**

(vi)ΔE = +1.8 **(vii)ΔE = +2.0** **(viii)ΔE = +2.3** **(ix)ΔE = +2.6** **(x)ΔE = +2.8**

(xi)ΔE = +3.7 **(xii)ΔE = +6.0** **(xiii)ΔE = +6.8** **(xiv)ΔE = +8.5** **(xv)ΔE = +8.5**

Figure 3.7(i-xv) Higher energy equilibrium structures of $CH_3COOH.5H_2O$. Zero point energy corrected relative energy (in kcal/mol) of the conformers with respect to minimum energy conformer of that size cluster is also given. Red balls represent oxygen, grey balls represent carbon and blue balls represent hydrogen atoms.

Seventeen of the higher energy equilibrium conformers of hexa-hydrate of acetic acid, not shown previously, are given in Figure 3.8. Structures shown in Figure 3.8 (i)-(iii) are very close in energy to the minimum energy conformer and hence are possible structures for the hexa-hydrated cluster of acetic acid. Three ionized conformers of the hexa-hydrate (see Figure 3.8 (xii),(xv),(xvii)-(xix)) are observed to be very high in energy compared to the minimum energy conformer.

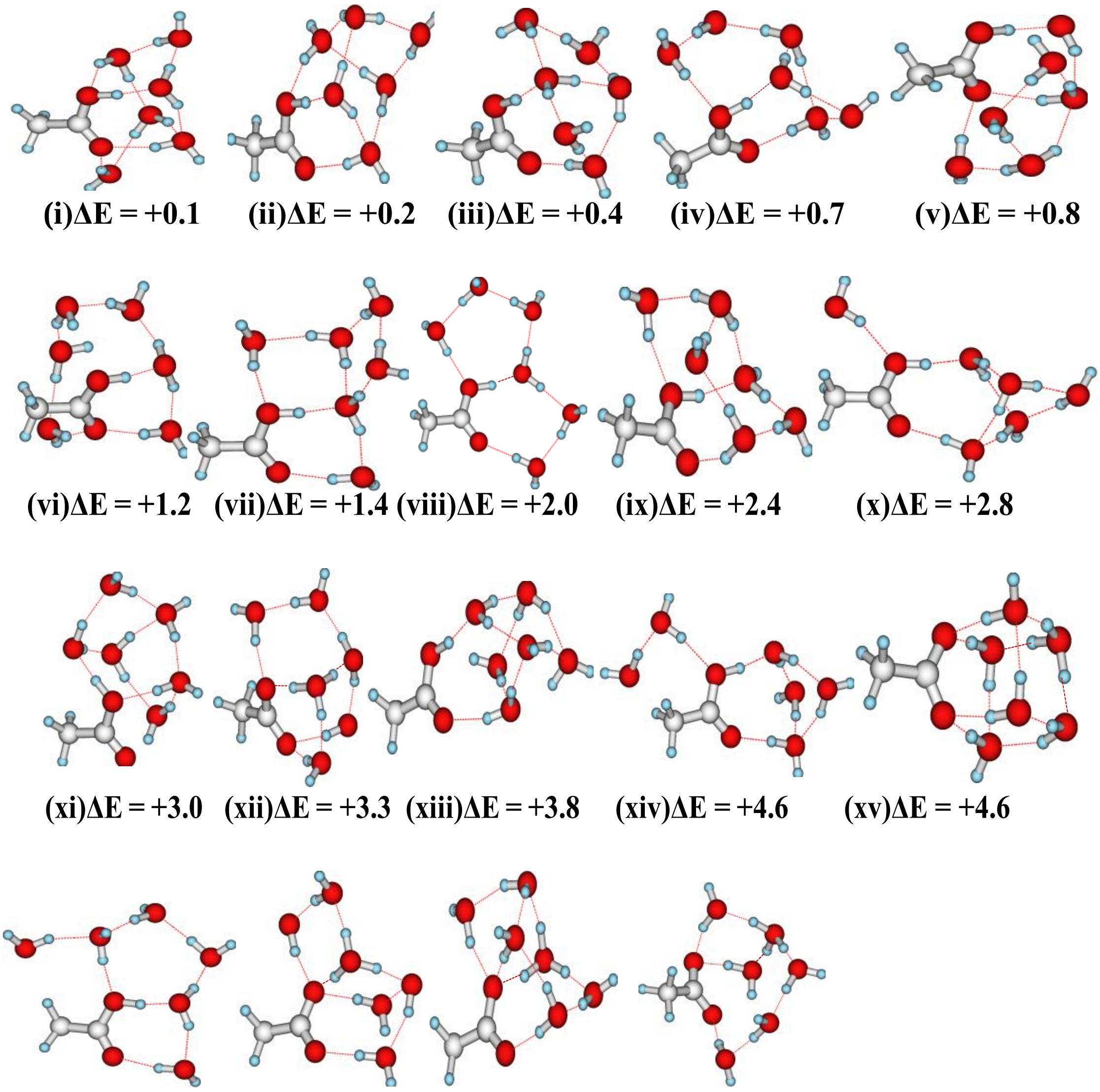

(i)ΔE = +0.1 **(ii)ΔE = +0.2** **(iii)ΔE = +0.4** **(iv)ΔE = +0.7** **(v)ΔE = +0.8**

(vi)ΔE = +1.2 **(vii)ΔE = +1.4** **(viii)ΔE = +2.0** **(ix)ΔE = +2.4** **(x)ΔE = +2.8**

(xi)ΔE = +3.0 **(xii)ΔE = +3.3** **(xiii)ΔE = +3.8** **(xiv)ΔE = +4.6** **(xv)ΔE = +4.6**

(xvi)ΔE = +5.4 **(xvii)ΔE = +5.8** **(xviii)ΔE = +6.5** **(xix)ΔE = +9.5**

Figure 3.8(i-xix) Higher energy equilibrium structures of $CH_3COOH.6H_2O$. Zero point energy corrected relative energy (in kcal/mol) of the conformers with respect to minimum energy conformer of that size cluster is also given. Red balls represent oxygen, grey balls represent carbon and blue balls represent hydrogen atoms.

Sixteen higher energy conformers of hepta-hydrate of acetic acid, other than those mentioned previously, are also provided in Figure 3.9. The structure shown in Figure 3.9(i) is also a possible conformation of the hepta-hydrate, its energy being higher than the minimum energy conformer by just 0.4 kcal/mol. Five conformers of the hepta-hydrate (see Figure 3.9 (x),(xii)-(xv)) show formation of ion pair. However their relative energy with respect to minimum energy conformer is > 5.0 kcal/mol and hence the probability of the hepta-hydrate to be in those conformations is very low.

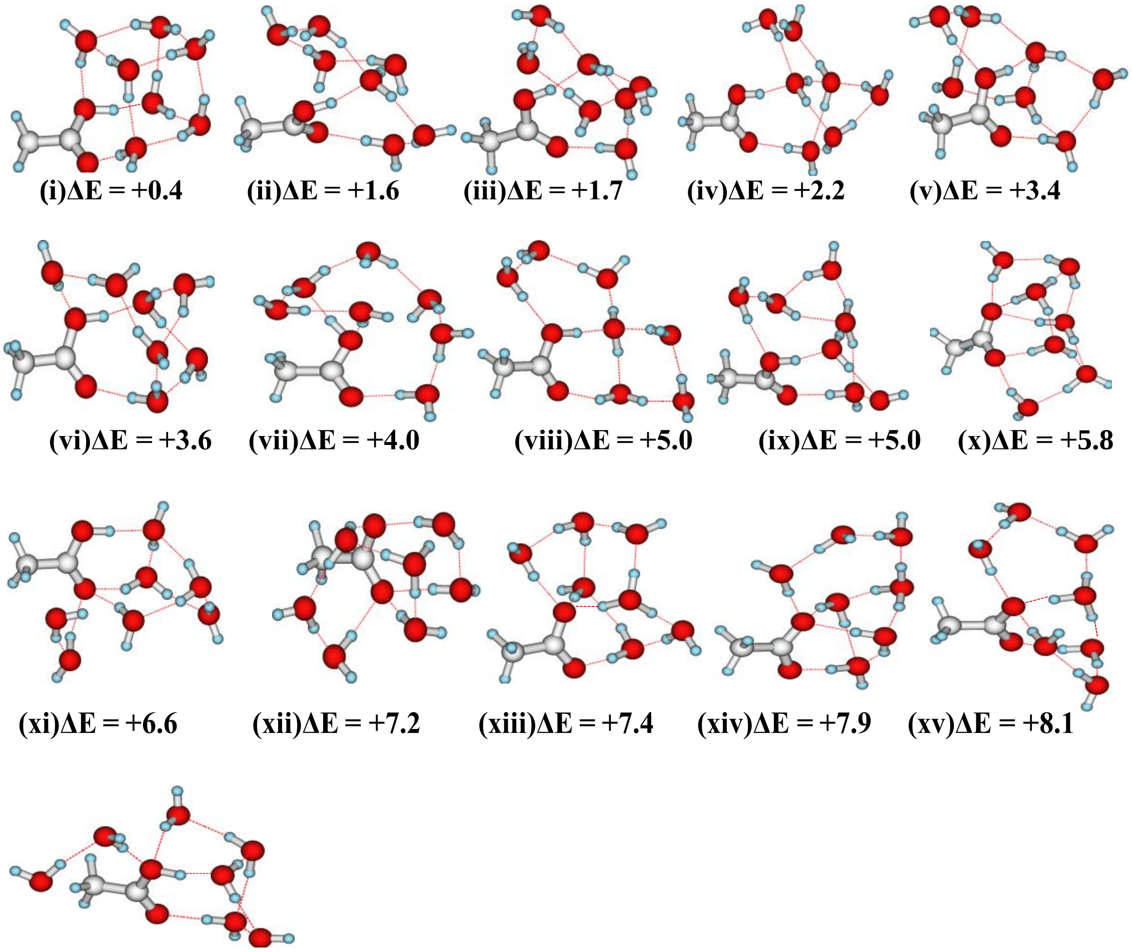

(i)$\Delta E = +0.4$ **(ii)**$\Delta E = +1.6$ **(iii)**$\Delta E = +1.7$ **(iv)**$\Delta E = +2.2$ **(v)**$\Delta E = +3.4$

(vi)$\Delta E = +3.6$ **(vii)**$\Delta E = +4.0$ **(viii)**$\Delta E = +5.0$ **(ix)**$\Delta E = +5.0$ **(x)**$\Delta E = +5.8$

(xi)$\Delta E = +6.6$ **(xii)**$\Delta E = +7.2$ **(xiii)**$\Delta E = +7.4$ **(xiv)**$\Delta E = +7.9$ **(xv)**$\Delta E = +8.1$

(xvi)$\Delta E = +8.9$

Figure 3.9 (i-xvi) Higher energy equilibrium structures of $CH_3COOH.7H_2O$. Zero point energy corrected relative energy (in kcal/mol) of the conformers with respect to minimum energy conformer of that size cluster is also given. Red balls represent oxygen, grey balls represent carbon and blue balls represent hydrogen atoms.

Other than the structures given previously, twenty conformers obtained for the octa-hydrate of acetic acid is given in Figure 3.10. All of them have relative energy >2.0 kcal/mol than the minimum energy conformer. It is observed that open chain conformations are not preferred. As can be seen from Figure 3.10, conformers showing formation of contact ion pair have relative energy 5.0 kcal/mol or higher compared to the most stable conformer. Hence it can be concluded that even in the presence of eight water molecules, acetic acid does not dissociate to form acetate anion and hydrated proton.

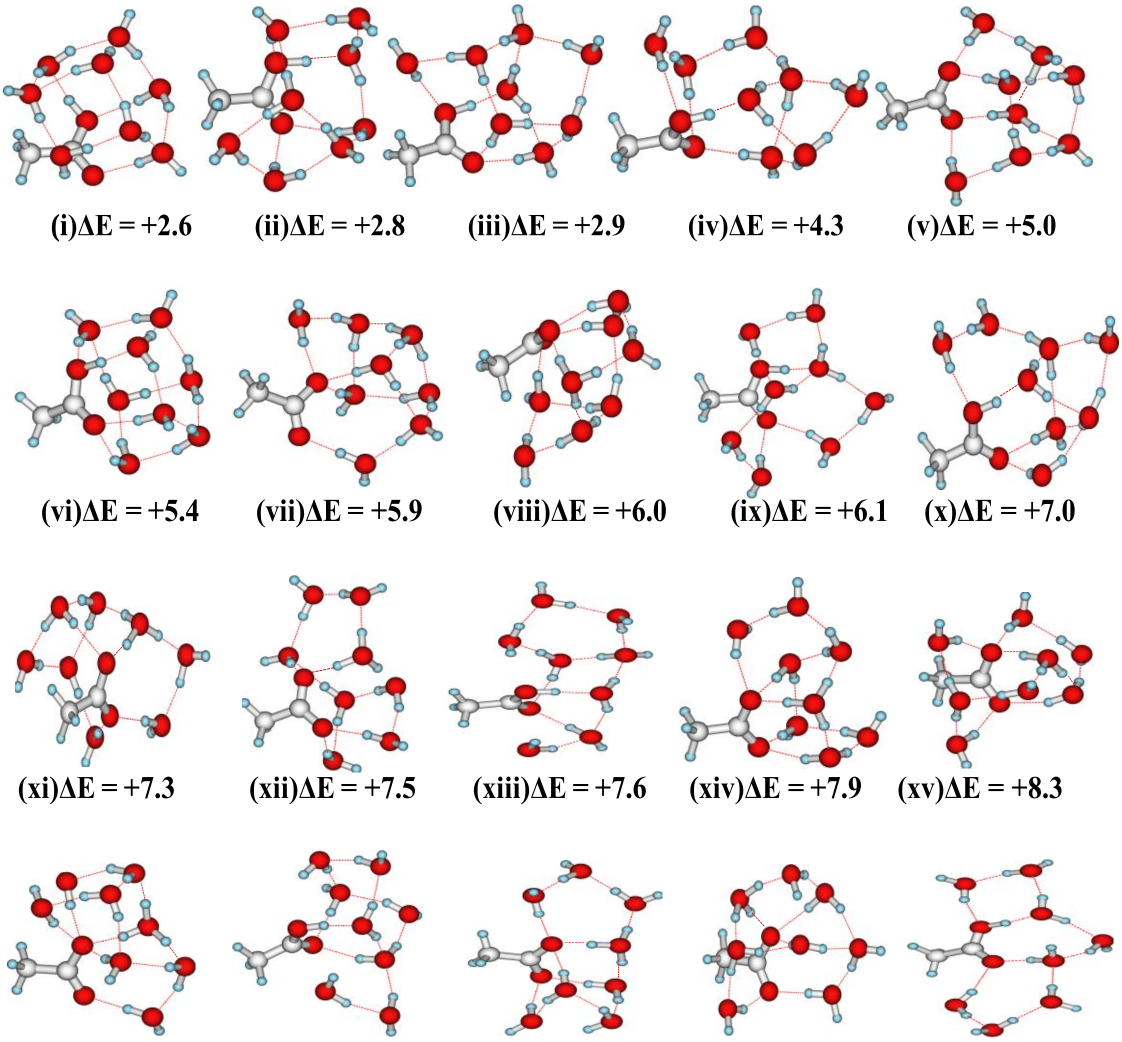

(i)ΔE = +2.6 **(ii)ΔE = +2.8** **(iii)ΔE = +2.9** **(iv)ΔE = +4.3** **(v)ΔE = +5.0**

(vi)ΔE = +5.4 **(vii)ΔE = +5.9** **(viii)ΔE = +6.0** **(ix)ΔE = +6.1** **(x)ΔE = +7.0**

(xi)ΔE = +7.3 **(xii)ΔE = +7.5** **(xiii)ΔE = +7.6** **(xiv)ΔE = +7.9** **(xv)ΔE = +8.3**

(xvi)ΔE = +9.3 **(xvii)ΔE = +9.3** **(xviii)ΔE = +9.4** **(xix)ΔE = +9.5** **(xx)ΔE = +12.8**

Figure 3.10 (i-xx) Higher energy equilibrium structures of $CH_3COOH.8H_2O$. Zero point energy corrected relative energy (in kcal/mol) of the conformers with respect to minimum energy conformer of that size cluster is also given. Red balls represent oxygen, grey balls represent carbon and blue balls represent hydrogen atoms.

3.2.4.3 Benzoic Acid (bza)

The pKa value of benzoic acid is 4.20, higher than that of formic acid. The +M effect of the phenyl ring makes the removal of proton from benzoic acid molecule difficult. At ωB97X-D/aug-cc-pVDZ level of theory, three equilibrium geometries are obtained for bza: a syn-conformer and two anti-conformers. The syn conformer has the COOH group and the phenyl ring in the same plane, with the O-H bond eclipsing the C=O bond, as shown in Figure 3.11 (a). It is more stable than the anti-conformers by 5.8 kcal/mol. The two anti-conformers are degenerate, with one having the COOH and phenyl ring in the same plane while the other having 22° angle between the two. However, neither gas phase electron diffraction[121] nor microwave studies[122] could detect the anti-conformer. The relative energy of the anti-conformer, calculated at MP2/6-311+G(d,p)[121] and B3LYP/cc-pVTZ[122] levels of theory, is more than 6 kcal/mol higher than the syn conformer. The calculated O1-H bond length of the minimum energy conformer of bza is 0.966 Å and C=O bond length is 1.210 Å, at present level of theory, which is comparable to the O1-H and C=O bond lengths at MP2/6-311+G(d,p)(0.968 and 1.213 Å respectively).

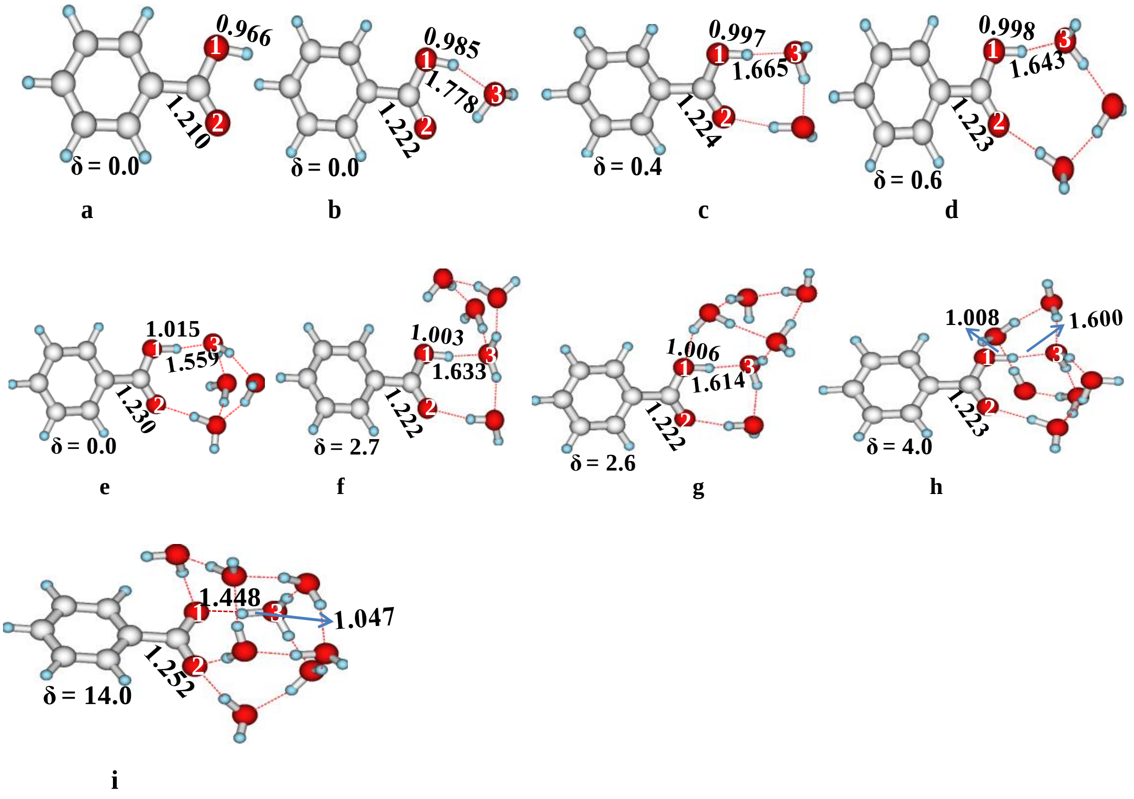

Figure 3.11 Minimum energy equilibrium structures of (a) C_6H_5COOH; (b) $C_6H_5COOH.1H_2O$; (c) $C_6H_5COOH.2H_2O$; (d) $C_6H_5COOH.3H_2O$; (e) $C_6H_5COOH.4H_2O$; (f) $C_6H_5COOH.5H_2O$; (g) $C_6H_5COOH.6H_2O$ (h) $C_6H_5COOH.7H_2O$; and (i) $C_6H_5COOH.8H_2O$. O1and O2 are hydroxyl and

carbonyl oxygen atoms of acid molecule. O3 is the oxygen atom on the water molecule closest to hydroxyl hydrogen atom of acid molecule. Red balls represent oxygen, grey balls represent carbon and blue balls represent hydrogen atoms.

Of the three equilibrium conformer obtained for the mono-hydrate of benzoic acid, bza.1H_2O, the minimum energy conformer is similar to the mono-hydrates of previously studied acid molecules, with the oxygen of the water molecule hydrogen bonded to the hydroxyl hydrogen of the acid molecule (see Figure 3.11 (b)). The O1-H bond length increases to 0.985 Å. The C=O2 and H-O3 bond distances are 1.222 and 1.778 Å respectively. The rotational constants determined using B3LYP/6-311++G(d,p) level of theory is previously reported to be closer to the experimentally determined values, when compared to those obtained from M06-2X or MP2 calculations.[99] The O1-H and H-O3 bond distances calculated at B3LYP, M06-2X & MP2 levels of theory are 0.990, 0.980 & 0.990 and 1.800, 1.780 & 1.760 Å respectively, which are close to the values obtained at present level of theory. A hydrogen bonded closed ring structure is the most stable conformer obtained for bza.2H_2O. As shown in Figure 3.11(c), the di-hydrate has O1-H bond length of 0.997 Å and H-O3 bond length of 1.665 Å. Of the five equilibrium conformers of the tri-hydrate, the minimum energy structure has the water molecules forming a hydrogen bonded closed ring connecting the carbonyl oxygen and hydroxyl hydrogen atom of the acid molecule, as seen in Figure 3.11 (d). The O1-H and H-O3 bond lengths of bza.3H_2O are 0.998 and 1.223 Å respectively. The structural motif of bza.4H_2O is similar to that predicted in the previous cases. It has a pyramid-like structure, with the four water molecules forming the base and the planar acid molecule forming the apex of the pyramid, as shown in Figure 3.11 (e). The O1-H bond length increases to 1.015 Å while there is a reduction in H-O3 bond distance to 1.559 Å. The minimum energy conformer, of the twelve equilibrium geometries of bza.5H_2O, consists of the water molecules forming two hydrogen bonded closed rings, one of which is H bonded to the acid molecule as shown in Figure 3.11 (f). The O1-H and H-O3 bond distances of the minimum energy conformer of bza.5H_2O are 1.003 and 1.633 Å respectively. With six water molecules, though the most stable conformer remains un-ionized, a few higher energy structures are obtained, containing contact ion pairs. However, the most stable ionized conformer is higher in energy than the minimum energy conformer by 5.4 kcal/mol. The minimum energy hexa-hydrated cluster of benzoic acid molecule has the water molecules forming many hydrogen bonded closed rings, connecting the acid molecule as well as each other (see Figure 3.11 (g)). The O1-H and H-O3 bond lengths are 1.006 and 1.614 Å respectively. The hepta-hydrate of benzoic acid molecule has a structural motif resembling that of bza.4H_2O (see Figure 3.11 (h)), with O1-H and H-O3 bond distances of 1.008 and 1.600 Å respectively. Out of the 11 equilibrium geometries determined, a higher energy hepta-hydrate shows the formation of charge-separated ion pair. This ionized structure (see Figure 3.12 (a)) is higher in energy than the minimum energy un-ionized conformer by 1.5 kcal/mol.

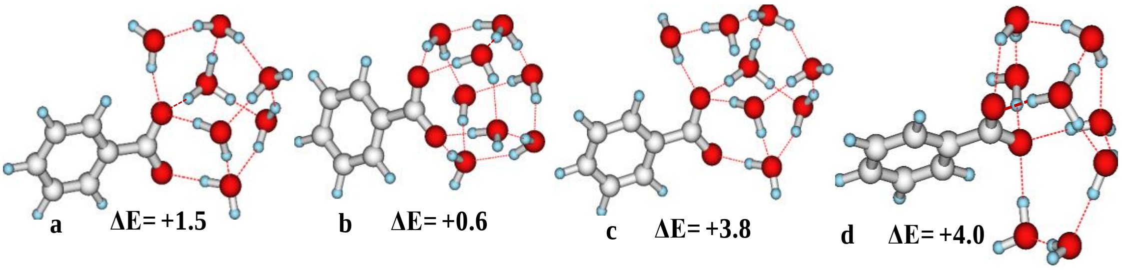

Figure 3.12 Higher energy equilibrium structures of (a)$C_6H_5COOH.7H_2O$ and (b)-(d) $C_6H_5COOH.8H_2O$ showing contact ion pair formation. Zero point energy corrected relative energy (in kcal/mol) of the conformers with respect to minimum energy conformer of that size cluster is also given. Red balls represent oxygen, grey balls represent carbon and blue balls represent hydrogen atoms.

The proton transfer from the acid molecule to the solvent water molecules occur with the addition of eight water molecules, as shown in Figure 3.11(i). The minimum energy conformer of bza.8H_2O has O1-H and H-O3 bond distances of 1.448 and 1.047 Å respectively, indicating that the acid molecule has dissociated and the proton now resides with the solvent water molecules. A few higher energy conformers obtained, also containing the dissociated acid molecule, are given in Figure 3.12 (b)-(d). Thus, a minimum of eight water molecules are needed to dissociate benzoic acid molecule, which is one water molecule greater than that required for formic acid molecule. The geometrical parameters of bza.nH_2O, n=0-8 are given in Table 3.5.[123]

Table 3.5 Selected bond lengths of $C_6H_5COOH.nH_2O$, n=0-8, calculated at ωB97X-D/aug-cc-pVDZ level of theory. r_{O1-H}, $r_{C=O2}$ and r_{H-O3} represent hydroxyl O-H and carbonyl C=O bond of the acid molecule and hydrogen bond between the hydroxyl hydrogen of acid molecule and oxygen of the nearest water molecule, respectively.

System	Bond distance (Å)		
	r_{O1-H}	$r_{C=O2}$	r_{H-O3}
C_6H_5COOH	0.966	1.210	-
$C_6H_5COOH.1H_2O$	0.985	1.222	1.778
$C_6H_5COOH.2H_2O$	0.997	1.224	1.665
$C_6H_5COOH.3H_2O$	0.998	1.223	1.643
$C_6H_5COOH.4H_2O$	1.015	1.230	1.559
$C_6H_5COOH.5H_2O$	1.003	1.222	1.633
$C_6H_5COOH.6H_2O$	1.006	1.222	1.614
$C_6H_5COOH.7H_2O$	1.008	1.223	1.600
$C_6H_5COOH.8H_2O$	1.448	1.252	1.047

The microwave rotational constants of benzoic acid and its mono-hydrate have been reported.[99,122] The reported rotational constants A, B and C for free benzoic acid molecule are 3872, 1227 and 933 MHz and that for bza.1H_2O are 3838, 652 and 558 MHZ, respectively. The calculated rotational constants, A, B and C of free benzoic acid molecule differ from the experimental values by +12, -2 and -2 MHZ while that of bza.1H_2O differ by +8, +5 and +4 MHZ respectively. Calculated microwave data are comparable to the experimental data.

Based on the many initial guess structures chosen, several other higher energy equilibrium structures are obtained for benzoic acid and its hydrated clusters. The higher energy conformers of benzoic acid molecule and mono, di, tri and tetra-hydrated benzoic acid molecules, along with their relative energy with respect to minimum energy conformer of that size cluster, is given in Figure 3.13.

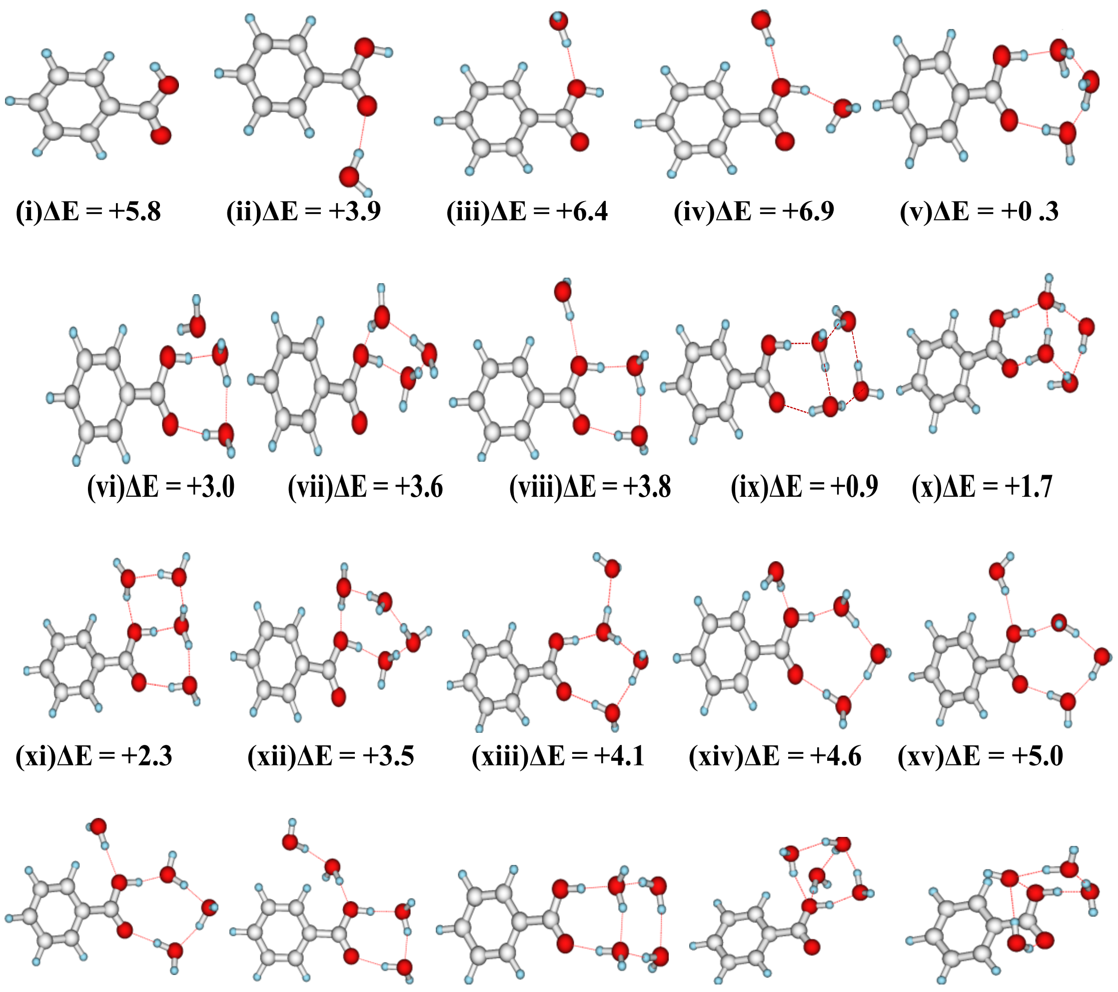

(i)$\Delta E = +5.8$ **(ii)$\Delta E = +3.9$** **(iii)$\Delta E = +6.4$** **(iv)$\Delta E = +6.9$** **(v)$\Delta E = +0 .3$**

(vi)$\Delta E = +3.0$ **(vii)$\Delta E = +3.6$** **(viii)$\Delta E = +3.8$** **(ix)$\Delta E = +0.9$** **(x)$\Delta E = +1.7$**

(xi)$\Delta E = +2.3$ **(xii)$\Delta E = +3.5$** **(xiii)$\Delta E = +4.1$** **(xiv)$\Delta E = +4.6$** **(xv)$\Delta E = +5.0$**

(xvi)$\Delta E = +5.3$ **(xvii)$\Delta E = +5.8$** **(xviii)$\Delta E = +6.2$** **(xix)$\Delta E = +6.5$** **(xx)$\Delta E = +7.0$**

Figure 3.13 Higher energy equilibrium structures of (i)C_6H_5COOH, (ii-iii) $C_6H_5COOH.1H_2O$, (iv) $C_6H_5COOH.2H_2O$, (v-viii) $C_6H_5COOH.3H_2O$ and (ix-xx) $C_6H_5COOH.4H_2O$. Zero point energy corrected relative energy (in kcal/mol) of the conformers with respect to minimum energy conformer of that size cluster is also given. Red balls represent oxygen, grey balls represent carbon and blue balls represent hydrogen atoms.

It can be seen that open chain conformers are not preferred and the water molecules in the hydrated clusters tend to remain near the carboxyl group of the acid molecule. The conformer shown in Figure 3.13(v) is very similar to the minimum energy conformer of the tri-hydrated benzoic acid and is just 0.3 kcal/mol higher in energy. The difference between the two structures is in the orientation of the closed ring motif formed by the three water molecules: while in the minimum energy conformer the ring is planar to the benzene ring, in the higher energy conformer it is perpendicular to the benzene ring. All other structures are found to be much higher in energy than their minimum energy counterparts. Eleven higher energy equilibrium structures are obtained for the penta-hydrate of benzoic acid (see Figure 3.14). Most of the conformers are observed to contain hydrogen bonded closed ring motifs formed by two or three water molecules.

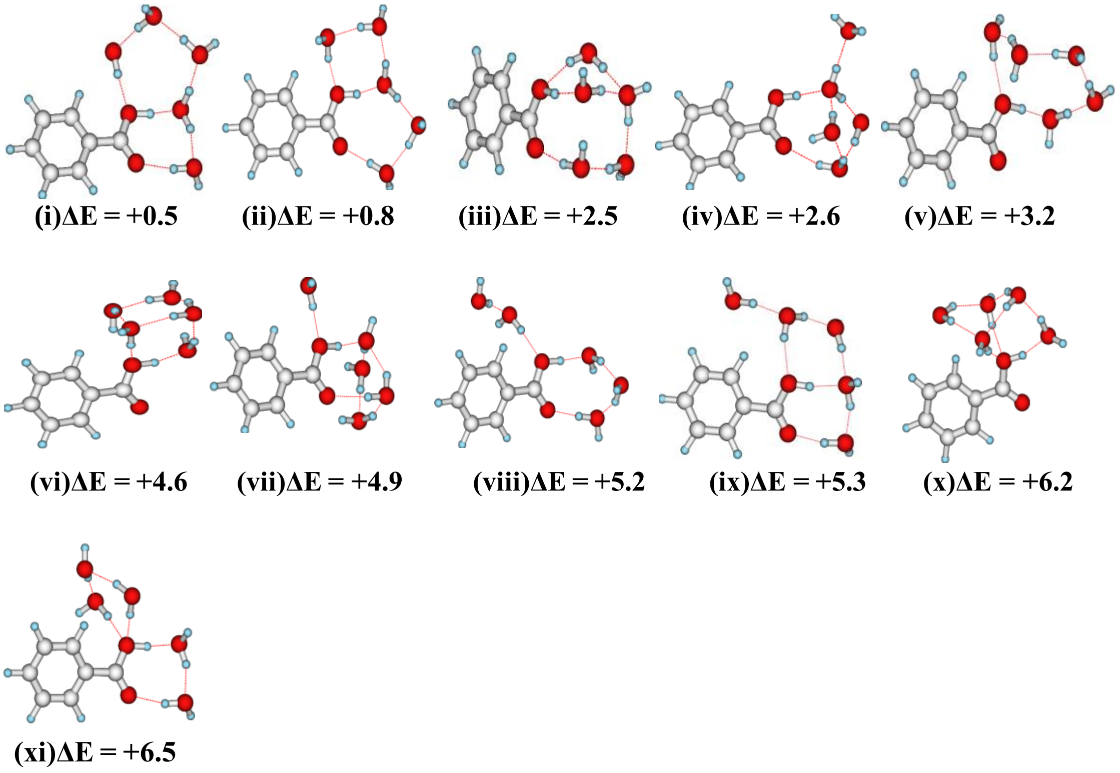

(i)ΔE = +0.5 **(ii)ΔE = +0.8** **(iii)ΔE = +2.5** **(iv)ΔE = +2.6** **(v)ΔE = +3.2**

(vi)ΔE = +4.6 **(vii)ΔE = +4.9** **(viii)ΔE = +5.2** **(ix)ΔE = +5.3** **(x)ΔE = +6.2**

(xi)ΔE = +6.5

Figure 3.14 (i-xi) Higher energy equilibrium structures of $C_6H_5COOH.5H_2O$. Zero point energy corrected relative energy (in kcal/mol) of the conformers with respect to minimum energy conformer of that size cluster is also given. Red balls represent oxygen, grey balls represent carbon and blue balls represent hydrogen atoms.

Of the twenty higher energy equilibrium structures obtained for the hexa-hydrated cluster, none showed the formation of contact ion-pair. As in previous cases, all the structures are observed to contain H-bonded closed ring motifs (see Figure 3.15). The structure shown in Figure 3.15(i) is a possible conformation of the hexa-hydrated cluster, being only 0.2 kcal/mol higher in energy than the minimum energy conformer.

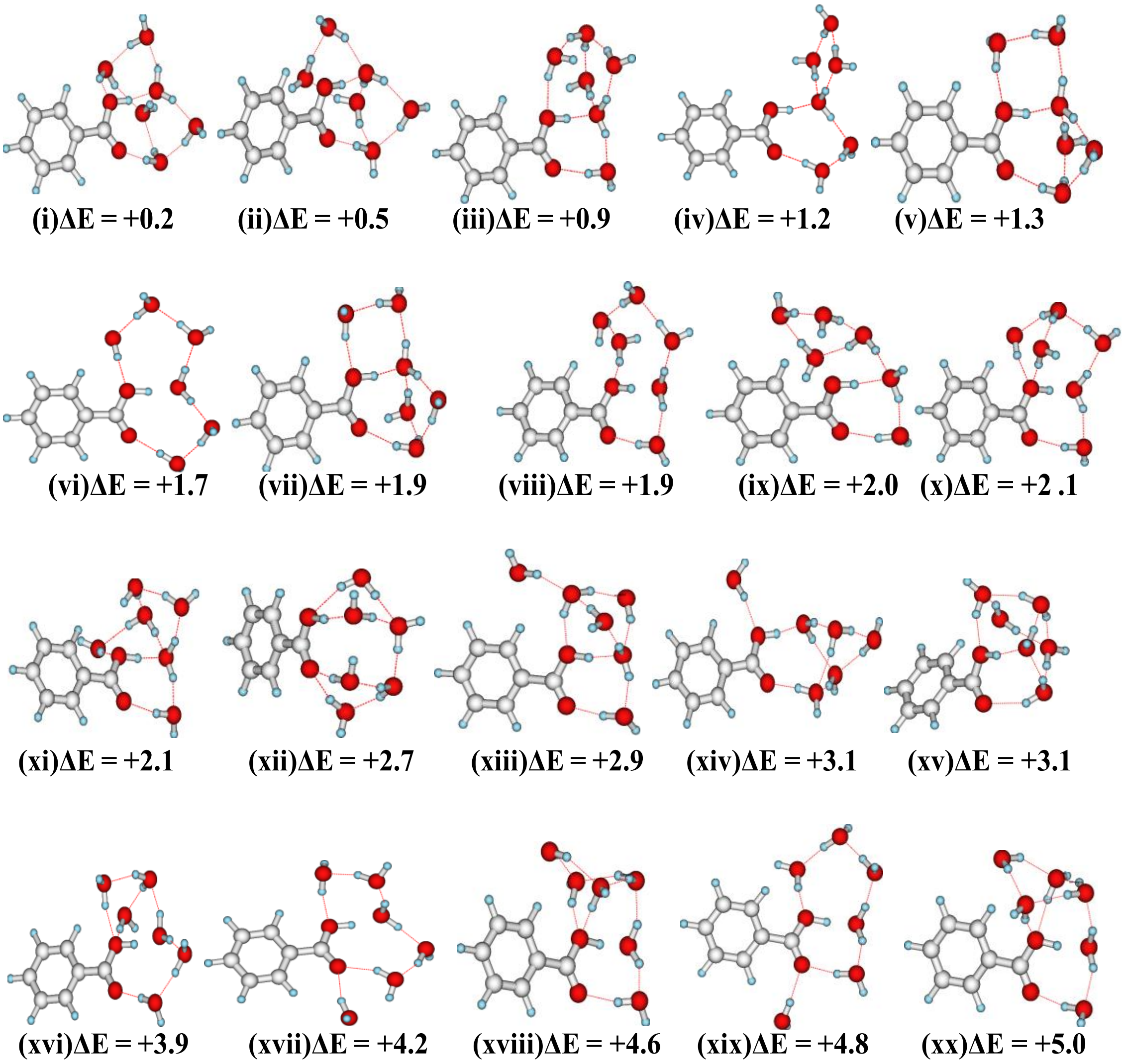
(i)ΔE = +0.2 **(ii)ΔE = +0.5** **(iii)ΔE = +0.9** **(iv)ΔE = +1.2** **(v)ΔE = +1.3**

(vi)ΔE = +1.7 **(vii)ΔE = +1.9** **(viii)ΔE = +1.9** **(ix)ΔE = +2.0** **(x)ΔE = +2 .1**

(xi)ΔE = +2.1 **(xii)ΔE = +2.7** **(xiii)ΔE = +2.9** **(xiv)ΔE = +3.1** **(xv)ΔE = +3.1**

(xvi)ΔE = +3.9 **(xvii)ΔE = +4.2** **(xviii)ΔE = +4.6** **(xix)ΔE = +4.8** **(xx)ΔE = +5.0**

Figure 3.15 (i-xx) Higher energy equilibrium structures of $C_6H_5COOH.6H_2O$. Zero point energy corrected relative energy (in kcal/mol) of the conformers with respect to minimum energy conformer of that size cluster is also given. Red balls represent oxygen, grey balls represent carbon and blue balls represent hydrogen atoms.

Nine other higher energy conformers of hepta-hydrated cluster of benzoic acid, which do not show formation of contact ion-pair, are shown in Figure 3.16. Interestingly none of these structures show the cage-like motif of hydrogen bonded network of water molecules, observed in case of acetic acid and trifluoroacetic acid.

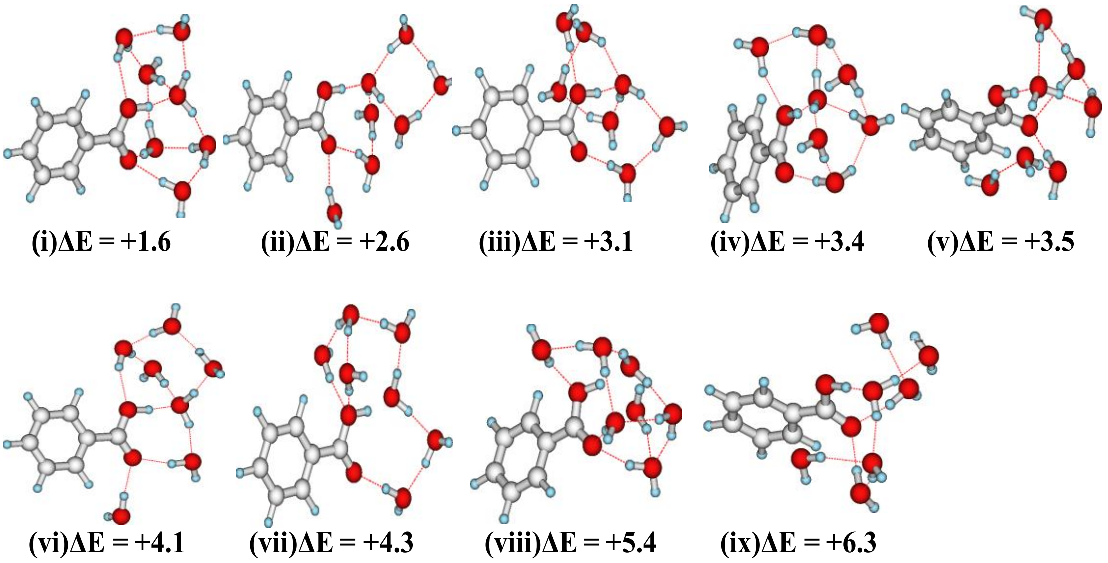

(i)$\Delta E = +1.6$ (ii)$\Delta E = +2.6$ (iii)$\Delta E = +3.1$ (iv)$\Delta E = +3.4$ (v)$\Delta E = +3.5$

(vi)$\Delta E = +4.1$ (vii)$\Delta E = +4.3$ (viii)$\Delta E = +5.4$ (ix)$\Delta E = +6.3$

Figure 3.16 (i-ix) Higher energy equilibrium structures of $C_6H_5COOH.7H_2O$. Zero point energy corrected relative energy (in kcal/mol) of the conformers with respect to minimum energy conformer of that size cluster is also given. Red balls represent oxygen, grey balls represent carbon and blue balls represent hydrogen atoms.

The higher energy conformations of the octa-hydrated cluster are shown in Figure 3.17. Another possible conformation of the octa-hydrate of benzoic acid is shown in Figure 3.17(i), which is just 0.3 kcal/mol less stable than the most stable conformer. It is observed that few of the higher energy conformers also show contact ion-pair formation. The proton in all the cases remain within the first shell of hydration, i.e., there is direct contact between the benzoate group and the hydrated proton.

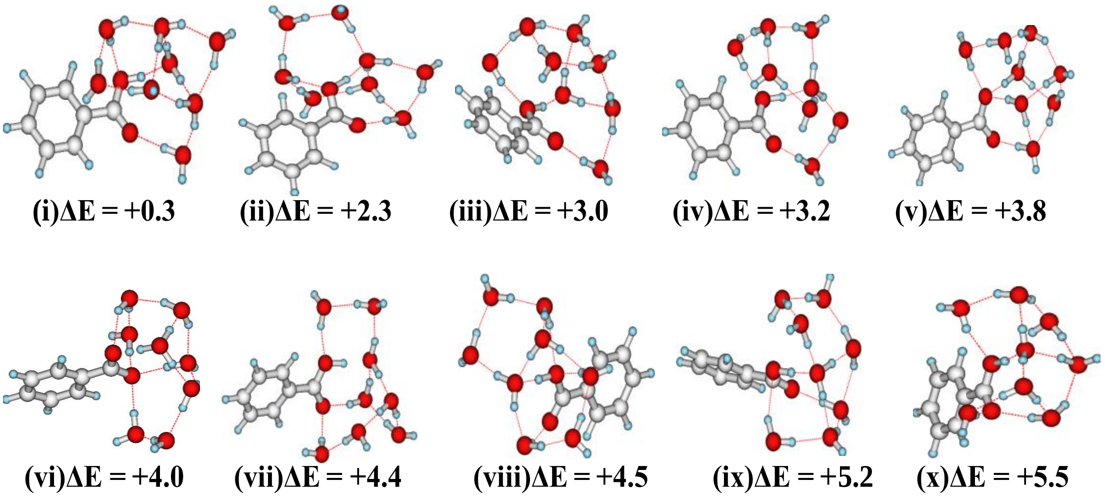

(i)$\Delta E = +0.3$ (ii)$\Delta E = +2.3$ (iii)$\Delta E = +3.0$ (iv)$\Delta E = +3.2$ (v)$\Delta E = +3.8$

(vi)$\Delta E = +4.0$ (vii)$\Delta E = +4.4$ (viii)$\Delta E = +4.5$ (ix)$\Delta E = +5.2$ (x)$\Delta E = +5.5$

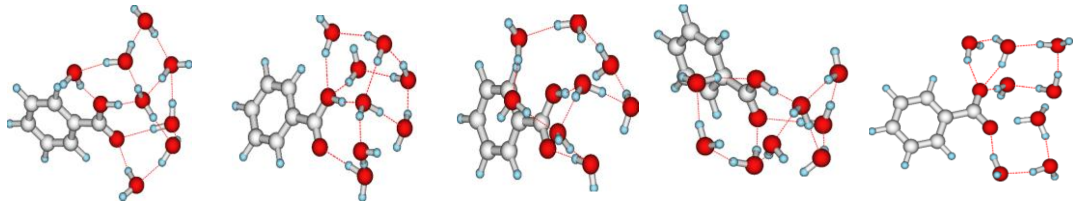

(xi)ΔE = +5.7 (xii)ΔE = +5.7 (xiii)ΔE = +6.4 (xiv)ΔE = +6.4 (xv)ΔE = +6.5

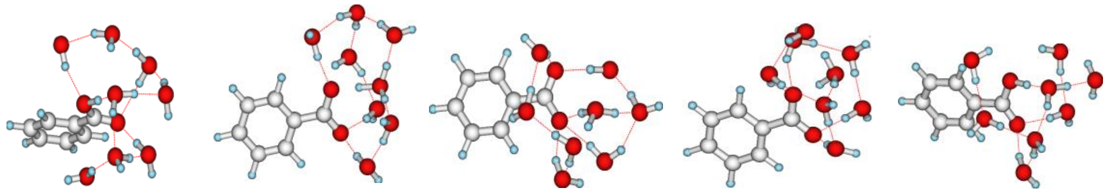

(xvi)ΔE = +6.7 (xvii)ΔE = +8.0 (xviii)ΔE = +8.4 (xix)ΔE = +8.5 (xx)ΔE = +9.5

Figure 3.17 (i-xx) Higher energy equilibrium structures of $C_6H_5COOH.8H_2O$. Zero point energy corrected relative energy (in kcal/mol) of the conformers with respect to minimum energy conformer of that size cluster is also given. Red balls represent oxygen, grey balls represent carbon and blue balls represent hydrogen atoms.

3.2.4.4 Oxalic Acid (oxa)

The simplest dicarboxylic acid, oxalic acid, has first pKa value of 1.25 and second pKa value of 3.81. Six equilibrium conformers are obtained for free oxalic acid (oxa) molecule. Three of the conformers have both the hydroxyl bonds on the same side of the C-C bond (cis) while other three have them on the opposite side (trans). The most stable structure is a planar trans conformer with both the hydroxyl bonds facing inward, as shown in Figure 3.18(a) and having O(H)-C-C-O(H) dihedral angle (δ) of 180°. This is consistent with the gas phase electron diffraction and IR study[124,125]. The gas phase electron diffraction study gives the C-C, C=O, C-O and O-H bond lengths to be 1.548, 1.208, 1.339 and 1.056 Å respectively[124], while the calculated bond lengths, at ωB97X-D/aug-cc-pVDZ level of theory are: 1.542, 1.205, 1.320 and 0.974 Å respectively. There is an excellent agreement for all the bond lengths except the O-H bond. It is under estimated by 0.082 Å at the present level of theory. A previous study at B3LYP/6-311++G(d,p) also shows this geometry to be the minimum energy conformer of free oxalic acid, with the O-H bond lengths being 0.975 Å.[100] The C-C, C=O, C-O and O-H bond lengths at MP2/6-311++G(3df,3pd) level of theory are 1.536, 1.207, 1.322 and 0.973 Å respectively while those at MP2/aug-cc-pVTZ are 1.527, 1.206, 1.319 and 0.974 Å respectively.[103] The minimum energy conformer is 2.7 kcal/mol lower in energy than the next stable conformer, which has a trans geometry, with one hydroxyl group facing outward and the other facing inward. The stability of the minimum energy conformer is justifiable as there are two intra-molecular hydrogen bonding interactions possible in this conformer, while the other conformers have one or none. The minimum energy conformer of mono-hydrate of oxalic acid, oxa.1H_2O, as shown in Figure 3.18(b), has the water molecule hydrogen bonded to one of the hydroxyl hydrogen atoms. The acid molecule is planar and there is an increase in O1-H bond length to 0.996 Å. The H-Oa bond length is 1.662 Å while there is only a marginal increase in the O2-H bond length, to 0.978 Å. These are comparable to the previously reported O1-H, O2-H and H-Oa bond lengths of 0.998, 0.979 and 1.669 Å respectively at B3LYP/6-311++G(d,p) level of theory.[100] The minimum energy conformer of di-hydrated oxalic acid molecule, oxa.2H_2O, has a hydrogen bonded closed ring planar conformation, as shown in Figure 3.18(c). It is observed that the O1-H bond length further increases to 1.004 Å but the O2-H bond length remains unchanged on addition of the second solvent water molecule. With three water molecules, the most stable geometry of oxa.3H_2O also forms a hydrogen bonded closed ring, planar structure (see Figure 3.18(d)), having O1-H and O2-H bond lengths as 1.009 and 0.979 Å respectively. It is seen that up to three water molecules, the minimum energy conformers have water molecules forming a closed hydrogen bonded network.

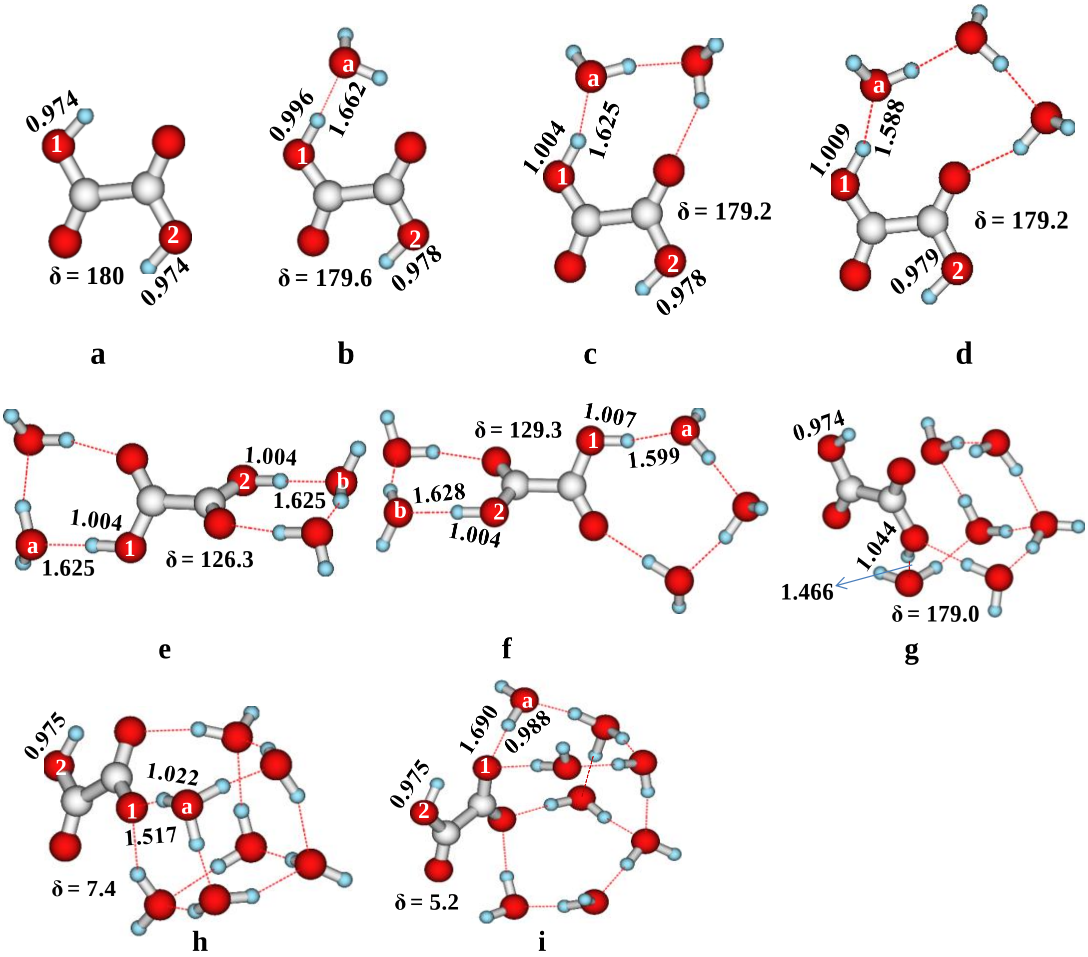

Figure 3.18 Minimum energy equilibrium structures of (a) $(COOH)_2$; (b) $(COOH)_2.1H_2O$; (c) $(COOH)_2.2H_2O$; (d) $(COOH)_2.3H_2O$; (e) $(COOH)_2.4H_2O$; (f) $(COOH)_2.5H_2O$; (g) $(COOH)_2.6H_2O$ (h) $(COOH)_2.7H_2O$; and (i) $(COOH)_2.8H_2O$. O1and O2 are hydroxyl oxygen atoms of acid molecule. Oa and Ob are the oxygen atoms on the water molecules closest to hydroxyl hydrogen atoms of acid molecule. Red balls represent oxygen, grey balls represent carbon and blue balls represent hydrogen atoms.

However, with four water molecules, the most stable conformer of oxa.$4H_2O$ is the one in which two water molecules form hydrogen bonded closed ring motif on one side of the acid molecule, while the other two water molecules form similar motif on the other side, giving rise to a symmetrical structure, as given in Figure 3.18(e). The planarity of the acid molecule is seen to be lost and the calculated O1-C-C-O2 dihedral angle is 126.3°. The bond length of O1-H and O2-H bonds is 1.004 Å while the distance of hydrogen bond between the dissociating protons and solvent water molecules (H-Oa and H-Ob) is 1.625 Å. This conformer is the most stable one and is more stable than the next stable conformer by 1.7 kcal/mol, where all the four water molecules form hydrogen bonded closed ring geometry on one side of the molecule. Out of the many equilibrium structures obtained for oxa.5H_2O, the minimum energy structure (see Figure 3.18(f)) has an un-ionized acid molecule, with three water molecules forming hydrogen bonded closed ring on one side and the two remaining water molecules forming a closed ring motif on the other side of the acid molecule. Calculated O1-H and O2-H bonds are 1.007 and 1.004 Å respectively, indicating that the proton transfer from acid molecule to water molecules has not occurred even after addition of five solvent water molecules. Calculated O1-C-C-O2 dihedral angle is 129.3°. An equilibrium geometry is obtained for the penta-hydrate, that is higher in energy than the structure shown in Figure 3.18(f) by only 0.4 kcal/mol. This structure has all the five water molecules forming closed hydrogen bonded network in one side of the acid molecule as shown in Figure 3.19(a). This conformer depicts the dissociation of one of the O-H bonds of the acid molecule and the formation of contact ion pair. The O1-H and H-Oa bond lengths are calculated as 1.418 and 1.051 Å respectively and the acid molecule remains planar. Since this is lower than the thermal energy, at room temperature, there is a possibility of dissociation of oxalic acid in the presence of five water molecules. It must be noted, however that hydrated oxalic acid systems are not stable at room temperature and are stable only at low temperature (~ 150 K or lower). Hence, the minimum number of water molecules needed for dissociating oxalic acid molecule cannot be five.

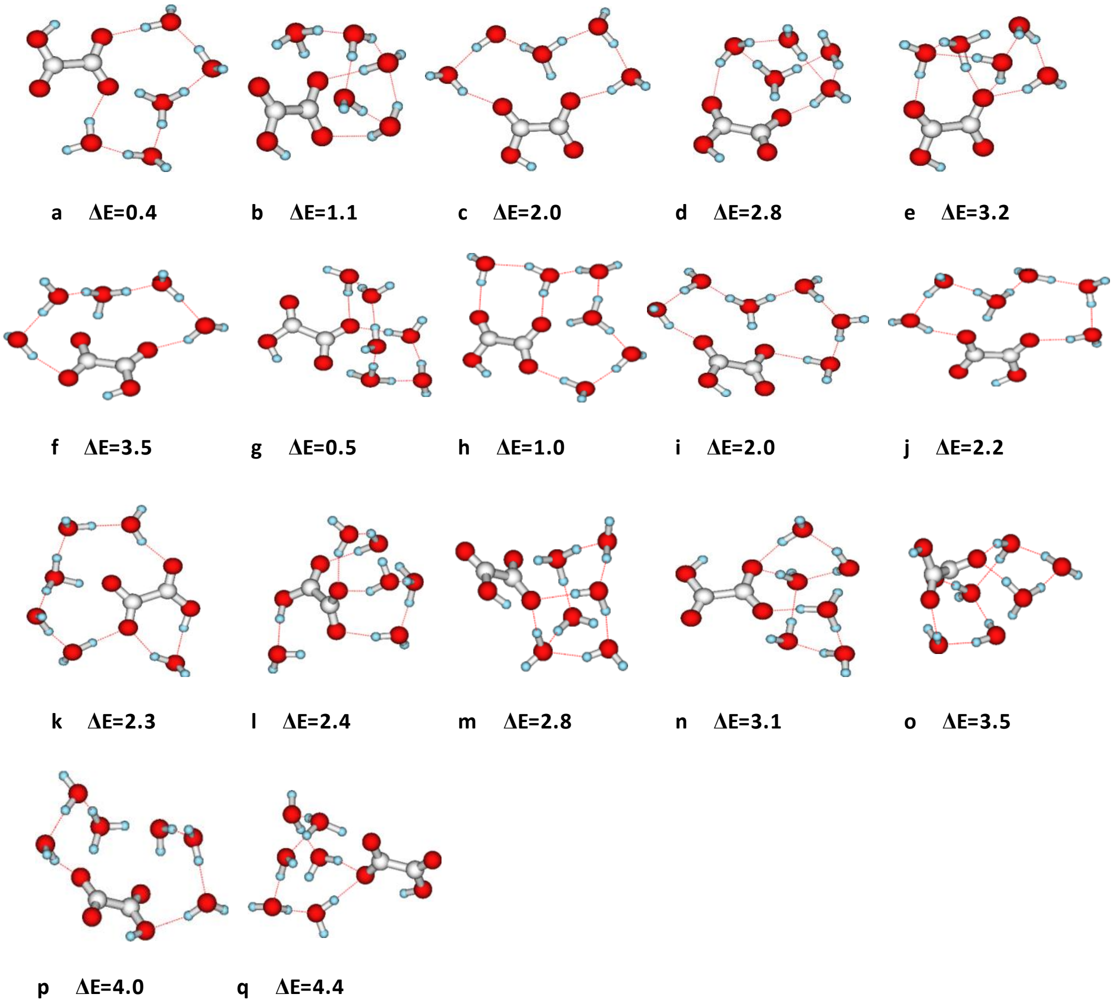

a ΔE=0.4 b ΔE=1.1 c ΔE=2.0 d ΔE=2.8 e ΔE=3.2

f ΔE=3.5 g ΔE=0.5 h ΔE=1.0 i ΔE=2.0 j ΔE=2.2

k ΔE=2.3 l ΔE=2.4 m ΔE=2.8 n ΔE=3.1 o ΔE=3.5

p ΔE=4.0 q ΔE=4.4

Figure 3.19 Higher energy equilibrium structures of (a)-(f) $(COOH)_2.5H_2O$ and (g)-(q) $(COOH)_2.6H_2O$ showing contact ion pair formation. Zero point energy corrected relative energy (in kcal/mol) of the conformers with respect to minimum energy conformer of that size cluster is also given. Red balls represent oxygen, grey balls represent carbon and blue balls represent hydrogen atoms.

The hexa-hydrate of oxalic acid molecule, oxa.$6H_2O$, gives an un-ionized conformer as the most stable geometry; very different from that reported by Tao et al.[100] The calculated most stable structure, as shown in Figure 3.18(g), has a hydrogen bonded network of the six water molecules connected to one of the hydroxyl hydrogen atoms of the acid molecule. The O1-H and O2-H bond lengths are 1.044 and 0.974 Å respectively, with the planarity of the acid molecule intact. However, another conformer having relative energy 0.5 kcal/mol higher than the minimum energy conformer is also predicted for the hexa-hydrate, which shows the formation of charge separated ion pair, as shown in Figure 3.189(g). The bond distances O1-H and H-Oa in this higher energy conformer are 1.443 and 1.047 Å respectively. In this structure, solvent water molecules form hydrogen bonded cluster which is connected to one side of the acid molecule through hydrogen bonds with hydroxyl hydrogen and carbonyl oxygen atoms. Contact ion-pair formation is also noted in some other higher energy conformers, which are given in Figure 3.19(h)-(q).

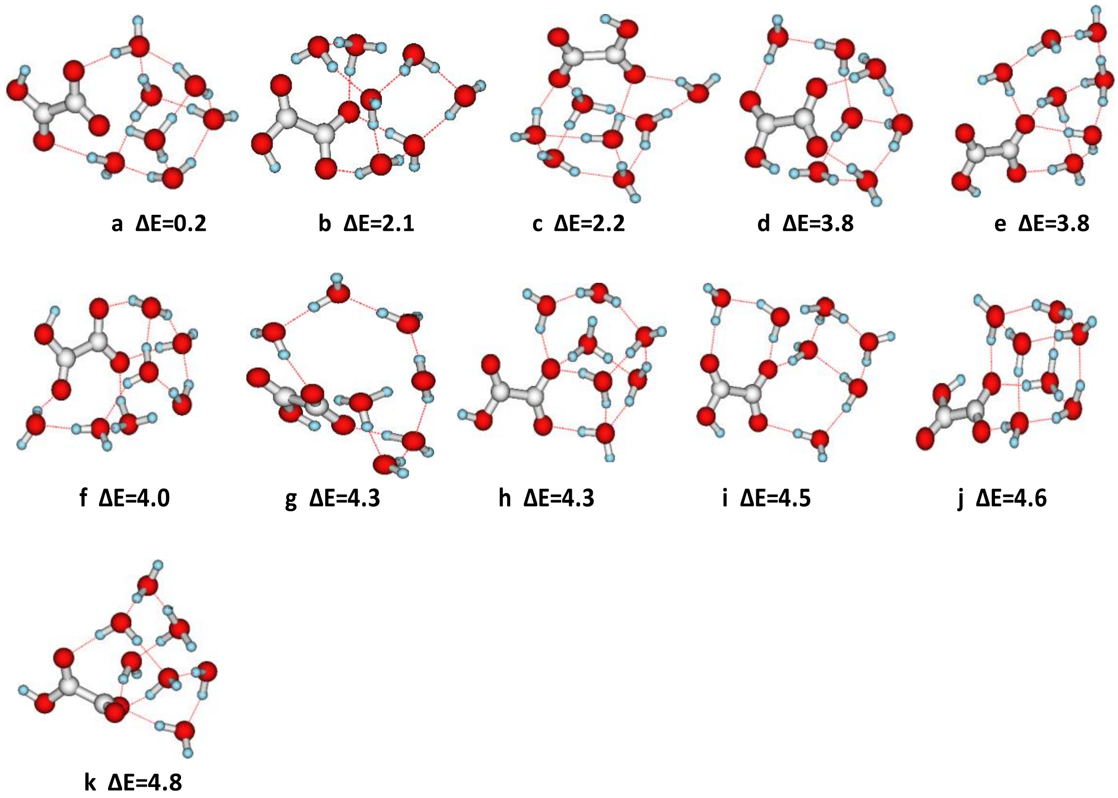
a ΔE=0.2 b ΔE=2.1 c ΔE=2.2 d ΔE=3.8 e ΔE=3.8

f ΔE=4.0 g ΔE=4.3 h ΔE=4.3 i ΔE=4.5 j ΔE=4.6

k ΔE=4.8

Figure 3.20 Higher energy equilibrium structures of $(COOH)_2.7H_2O$ showing contact ion pair formation. Zero point energy corrected relative energy (in kcal/mol) of the conformers with respect to minimum energy conformer of that size cluster is also given. Red balls represent oxygen, grey balls represent carbon and blue balls represent hydrogen atoms.

In case of hepta-hydrated oxalic acid cluster, the minimum energy structure shows dissociation of one of the hydroxyl hydrogen atoms of the oxalic acid molecule, as shown in Figure 3.18(h). It has hydrogen bonded cage-like structure, with O1-H and H-Oa bond distances equal to 1.517 and 1.022 Å respectively, and the acid molecule is planar. Higher energy conformers of hepta-hydrate, showing contact ion-pair formation is given in Figure 3.20(a)-(k). The minimum energy equilibrium geometry for octa-hydrated oxalic acid molecule, oxa.8H_2O, is a solvent separated ion-pair, as shown in Figure 3.18(i). Solvent water molecules are present between the acid molecule and hydronium ion in the hydrated cluster.

Table 3.6. Selected bond lengths of $(COOH)_2.nH_2O$, n=0-7, calculated at ωB97X-D/aug-cc-pVDZ level of theory. r_{O1-H}, r_{O2-H}, r_{H-Oa} and r_{H-Ob} represent hydroxyl O-H and hydrogen bond between the hydroxyl hydrogen of acid molecule and oxygen of the nearest water molecule, respectively.$\delta_{O1-C-C-O2}$ gives the dihedral angle between the C-O bonds

System	r_{O1-H}	r_{O2-H}	r_{H-Oa}	r_{H-Ob}	$\delta_{O1-C-C-O2}$
	(Å)				(degree)
$(COOH)_2$	0.974	0.974	-	-	180.0
$(COOH)_2.1H_2O$	0.996	0.978	1.661	-	179.6
$(COOH)_2.2H_2O$	1.004	0.978	1.625	-	179.2
$(COOH)_2.3H_2O$	1.009	0.979	1.588	-	179.2
$(COOH)_2.4H_2O$	1.004	1.004	1.625	1.625	126.3
$(COOH)_2.5H_2O$	1.007	1.004	1.599	1.628	129.3
$(COOH)_2.6H_2O$	1.044	0.974	1.466	-	179.0
$(COOH)_2.7H_2O$	1.517	0.975	1.022	-	174.1

An interesting observation is that in the smaller hydrated clusters, the water molecules are distributed across the oxalic acid molecule while in larger size clusters, the water molecules prefer a particular region of the acid molecule. A possible explanation for this observation is that, in case of smaller clusters, there is not much weakening of bonds in the acid molecule. The water molecules arrange themselves uniformly across the acid molecule to form stabilizing hydrogen bonds. In larger clusters, the hydroxyl bonds weaken due to hydrogen bonding with solvent water molecules and their polar character increases, attracting the water molecules to those regions. Another point noted is that the distribution of water molecules on either side of the acid molecule leads to loss in planarity of the acid molecule, implying that the hydrogen bonding, between the acid molecule and water molecules as well as between the water molecules, are strong enough to break the planarity of the oxalic acid molecule.

As the number of possible input geometries increases largely with increase in size of the hydrated oxalic acid cluster, only the first dissociation of oxalic acid is presently considered. Based on a rough estimate, second ionization was not observed in the minimum energy conformer, even up to twelve water molecules. However, as the possibility of missing out important conformers is large in large size clusters, a conclusive statement cannot be given. Selected geometrical parameters of oxa.nH_2O, n=1-7 are given in Table 3.6.[126]

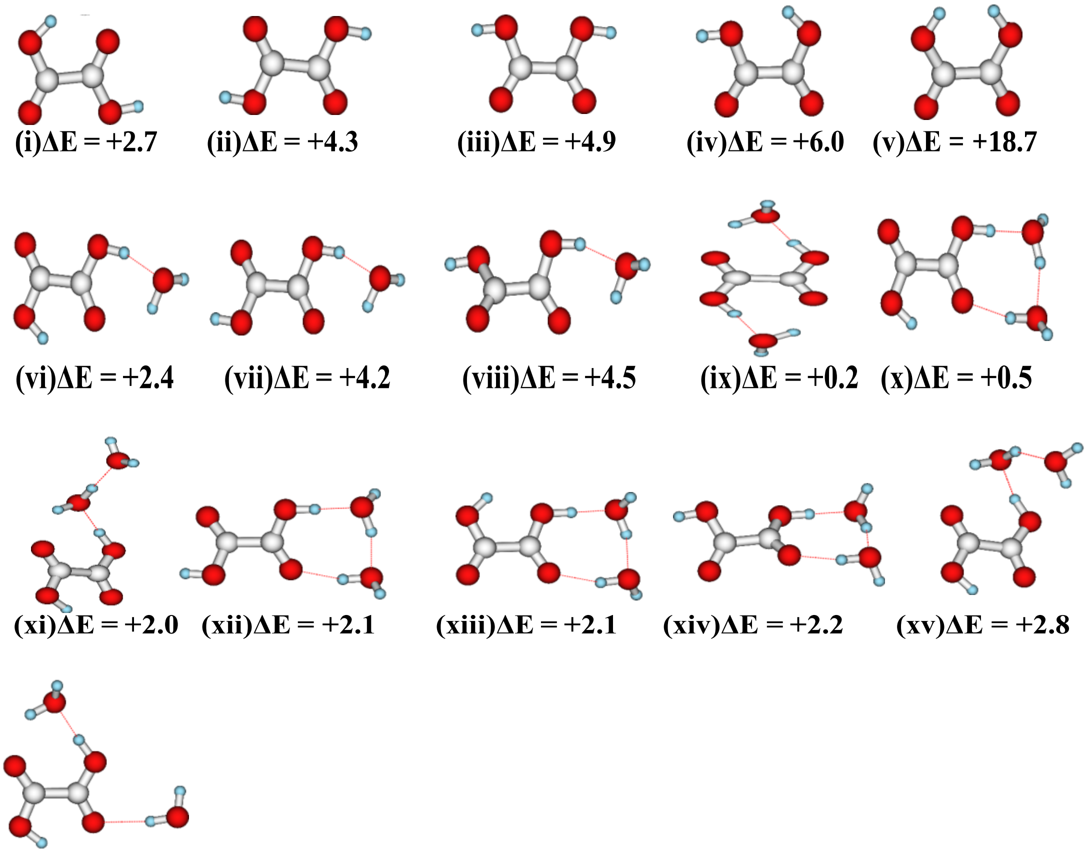

(i)ΔE = +2.7 **(ii)ΔE = +4.3** **(iii)ΔE = +4.9** **(iv)ΔE = +6.0** **(v)ΔE = +18.7**

(vi)ΔE = +2.4 **(vii)ΔE = +4.2** **(viii)ΔE = +4.5** **(ix)ΔE = +0.2** **(x)ΔE = +0.5**

(xi)ΔE = +2.0 **(xii)ΔE = +2.1** **(xiii)ΔE = +2.1** **(xiv)ΔE = +2.2** **(xv)ΔE = +2.8**

(xvi)ΔE = +4.8

Figure 3.21 Higher energy equilibrium structures of (i-v) $(COOH)_2$, (vi-viii) $(COOH)_2.1H_2O$, (ix-xvi) $(COOH)_2.2H_2O$. Zero point energy corrected relative energy (in kcal/mol) of the conformers with respect to minimum energy conformer of that size cluster is also given. Red balls represent oxygen, grey balls represent carbon and blue balls represent hydrogen atoms.

Many input geometries for each size hydrated oxalic acid cluster have been tried, to ensure that the most stable conformer is obtained. This has resulted in many higher energy equilibrium conformers of oxalic acid and its hydrated clusters. Higher energy conformers of free, mono and di-hydrates of oxalic acid and their relative energy with respect to the minimum energy conformer of that size cluster are given in Figure 3.21. All the conformers of free oxalic acid molecule given in Figure 3.21(i)-(v) are more than 2.0 kcal/mol higher in energy than the global minimum. The planarity of the acid molecule is lost in one of the three conformers of the mono-hydrate of oxalic acid (see Figure 3.21(viii)), which is 4.5 kcal/mol higher in energy than its minimum energy conformer.

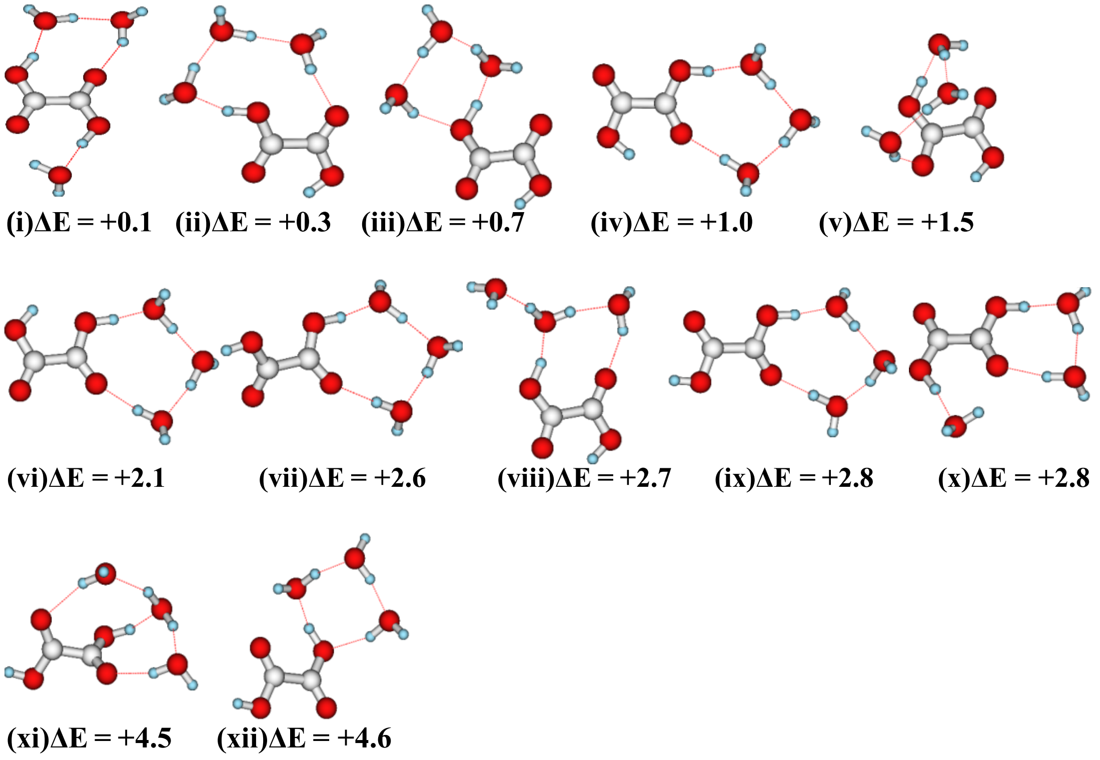
(i)ΔE = +0.1 **(ii)ΔE = +0.3** **(iii)ΔE = +0.7** **(iv)ΔE = +1.0** **(v)ΔE = +1.5**

(vi)ΔE = +2.1 **(vii)ΔE = +2.6** **(viii)ΔE = +2.7** **(ix)ΔE = +2.8** **(x)ΔE = +2.8**

(xi)ΔE = +4.5 **(xii)ΔE = +4.6**

Figure 3.22 (i-xii) Higher energy equilibrium structures of $(COOH)_2.3H_2O$. Zero point energy corrected relative energy (in kcal/mol) of the conformers with respect to minimum energy conformer of that size cluster is also given. Red balls represent oxygen, grey balls represent carbon and blue balls represent hydrogen atoms.

12 higher energy equilibrium conformers are obtained for tri-hydrate of oxalic acid, as shown in Figure 3.22(i)-(xii). Four of them are less than 1.0 kcal/mol higher in energy than the most stable conformer. It is seen that the planarity of the acid molecule is lost in few of the higher energy conformers. Another interesting observation is that clusters with similar hydrogen bonded water ring motifs differ very much in energy depending on the conformation of the acid molecule. Open chain motifs of water molecules are not observed.

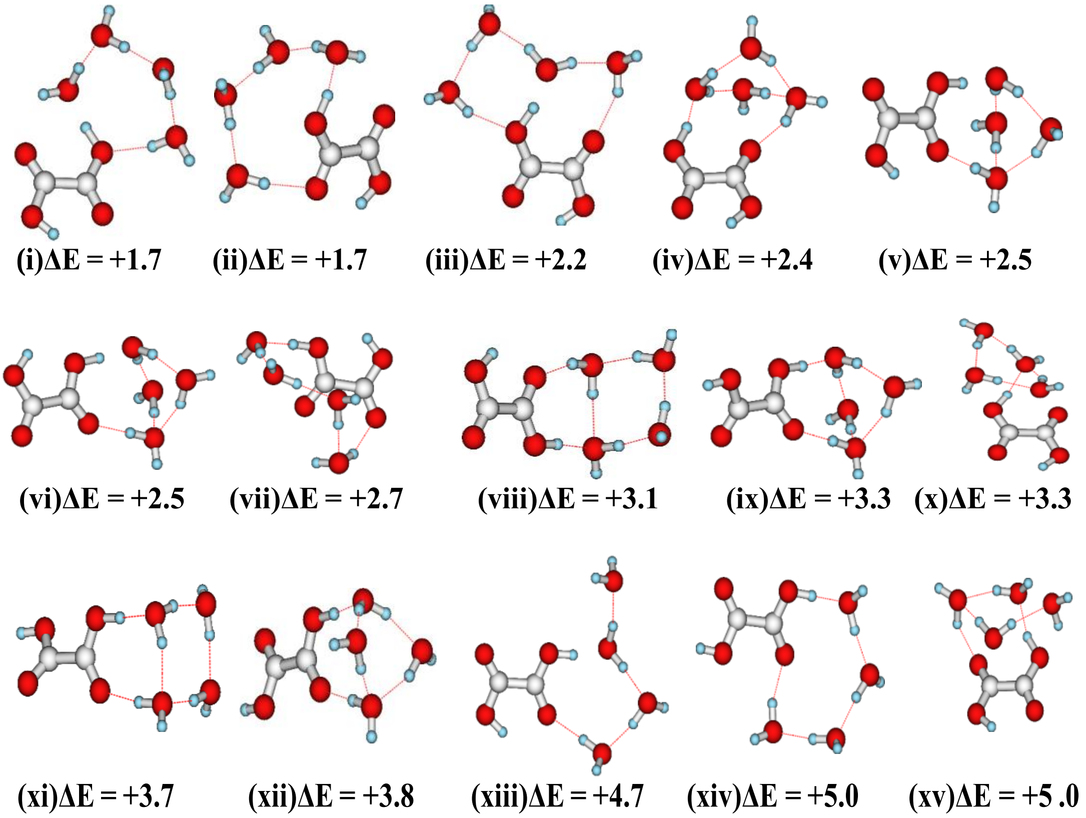

(i)ΔE = +1.7 **(ii)ΔE = +1.7** **(iii)ΔE = +2.2** **(iv)ΔE = +2.4** **(v)ΔE = +2.5**

(vi)ΔE = +2.5 **(vii)ΔE = +2.7** **(viii)ΔE = +3.1** **(ix)ΔE = +3.3** **(x)ΔE = +3.3**

(xi)ΔE = +3.7 **(xii)ΔE = +3.8** **(xiii)ΔE = +4.7** **(xiv)ΔE = +5.0** **(xv)ΔE = +5 .0**

Figure 3.23 (i-xv) Higher energy equilibrium structures of $(COOH)_2.4H_2O$. Zero point energy corrected relative energy (in kcal/mol) of the conformers with respect to minimum energy conformer of that size cluster is also given. Red balls represent oxygen, grey balls represent carbon and blue balls represent hydrogen atoms.

Fifteen higher energy equilibrium geometries obtained for the tetra-hydrate of oxalic acid is shown in Figure 3.23. It is observed that hydrogen bonded closed ring motifs are preferred. All the structures obtained are more than 1.0 kcal/mol higher in energy than the minimum energy conformer. Conformer with structural motifs similar to those observed in minimum energy equilibrium conformers of tetra-hydrates of trifluoroacetic acid, acetic acid and benzoic acid molecules are found to be much higher in energy in case of oxalic acid.

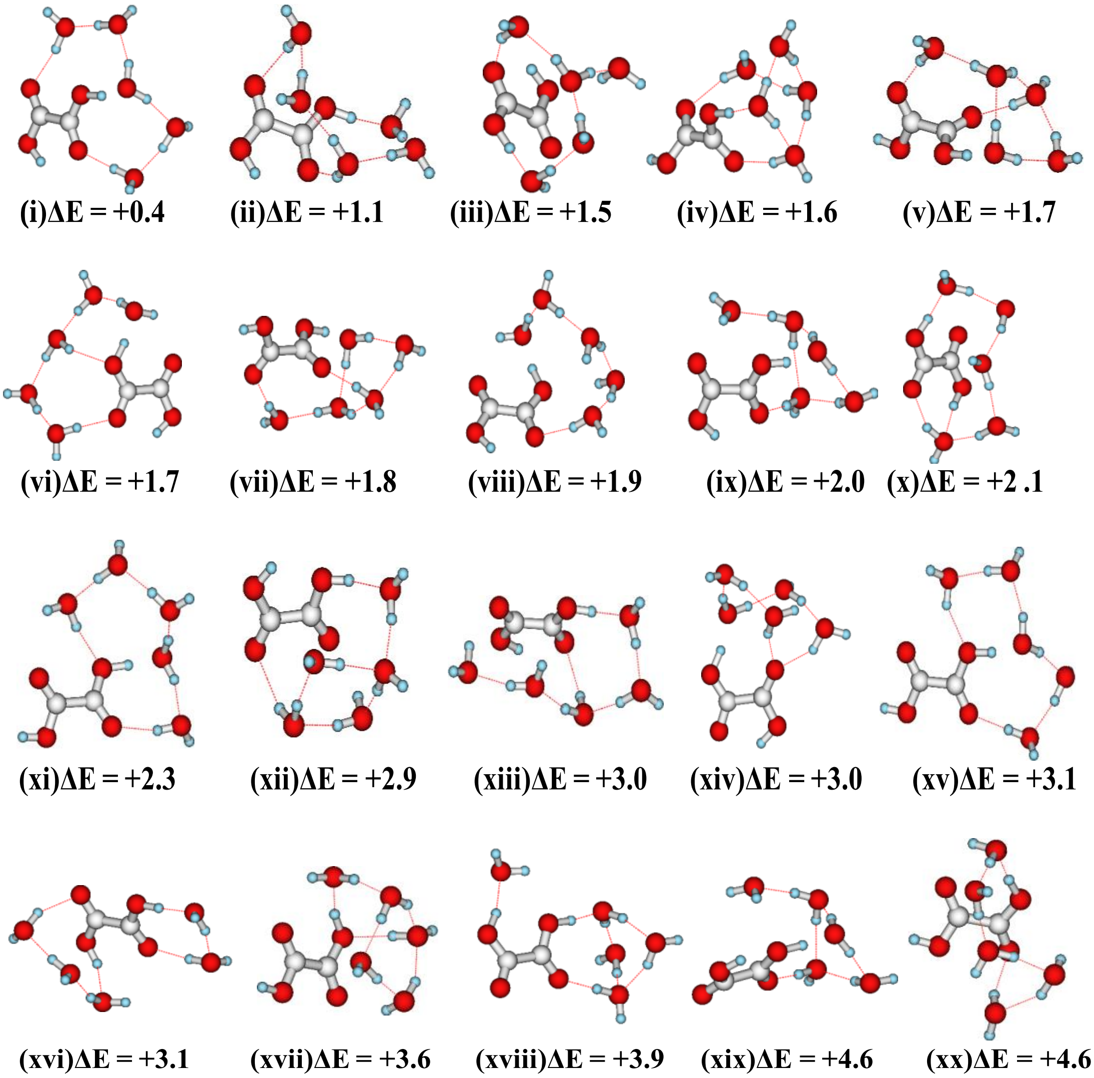

(i)ΔE = +0.4 **(ii)ΔE = +1.1** **(iii)ΔE = +1.5** **(iv)ΔE = +1.6** **(v)ΔE = +1.7**

(vi)ΔE = +1.7 **(vii)ΔE = +1.8** **(viii)ΔE = +1.9** **(ix)ΔE = +2.0** **(x)ΔE = +2 .1**

(xi)ΔE = +2.3 **(xii)ΔE = +2.9** **(xiii)ΔE = +3.0** **(xiv)ΔE = +3.0** **(xv)ΔE = +3.1**

(xvi)ΔE = +3.1 **(xvii)ΔE = +3.6** **(xviii)ΔE = +3.9** **(xix)ΔE = +4.6** **(xx)ΔE = +4.6**

Figure 3.24 (i-xx) Higher energy equilibrium structures of $(COOH)_2.5H_2O$. Zero point energy corrected relative energy (in kcal/mol) of the conformers with respect to minimum energy conformer of that size cluster is also given. Red balls represent oxygen, grey balls represent carbon and blue balls represent hydrogen atoms.

Twenty higher energy equilibrium conformers of penta-hydrate of oxalic acid, other than the ionized conformers given previously, are given in Figure 3.24. One of them (Figure 3.24(i)) is just 0.4 kcal/mol higher in energy than the minimum energy conformer. The water molecules are observed to form hydrogen bonded closed ring motifs. Structures where water molecules have dangling hydrogen bonds are less preferred. The relative energy of the penta-hydrates with similar hydrogen bonded motifs of water molecules vary greatly, depending on the conformation of the acid molecule.

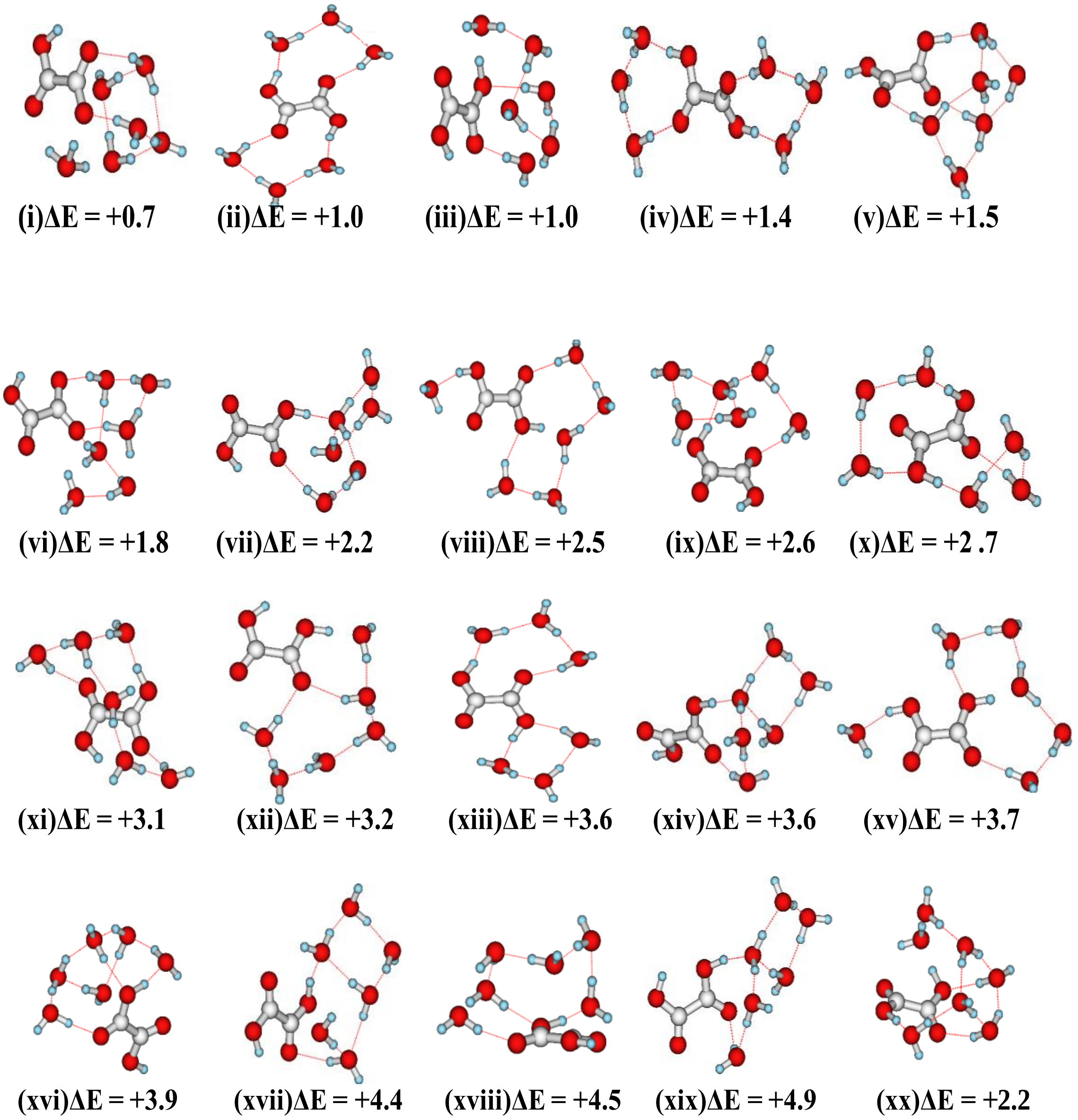

(i)$\Delta E = +0.7$ (ii)$\Delta E = +1.0$ (iii)$\Delta E = +1.0$ (iv)$\Delta E = +1.4$ (v)$\Delta E = +1.5$

(vi)$\Delta E = +1.8$ (vii)$\Delta E = +2.2$ (viii)$\Delta E = +2.5$ (ix)$\Delta E = +2.6$ (x)$\Delta E = +2 .7$

(xi)$\Delta E = +3.1$ (xii)$\Delta E = +3.2$ (xiii)$\Delta E = +3.6$ (xiv)$\Delta E = +3.6$ (xv)$\Delta E = +3.7$

(xvi)$\Delta E = +3.9$ (xvii)$\Delta E = +4.4$ (xviii)$\Delta E = +4.5$ (xix)$\Delta E = +4.9$ (xx)$\Delta E = +2.2$

Figure 3.25 Higher energy equilibrium structures of (i-xix) $(COOH)_2.6H_2O$ and (xx) $(COOH)_2.7H_2O$. Zero point energy corrected relative energy (in kcal/mol) of the conformers with respect to minimum energy conformer of that size cluster is also given. Red balls represent oxygen, grey balls represent carbon and blue balls represent hydrogen atoms.

Higher energy equilibrium conformers of hexa and hepta-hydrates of oxalic acid, other than those discussed previously, along with the relative stability of each conformer with respect to the minimum energy conformer of that size cluster, are given in Figure 3.25. As can be seen from the figure, open-chain conformers are not observed. It is seen that the planarity of the acid molecule is lost in a few of the higher energy conformers. Most of the higher energy conformers of the hepta-hydrate also show contact ion pair formation, and are given in Figure 3.20. As in previous cases, hydrogen bonded closed ring motifs of water molecules are preferred.

3.3 Conclusion

Range-separated, dispersion-corrected, correlated hybrid density functional, namely, ωB97X-D, is applied along with aug-cc-pVDZ basis sets for determining the minimum number of water molecules needed to dissociate trifluoroacetic acid, acetic acid, benzoic acid and oxalic acid molecules. Available macroscopic solvation models cannot fully describe acid−water systems, which are important in many phenomena ranging from biological to atmospheric. From the present study it is concluded that implicit macroscopic solvation model fails to accurately describe the effect of hydration on the structure of carboxylic acid molecules. Explicit hydration (microhydration), leading to dissociation, of trifluoroacetic acid, acetic acid, benzoic acid and oxalic acid molecules are studied. Various initial guess structures are considered for each size hydrated acid clusters for geometry optimization to determine the most stable conformers.

The structure of a hydrated acid cluster depends on the delicate balance between the hydrogen bond stabilization, coulombic attraction and proton transfer energy. An interesting point noted is the extra stability of hydrogen bonded closed ring conformers of the hydrated acid clusters, relative to open chain conformers. This is not surprising as the number of stabilizing hydrogen bonds are more in case of the closed ring conformers.

An elongation is seen in the acidic O-H bonds of the hydrated acid clusters, in all cases, with increase in number of water molecules. This is expected as the hydrogen bonds between the acid molecule and the water molecules causes weakening of the acidic hydroxyl bonds. It is observed that a minimum of six water molecules are needed to dissociate trifluoroacetic acid molecule while eight water molecules are needed for the dissociation of benzoic acid molecule. In case of oxalic acid molecule, the dissociation of the first acidic proton requires the presence of at least seven water molecules. The structure of the ionized acid-water cluster resembles that of the Eigen cation interacting with the carboxylate anion surrounded by the remaining water molecules. The proton transfer in $CH_3COOH.nH_2O$ and second proton transfer in $(COOH)_2.nH_2O$ are not observed even when n=8. The proton transfer from an acid molecule to the solvent water molecules in a hydrated acid cluster can be explained by the stronger stabilization of the contact ion pairs upon hydration, compared to the neutral acid molecule. As the possibility of missing out important conformers increases with increase in size of the hydrated clusters, the present study is limited to octa-hydrates. Geometrical parameters like bond length and microwave rotational constants, of the minimum energy conformers of the hydrated acid clusters, are found to be comparable to the available experimental data.

Chapter 4

Energetics of Hydrated Carboxylic acid Clusters

The whole is more than the sum of the parts

- Aristotle

The stability of the hydrated acid clusters at a finite temperature can be understood by studying their thermodynamic parameter. The free energy of formation, ΔG, determines the feasibility of formation and thermodynamic stability of the microhydrated acid clusters. The interactions of the solvent water molecules with solute acid molecule can be qualitatively analyzed by solvent stabilization energy and interaction energy.

In the present chapter, the free energy of formation of the hydrated clusters of carboxylic acids is calculated at different conditions to determine the temperature and pressure dependence on their stability. The solvent stabilization energy and interaction energy of the hydrated carboxylic acid clusters are also defined and their variation is monitored with increase in size of the hydrated acid cluster.

4.1 Theoretical Methods

The geometries are optimized and the most stable conformers of each size hydrated clusters of carboxylic acids are selected, as mentioned in Chapter 3. The free energy calculations are carried out for the most stable conformers of each size hydrated cluster of carboxylic acid molecule at ωB97X-D/aug-cc-pVDZ level of theory. The free energy of formation of a hydrated cluster is calculated as the difference in free energy of the product and the individual reactant molecules. The free energy of individual reactants and the product is calculated applying principles of statistical thermodynamics, assuming a non-interacting NVT ensemble, which is obtained during Hessian calculations.

Based on the geometry of the most stable conformers of free and hydrated carboxylic acids optimized at ωB97X-D/aug-cc-pVDZ level of theory, energy parameters are defined to understand the molecular interactions existing within the hydrated acid clusters. Solvent-induced stabilization energy of hydrated clusters of the acid molecule, $RCOOH.nH_2O$, is defined as:

$$E_{stab} = E_{RCOOH.nH2O} - (nE_{H2O} + E_{RCOOH}) \qquad 4.1$$

where, $E_{RCOOH.nH2O}$ refers to the energy of the hydrated acid cluster, $RCOOH.nH_2O$, E_{H2O} and E_{RCOOH} correspond to the energy of a single water and acid molecule, respectively.

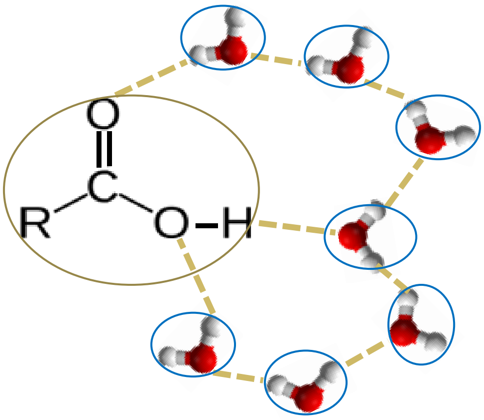

Figure 4.1 Schematic diagram depicting the solvent stabilization energy, E_{stab}, for a hydrated carboxylic acid system, $RCOOH.nH_2O$. This energy parameter includes solute-solvent as well as solvent-solvent interactions. The red and white balls represent oxygen and hydrogen atoms respectively of water molecule.

By definition, E_{stab} represents stabilization of the acid molecule due to its interactions with the solvent water molecules. E_{stab} gives the stabilization of the acid molecule on account of addition of solvent water molecules, which includes both solute–solvent as well as solvent–solvent interactions, as depicted in Figure 4.1. To isolate the solute–solvent interactions from the solvent stabilization energy, excluding any solvent–solvent stabilization, interaction energy, E_{int} is defined as:

$$E_{int} = E_{RCOOH \cdot nH2O} - (E_{(H2O)n} + E_{RCOOH*}) \qquad 4.2$$

$E_{(H2O)n}$ and E_{RCOOH*} correspond to the energy of the water cluster and the acid molecule, respectively, in the same geometry as is present in the hydrated acid cluster.

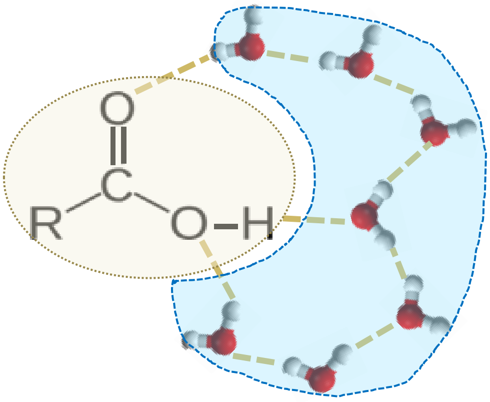

Figure 4.2 Schematic diagram depicting the interaction energy, E_{int}, for a hydrated carboxylic acid system, $RCOOH.nH_2O$. This energy parameter contains only solute-solvent interactions. The red and white balls represent oxygen and hydrogen atoms respectively of water molecule.

For evaluation of $E_{(H2O)n}$, solute part RCOOH is deleted from the optimized geometry of the cluster, followed by a single-point energy calculation. Following a similar procedure for the evaluation of E_{RCOOH}, the $(H_2O)_n$ part is removed from the optimized geometry of the hydrated cluster, followed by a single-point energy calculation. The interaction energy includes only solute-solvent interactions, removing all solvent-solvent interactions as depicted in Figure 4.2. The calculations are done at ωB97X-D/aug-cc-pVDZ level of theory. The energy parameters are improved applying CCSD(T) level of theory/6-311++G(d,p).

4.2 Results and Discussion

4.2.1 Free energy of formation

The calculated free energy of formation, at room temperature and atmospheric pressure (${}_{1atm}\Delta G^{298K}$), of hydrated clusters of tfa, acoh, bza and oxa are given in Table 4.1. In case of trifluoroacetic acid, the calculated free energy of formation at room temperature and atmospheric pressure are negative only for mono, di, tri and tetra-hydrates while for penta, hexa and hepta-hydrates, it is +1.1, +2.1 and +3.3 kcal/mol respectively.

Table 4.1 Free energy of formation, at room temperature/atmospheric pressure ($_{1atm}\Delta G^{298K}$) and 100K/1μTorr ($_{\mu Torr}\Delta G^{100K}$), of $CF_3COOH.nH_2O$, $CH_3COOH.nH_2O$, $C_6H_5COOH.nH_2O$ and $(COOH)_2.nH_2O$, n=1-8, calculated at ωB97X-D/aug-cc-pVDZ level of theory.[a]

n	$CF_3COOH.nH_2O$		$CH_3COOH.nH_2O$		$C_6H_5COOH.nH_2O$		$(COOH)_2.nH_2O$	
	$_{\mu Torr}\Delta G^{100K}$	$_{1atm}\Delta G^{298K}$	$_{\mu Torr}\Delta G^{100K}$	$_{1atm}\Delta G^{298K}$	$_{\mu Torr}\Delta G^{100K}$	$_{1atm}\Delta G^{298K}$	$_{\mu Torr}\Delta G^{100K}$	$_{1atm}\Delta G^{298K}$
	(kcal/mol)							
1	-4.3	-1.1	-2.7	+1.8	-3.3	+0.03	-3.4	+0.0
2	-9.2	-2.5	-6.9	+0.3	-7.7	-1.1	-5.9	+0.2
3	-10.8	-1.2	-8.6	+0.9	-9.3	-0.3	-8.2	+0.8
4	-14.2	-0.4	-10.9	+2.9	-11.6	+1.7	-11.6	+2.1
5	-16.4	+1.1	-12.7	+3.0	-12.4	+3.9	-13.6	+2.6
6	-18.2	+2.1	-14.8	+5.7	-14.7	+5.6	-15.7	+5.1
7	-23.4	+3.3	-18.9	+6.3	-18.3	+5.5	-22.0	+4.1
8	-	-	-22.8	+7.2	-21.8	+7.5	-	-

[a] References [117,119,126,127]

Similarly, it is seen that the hydrated clusters of acetic acid have positive free energy of formation at room temperature and atmospheric pressure. The positive value of the calculated free energy of formation of the hydrated clusters of benzoic acid and oxalic acid also indicate that not all sized hydrated clusters of carboxylic acids are stable at room temperature and atmospheric pressure.

Free energy of formation of the hydrated clusters of the carboxylic acids is also calculated at a lower temperature (100 K) and pressure (1 μTorr), mimicking the conditions of upper atmosphere. Calculated data is provided in Table 4.1 as $_{\mu Torr}\Delta G^{100K}$. It is observed that all the hydrated acid clusters are thermodynamically stable under such conditions. The calculated free energy of formation of mono, di, tri, tetra, penta, hexa and hepta-hydrates of trifluoroacetic acid at 100K and 1μTorr are -4.3, -9.2, -10.8, -14.2, -16.4, -18.2 and -23.4. Similarly, at 100 K and 1 μTorr pressure, it is seen that there is a near linear increase in the ΔG value of the $acoh\cdot nH_2O$ clusters, with an increase in the number of water molecules. The free energy change for acoh·$1H_2O$ is −2.7 kcal/mol at 100 K and 1 μTorr pressure. With the addition of another water molecule, the free energy change for di-hydrate is −6.9 kcal/mol. At 100 K and 1 μTorr pressure, ΔG for acoh·$3H_2O$, acoh·$4H_2O$, acoh.$5H_2O$, acoh·$6H_2O$, acoh·$7H_2O$, and acoh·$8H_2O$ are, respectively, −8.6, −10.9, −12.7, −14.8, −18.9, and −22.8 kcal/mol. At 100K and 1μTorr pressure, the calculated free energy of formation for all the hydrated clusters of benzoic acid is found to be negative. The calculated free energy of formation at 100 K and 1 μTorr, for mono, di, tri, tetra, penta, hexa and hepta-hydrate of oxalic acid are -3.4, -5.9, -8.2, -11.6, -13.6, -15.7 and -22.0 kcal/mol respectively, indicating that they too are stable at low temperature and pressure. The negative value of the free energy of formation of the hydrated carboxylic acid clusters at low temperature and pressure implies that there is a possibility for their existence in the upper atmosphere, where these acid molecules are known to be present, along with water vapor. These hydrated acid clusters determine many atmospheric phenomena such as cloud nucleation, aerosol formation, etc. The microhydration studies of carboxylic acid molecules are environmentally relevant and can help in developing theoretical models that accurately describe the atmosphere. For that, understanding the intermolecular interactions of these hydrated acid clusters is important. These interactions can be qualitatively analyzed by solvent stabilization energy and interaction energy

4.2.2 Solvent Stabilization Energy

Solvent stabilization energy (E_{stab}) of tfa·nH_2O clusters, calculated applying ωB97X-D/aug-cc-pVDZ level of theory, is supplied in Table 4.2. It is noted that E_{stab} changes linearly with the addition of solvent water molecules. This is understandable because the E_{stab} value corresponds to the internal energy that increases with the increase in size of the hydrated cluster.

Table 4.2 Solvent stabilization energy and Interaction energy of $CF_3COOH.nH_2O$, $CH_3COOH.nH_2O$, $C_6H_5COOH.nH_2O$ and $(COOH)_2.nH_2O$, n=1-8, calculated at ωB97X-D/aug-cc-pVDZ level of theory.[a]

n	$CF_3COOH.nH_2O$		$CH_3COOH.nH_2O$		$C_6H_5COOH.nH_2O$		$(COOH)_2.nH_2O$	
	E_{stab}	E_{int}	E_{stab}	E_{int}	E_{stab}	E_{int}	E_{stab}	E_{int}
	(kcal/mol)							
1	-11.6	-12.3	-10.8	-11.5	-11.0	-11.8	-10.9	-13.7
2	-24.1	-22.1	-22.7	-20.3	-23.0	-20.8	-20. 6	-19.3
3	-32.8	-25.2	-31.5	-21.7	-31.8	-22.1	-30.3	-22.5
4	-44.4	-32.2	-42.4	-28.4	-42.5	-29.8	-42.0	-42.1
5	-54	-39.6	-51.2	-25.7	-51.2	-22.8	-51.2	-44.0
6	-62.3	-96.2	-62.4	-23.3	-61.3	-33.8	-62.4	-31.8
7	-78.2	-150.3	-74.9	-35.7	-73.7	-27.6	-78.5	-124.7
8	-	-	-88.3	-33.4	-85.3	-109.8	-	-

[a]References [117,119,126,127]

Similarly, for microhydrated clusters of acetic acid molecule, E_{stab} varies linearly with the addition of water molecules. E_{stab} of hydrated clusters of benzoic acid and oxalic acid molecules also increase linearly with addition of water molecules, as expected, and does not provide any information regarding the ionization of the acid molecule.

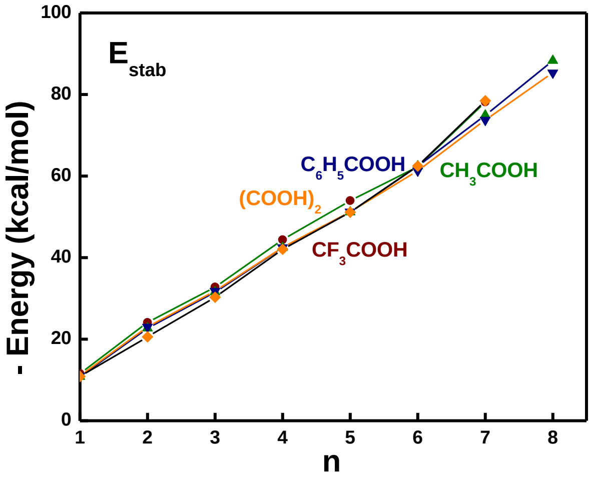

Figure 4.3 Variation of solvent stabilization energy (E_{stab}) of hydrated clusters of carboxylic acids with increase in size of the hydrated cluster (n). The brown, green, blue and orange line

shows solvent stabilization energies of $CF_3COOH.nH_2O$, $CH_3COOH.nH_2O$, $C_6H_5COOH.nH_2O$ and $(COOH)_2.nH_2O$, n=1-8, clusters respectively, calculated at ωB97X-D/aug-cc-pVDZ level of theory.

This cumulative solvent stabilization masks the solute-solvent interactions which is the focus of our study. The plotted energy profile of E_{stab} does not display any characteristic feature to indicate the formation of an ion pair for any of the hydrated acid clusters studied at present, as shown in Figure 4.3.

4.2.3 Interaction Energy

Interaction energy (E_{int}) essentially represents the net interaction of the acid molecule with $(H_2O)_n$ systems in these hydrated acid clusters. Interaction energy of the $RCOOH.nH_2O$ (n = 1−8) clusters, calculated applying ωB97X-D/aug-cc-pVDZ method is tabulated in Table 4.2. One may easily notice that stabilization and interaction energy are very close in mono and di-hydrated clusters of tfa. But when intermolecular hydrogen bonds among solvent water molecules start building up, the E_{stab} exceeds interaction energy. Calculated interaction energy is significantly smaller than E_{stab} for the hydrated cluster of size n = 3−5 of tfa.

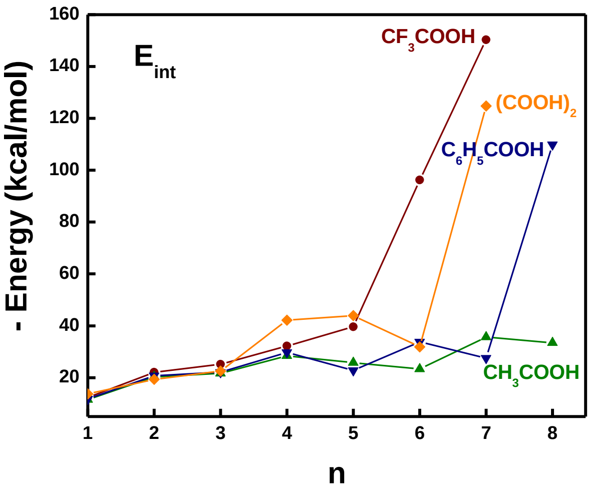

Figure 4.4 Variation of interaction energy (E_{int}) for hydrated carboxylic acid clusters with increase in size of the hydrated cluster (n). The brown, orange, blue and green lines show interaction energy profiles for $CF_3COOH.nH_2O$, $(COOH)_2.nH_2O$, $C_6H_5COOH.nH_2O$ and

$CH_3COOH.nH_2O$, n=1-8, clusters respectively, calculated at ωB97X-D/aug-cc-pVDZ level of theory.

The interaction energy profile shows a sharp increase for hexa- and hepta- hydrated clusters of tfa. This increase in E_{int} values over E_{stab} may be explained from the definition of these two energy parameters. In the case of hexa and hepta-hydrated clusters of tfa, the O−H bond of tfa is close to dissociation limit. However, by definition of E_{stab}, the energy of tfa with equilibrium O−H bond length is considered. This makes E_{stab} lower than E_{int}, where energy of the system with actual geometrical parameters is calculated. The difference between the two energy parameters, E_{stab} and E_{int}, for hydrated clusters up to n = 5 should be the measure of inter-water hydrogen bonding energy. The interaction energy profiles clearly point out that six solvent water molecules are enough to dissociate tfa to form a contact ion pair. The absence of ion pair formation is reflected in the interaction energy profile of hydrated clusters of acetic acid. E_{int} varies irregularly with the addition of water molecules, depending on the geometry of the hydrated acetic acid cluster. The interaction energy profile of the hydrated clusters of carboxylic acid molecules is shown in Figure 4.4. It should be noted that except for the mono-hydrate, the solvent stabilization energies of acetic acid clusters are higher than solvent interaction energies. This is justified as the solvent stabilization energy includes solvent−solvent dispersion interactions whereas the interaction energy accounts only for the net dispersion interaction between solute and solvent clusters. Observations similar to the case of tfa are noted for benzoic acid and oxalic acid hydrated clusters. While the solvent stabilization energy of acid-water systems increases linearly with the addition of water molecules, a sharp increase of interaction energy is observed when moving from unionized to ionized system. For benzoic acid system, from hepta to octa hydrate, the interaction energy increases steeply from -27.6 kcal/mol to -109.8 kcal/mol. A sharp increase is seen in the interaction energy of the hydrated oxalic acid cluster on moving from unionized hexa-hydrate to ionized hepta-hydrate, as depicted in Figure 4.4.

Table 4.3 Solvent stabilization energy (E_{stab}) and Interaction energy (E_{int}) of $CF_3COOH.nH_2O$, $CH_3COOH.nH_2O$, $C_6H_5COOH.nH_2O$ and $(COOH)_2.nH_2O$, n=1-8, clusters calculated at CCSD(T)/6-311++G(d,p) level of theory.[a]

n	$CF_3COOH.nH_2O$		$CH_3COOH.nH_2O$		$C_6H_5COOH.nH_2O$		$(COOH)_2.nH_2O$	
	E_{stab}	E_{int}	E_{stab}	E_{int}	E_{stab}	E_{int}	E_{stab}	E_{int}
1	-11.4	-12.2	-10.2	-11.1	-10.6	-11.5	-10.2	-13.4
2	-23.8	-21.6	-22.1	-19.7	-22.8	-20.4	-21.3	-20.2
3	-32.9	-24.4	-32.0	-21.5	-32.7	-22.2	-31.8	-23.6
4	-44.7	-31.4	-42.2	-27.4	-42.6	-28.9	-43.9	-41.3
5	-54.8	-39.3	-52.3	-25.4	-52.1	-22.3	-54.2	-43.7
6	-63.9	-94.9	-63.4	-23.1	-	-	-66.3	-34.0
7	-78.5	-128.7	-76.3	-35.5	-	-	-80.7	-123.1
8	-	-	-89.3	-32.8	-	-	-	-

[a]References [117,119,126,127]

It is observed that the stabilization energy dominates the interaction energy in the unionized hydrated acid clusters while the trend reverses for ionized clusters. This becomes obvious when we understand that the stabilization energy incorporates the weak van der Waals interactions which are present in the hydrogen bonded systems while the interaction energy takes into account the electrostatic interactions involved, which rises sharply in the ionized cluster.

To confirm that the above data is not a computational artifact, the interaction energy and stabilization energy values are further improved applying CCSD(T)/6-311++G(d,p) level of theory (see Table 4.3). Due to resource limitations, coupled cluster calculations on systems beyond penta-hydrated clusters of benzoic acid could not be performed at present. However, one can clearly see that the energy variation follow similar trend at both levels of theory. To correlate the solvent stabilization energy and interaction energy, a plot depicting the two energy profiles, calculated at both DFT and Coupled Cluster levels of theory, for oxalic acid-water clusters, is shown in

Figure **4.5**, as an example. The two intersecting energy curves do indicate the formation of charge-separated ion pair of oxalic acid in the case of hepta-hydrated cluster. As can be seen from the figure, the E_{stab} and E_{int} profiles, obtained from DFT and coupled cluster calculations, remain similar verifying the ωB97X-D/aug-cc-pVDZ level data as reliable. Similar plots are obtained for of all the carboxylic acids studied.

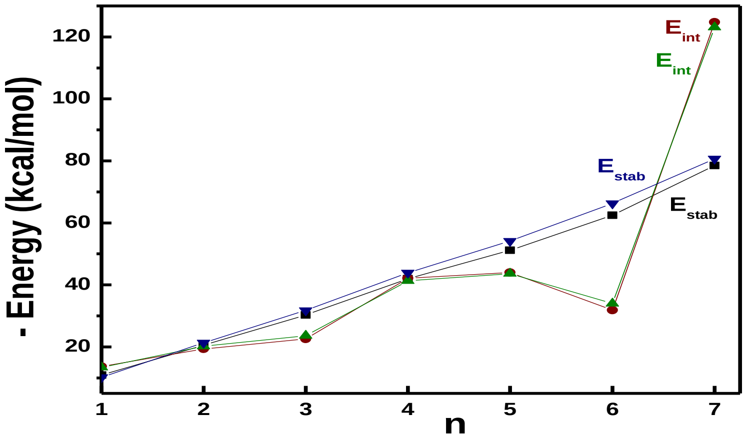

Figure 4.5 Variation of solvent stabilization energy (E_{stab}) and interaction energy (E_{int}) of hydrated oxalic acid clusters, $(COOH)_2.nH_2O$, n=1-7, with increase in size of the cluster (n). The blue and black lines show E_{stab} profiles calculated at CCSD(T)/6-311++G(d,p) and ωB97X-D/aug-cc-pVDZ levels of theory while green and brown lines show E_{int} profiles calculated at CCSD(T)/6-311++G(d,p) and ωB97X-D/aug-cc-pVDZ levels of theory, respectively.

The molecular cluster calculations suffer from Basis Set Super position Error (BSSE) which leads to artificial inter-molecular distances and energies. These errors become very pronounced when small basis sets are used. The BSSE calculations based on counterpoise procedure, reveal that the errors are negligible.The BSSE energy is calculated as 0.4, 0.6, and 0.8 kcal/mol for mono, di, and tri-hydrated clusters of tfa, respectively. For mono, di, tri and tetra-hydrate of acetic acid, the calculated BSSE energy is 0.4, 0.6, 0.7 and 0.9 kcal/mol respectively. BSSE for $C_6H_5COOH.nH_2O$, n=1-8 are 0.5, 0.7, 0.8, 1.0, 1.1, 1.1, 1.5 and 2.1 kcal/mol respectively, which are negligible compared to the stabilization and interaction energies obtained. The BSSE energy for the hydrated oxalic acid clusters are also determined to be very low compared to the interaction energy. The BSSE up to tetra-hydrate oxalic acid clusters are found to be less than 2 kcal/mol.

4.3 Conclusion

Free energy calculations show that the microhydrated clusters of carboxylic acid molecules are not favoured at room temperature and atmospheric pressure. They are stable only at very low temperature and pressure (100 K and 1 μTorr). The thermodynamic stability of the $RCOOH.nH_2O$ systems at low temperature and pressure implies the possibility of their existence in the upper atmosphere. The interaction and stabilization energy are calculated for $RCOOH\cdot nH_2O$ clusters ($n = 1-8$). The calculated stabilization energy increases linearly on successive addition of solvent water molecules whereas the interaction energy increases largely for ionized clusters. Similar results are obtained upon improving these energy parameters applying CCSD(T)/6-311++G(d,p) level of theory. No characteristic feature is observed in the plot of interaction energy v/s size of the cluster, for acetic acid hydrated clusters, indicating that more than eight water molecules are needed for its dissociation. As these acids are known to assist cloud nuclei formation and aerosol production, further studies, both theoretical and experimental, in this respect would be helpful for environmental modelling.

Chapter 5

Selected Properties of Hydrated Carboxylic acid Clusters

Who has seen the wind? Neither you nor I; But when the trees bow down their heads, the wind is passing by.

- Christina G. Rossetti 1830-1894

The addition of solvent water molecules to carboxylic acid molecule, leading to the formation of ion pair, should be reflected in some of the properties of the hydrated acid clusters. This chapter analyses a few properties of the hydrated acid clusters and their variation with the size of the cluster. It must be noted that as the rate of evolution of different properties of the hydrated acid systems may be different along the proton-transfer coordinate, measurement of these properties may suggest difference in the position of the proton along the proton transfer coordinate. Static polarizability, dipole moment, bond dipole moment, IR spectrum, bond dissociation curve and hydrogen bond energy of carboxylic acid molecules and their hydrated clusters have been examined.

Intermolecular interactions in a solvated system can be understood by the system's response to an external electric field, which is given by its electronic polarizability. Electronic polarizability is an important property for understanding the process of solvation in the hydrated clusters. The variation of static polarizability of the hydrated acid clusters, with increase in the size of the cluster, is studied.

The addition of water molecules to the acid molecule causes a weakening of the acidic O-H bond. The elongation of the hydroxyl bond of the acid molecule due to hydrogen bonding with solvent water molecules causes a change in the dipole moment of the hydrated acid clusters. Hence, dipole moment can be a property which can be monitored to determine the proton transfer in carboxylic acid-water cluster.

Water clusters encapsulating carboxylic acid molecule are stable due to the formation of hydrogen bonds between the acid molecule and neighboring water molecules as well as between the water molecules. Peak positions in IR spectra due to O−H stretching modes of the acid and water molecules are expected to shift compared with that of free acid and water, due to H-bonding interactions. Thus, simulating the IR spectra of the hydrated acid clusters can serve to keep track of the weakening of the O−H bond of the acid molecule. It can also help in determining the proton transfer from the solute acid molecule to solvent water molecules, as the presence of hydrated proton introduces new peaks in the IR spectrum. Comparing the simulated IR spectrum of the hydrated acid cluster with that of experimental gas phase IR spectrum can help in verifying the structures predicted. Hence Hessian calculation for the most stable structure of each size hydrated acid cluster is carried out.

The dissociation energy curve of the hydrated acid clusters is useful in obtaining information about the proton transfer barrier of the cluster. The dissociation energy curve is obtained by carrying out a rigid potential energy scan of the acidic hydroxyl bond of the hydrated acid cluster.

Two bonds crucial in the study of dissociation of the acid molecule are: the acidic O-H bond and the hydrogen bond between the acidic H atom and the O atom of the neighboring water molecule. The breaking of the former and the formation of the latter bonds can be studied from their hydrogen bond energy.

5.1 Theoretical Methods

5.1.1 Isotropic Polarizability

The charge density of a molecule can rearrange in the presence of an external electric field, E. This leads to a change in the electric dipole moment of the molecule which can be described by the tensor equation:

$$\mu = \mu_0 + \alpha : E + \frac{1}{2}\beta : EE + ... \tag{5.1}$$

where μ_0 is the dipole moment of the molecule in the absence of electric field, α is a second rank tensor called the polarizability tensor and β is the first in an infinite series of dipole hyperpolarizabilities. The isotropic polarizability, α, of hydrated acid clusters are calculated from the diagonal elements of the polarizability tensor.

$$\alpha = 1/3(\alpha_{xx} + \alpha_{yy} + \alpha_{zz}) \tag{5.29}$$

Isotropic polarizabilities of the most stable structures of each size hydrated acid cluster are calculated applying ωB97X-D/aug-cc-pVDZ level of theory.

5.1.2 O-H Bond Dipole Moment

The weakening of the acidic O-H bond will be reflected in its bond dipole moment. The bond dipole moment is calculated as the sum of products of density matrix and dipole moment integrals between the basis functions involved in the selected bond. It gives the electric dipole moment around the geometric centre of the two atoms involved. The bond dipole moments are calculated using Multiwfn - A Multifunctional Wavefunction Analyzer.[128]

5.1.3 IR Spectra

Vibrational frequency calculations are carried out by determining the second derivative of energy with respect to Cartesian nuclear coordinates of the molecular cluster and transforming to mass-weighted coordinates. Hessian calculations for the most stable structure of RCOOH.nH_2O cluster ($n = 1-8$), bare H_2O and RCOOH are carried out at ωB97X-D/aug-cc-pVDZ level of theory. The Lorentzian line shape has been applied with a peak half-width of 10 cm^{-1} for all the vibrational spectra plots. Hessian calculations are based on harmonic approximation. As full length anharmonicity calculations are expensive, a scaling factor is used to account for the anharmonicity in vibration. Since the main focus of this study is the hydroxyl stretching frequency of the acid molecule, the scaling factor is taken as the ratio of experimental to calculated O-H stretching frequency of the acid molecule.

5.1.4 O-H Bond Dissociation Curve

A dissociation energy curve is obtained from a rigid potential energy scan of the hydrated acid cluster, keeping all but the length of dissociating O-H bond constant. This energy profile can explain the process of proton transfer, which occurs only in a few hydrated acid clusters. A single point energy calculation varying only the acidic O-H bond is carried out for the most stable conformers of each size hydrated cluster. The relative energy of each variation with respect to the equilibrium energy of that size conformer is plotted against the O-H bond length, to obtain the dissociation energy curve. The calculations are done at ωB97X-D/aug-cc-pVDZ level of theory.

5.1.5 Hydrogen Bond Energy

The proton transfer from the acid molecule to the water molecule will be indicated by the hydrogen bond energy of the forming and dissociating bonds. Hydrogen bond energy is obtained as $E_{HB}= 0.5V(rcp)$, where V(rcp) is potential energy density at bond critical point.[129] The hydrogen bond energies are calculated for the most stable conformers of each size hydrated clusters of the acid molecule.

5.2 Results and Discussion

5.2.1 Isotropic Polarizability

The variation of isotropic polarizability (α) with the size (n) of hydrated clusters of carboxylic acids is observed to be linear. The isotropic polarizabilities of the hydrated clusters of the carboxylic acids are given in Table 5.1.

Table 5.1 Comparison of isotropic polarizability of RCOOH.nH_2O (n = 0−8) clusters calculated at ωB97X-D/aug-cc-pVDZ level of Theory

n	$CF_3COOH.nH_2O$	$CH_3COOH.nH_2O$	$C_6H_5COOH.nH_2O$	$(COOH)_2.nH_2O$
	in $Bohr^3$			
0	35.4	33.8	89.2	38.6
1	45.0	43.6	99.9	49.0
2	55.2	53.9	110.6	59.2
3	64.7	63.9	120.8	69.5
4	74.5	73.2	130.3	80.0
5	83.9	83.3	140.1	90.1
6	95.8	92.3	150.0	98.2
7	103.4	100.7	159.1	106.7
8	-	109.6	168.5	-

The calculated isotropic polarizability of CF_3COOH is 35.4. The addition of a single water molecule increases the value to 45.0. The calculated isotropic polarizability for $CF_3COOH.nH_2O$, n=2-7 are 55.2, 64.7, 74.5, 83.9, 95.8 and 103.4 respectively. The variation in α with the size of the hydrated clusters of trifluoroacetic acid is linear and best fitted as:

$$\alpha = 35.3 + 9.8n \qquad 5.30$$

with a regression value > 0.99.

Isotropic polarizability of acetic acid molecule is calculated as 33.8 $Bohr^3$ at the present level of theory. A linear increase in the isotropic polarizability, with increase in size of the acetic acid hydrated clusters, is observed, similar to that seen in trifluoroacetic acid-water clusters. For the most stable conformer of mono-hydrate of acetic acid cluster, isotropic polarizability is 43.6 $Bohr^3$ and that for di-hydrate, tri-hydrate, and tetra-hydrate are 53.9, 63.9, and 73.2 $Bohr^3$, respectively. With five, six, seven, and eight water molecules, the isotropic polarizability of the hydrated acetic acid clusters increases to 83.3, 92.3, 100.7, and 109.6 Bohr^3, respectively. This linear relation is best fitted, with a regression value of 0.99, as:

$$\alpha = 34.6 + 9.5n \tag{5.4}$$

where n is the number water molecules present in the cluster.

The calculated isotropic values of benzoic acid-water clusters are also seen to increase linearly with size of the cluster. α for $C_6H_5COOH.nH_2O$, n=0-8 are given in Table 5.1. With a regression value > 0.99, the linear variation in calculated isotropic polarizability with increase in size of the cluster is best fitted as:

$$\alpha = 90.3 + 9.9n \tag{5.5}$$

Similarly, for oxalic acid molecule the linear variation in calculated isotropic polarizability is observed to best fit in the equation:

$$\alpha = 39.5 + 9.8n \tag{5.6}$$

These linear fittings have a correlation coefficient > 0.99, showing the reliable predictability of the polarizability of larger size clusters. However, it is noted that calculated isotropic polarizability does not show any characteristic feature indicating the formation of ion pair. Isotropic polarizability cannot be used in monitoring the breaking of the acidic hydroxyl bond in carboxylic acid clusters.

5.2.2 Dipole moment

The elongation of the hydroxyl bond of the hydrated acid clusters, compared to free acid molecule, makes dipole moment a property which can be studied to determine the proton transfer in acid-water clusters. It would be interesting to understand the variation of dipole moment (μ) of the hydrated acid cluster with increase in the size of the hydrated cluster. It has been previously reported that the cumulative effect of aligning dipoles due to the water molecules create an electric field which induces acid dissociation in hydrated acid clusters.[130,131] The net dipole moment of the hydrated clusters of the carboxylic acid molecules are given in Table 5.2.

Table 5.2 Net dipole moment and acidic O-H bond dipole moments of the most stable conformers of hydrated carboxylic acid, $RCOOH.nH_2O$, n=0-8 systems.

n	$CF_3COOH.nH_2O$		$CH_3COOH.nH_2O$		$C_6H_5COOH.nH_2O$		$(COOH)_2.nH_2O$	
	μ	μ_{O-H}	μ	μ_{O-H}	μ	μ_{O-H}	μ	μ_{O-H}
	in Debye							
0	2.2	1.0	1.8	1.1	2.1	1.3	0.0	0.9
1	3.4	1.1	1.4	1.2	1.7	1.5	2.2	1.1
2	2.9	1.3	0.5	1.4	1.0	1. 8	2.6	1.1
3	4.4	1.3	1.0	1.4	1.3	1. 8	2.6	1.1
4	4.8	1.4	3.3	1.5	4.5	1. 8	0.1	1.3
5	4.9	1.3	2.3	1.4	3.1	2.0	0.9	1.3
6	4.2	1.0	0.5	1.5	2.7	1. 8	2.5	1.1
7	3.6	1.0	5.0	1.4	2.8	2.5	4.4	0.8
8	-	-	3.7	1.3	5.0	1.5	-	-

However no characteristic feature corresponding to dissociation of the acid molecules or formation of ion-pair is noted in the net dipole moment of the hydrated acid clusters. This is not surprising as the net dipole moment depends on geometry of the cluster. The direction of the net dipole moment vector need not be in the direction of the dissociating hydroxyl-bond. Hence the bond dipole moment of acidic O-H bond (μ_{O-H}), which is in the direction of the dissociating hydroxyl-bond, is calculated for the hydrated acid clusters.

Interestingly, calculated acidic O-H bond dipole moments of the microhydrated clusters shows a characteristic feature indicating formation of ion pair. The O-H bond dipole moment (μ_{O-H}) of CF_3COOH is 1.0 D. With the addition of a single water molecule, it increases to 1.1 D. The variation in O-H bond dipole moment of hydrated acid clusters is given in Table 5.2. It is seen that there is a sharp decrease in $\mu_{O\text{-}H}$ on going from penta to hexa-hydrate of trifluoroacetic acid. This is understandable as the bond dipole moment becomes insignificant when the distance between the atoms connected by the bond becomes large, as in the case of the ionized acid cluster. A similar feature is absent in the case of hydrated acetic acid clusters, as the formation of an ion pair does not take place. A sharp decrease in $\mu_{O\text{-}H}$ is observed for octa-hydrate of benzoic acid, from 2.5 to 1.5 D, and it is seen that from hexa to hepta-hydrate of oxalic acid, there is a clear decrease of the most acidic O-H bond dipole moment, from 1.1 to 0.8 D. Figure 5.1 shows the variation of O–H bond dipole moment of trifluoroacetic acid, acetic acid, benzoic acid and oxalic acid, with increase in size of the hydrated cluster.

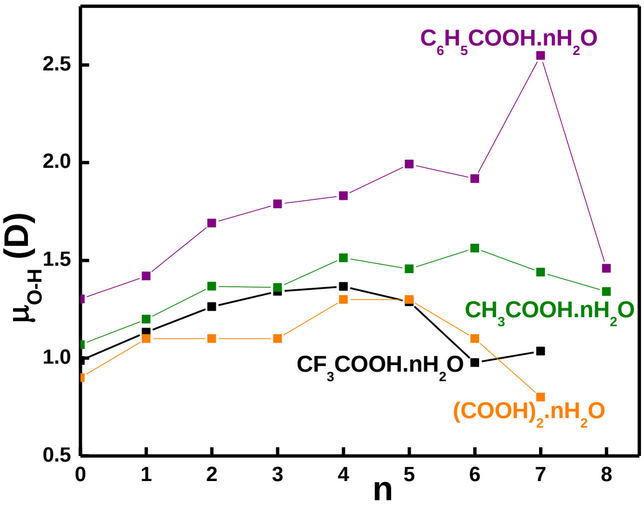

Figure 5.1 Variation of acidic O-H bond dipole moment ($\mu_{O\text{-}H}$) of hydrated clusters of carboxylic acids with increase in size of the hydrated cluster (n). The violet, green, black and orange line shows the bond dipole moments of the most acidic O-H bonds of $C_6H_5COOH.nH_2O$, $CH_3COOH.nH_2O$, $CF_3COOH.nH_2O$ and $(COOH)_2.nH_2O$, n=1-8, clusters respectively, calculated at ωB97X-D/aug-cc-pVDZ level of theory.

It is observed that the variation of bond dipole moment with number of water molecules is not regular. This is because the bond dipole moment depends on the geometry of the hydrated clusters. However, a sharp decrease in $\mu_{O\text{-}H}$ on moving from a lower to higher hydrate can be taken as an indication for acid ionization. In the case of trifluoroacetic acid, benzoic acid and oxalic acid, proton transfer from the acid molecule to solvent water molecules occurs in the presence of six, eight and seven water molecules, respectively. The plot shows a decrease in the O−H bond dipole moment corresponding to n = 6 for trifluoroacetic acid, n = 8 for benzoic acid and n = 7 for oxalic acid hydrated clusters, whereas there is no such significant variation in case of acetic acid hydrated clusters, where even with eight water molecules, proton transfer is not observed.

5.2.3 IR spectra

On the basis of the previously reported experimental values[114,115] of stretching frequency of CF_3COOH ($\nu_{O\text{-}H}$ = 3587 cm^{-1}) and calculated harmonic data ($\omega_{O\text{-}H}$ = 3822 cm^{-1}) at ωB97X-D/aug-cc-pVDZ level, 0.94 is considered to be the anharmonic scaling factor for tfa and its hydrated clusters. The ratio of experimental stretching frequency of H_2O (ν_{sym} = 3657 cm^{-1}, ν_{asym} = 3756 cm^{-1}) to calculated harmonic data (ω_{sym} = 3881 cm^{-1}, ω_{asym} = 3992 cm^{-1}), at ωB97X-D/aug-cc-pVDZ level, is also 0.94. Scaled frequencies for free water are thus calculated as 3645 and 3753 cm^{-1}, respectively, for symmetrical stretching (ω_{sym}) and asymmetrical stretching (ω_{asym}). Present calculated scaled stretching frequencies of C-F, C=O and O−H bonds in free tfa are 1143, 1783, and 3592 cm^{-1}, respectively. Frequencies of hydrated clusters of tfa are also calculated with the same scaling factor, and the acidic O-H stretching frequencies and their red-shift, with respect to free acid, are supplied in Table 5.3. Simulated IR spectrum of isolated free water molecule is presented in Figure 5.2 (a). IR peaks due to asymmetric stretching, symmetric stretching and bending modes in H_2O are computed at 3753, 3645 and 1530 cm^{-1}, respectively. The IR spectrum of free tfa molecule in the gas phase is displayed in Figure 5.2 (b), showing a peak at 3592 cm^{-1} corresponding to O−H stretching mode and at 1783 cm^{-1} corresponding to C=O stretching. The peak at 1357 cm^{-1} in the IR spectrum is for C−C stretching mode, and large intensity peaks around 1100 cm^{-1} correspond to different stretching modes of C−F bonds.

Table 5.3 Scaled IR stretching frequency of acidic O-H bond (ν_{O-H}) of hydrated carboxylic acid, RCOOH.nH$_2$O, n=0-8 systems. The red-shift of the O-H stretching frequency ($\Delta\nu_{O-H}$) of the carboxylic acid of the hydrated clusters, with respect to free acid molecule is also given.[a]

n	$CF_3COOH.nH_2O$		$CH_3COOH.nH_2O$		$C_6H_5COOH.nH_2O$		$(COOH)_2.nH_2O$	
	ν_{O-H}	$\Delta\nu_{O-H}$	ν_{O-H}	$\Delta\nu_{O-H}$	ν_{O-H}	$\Delta\nu_{O-H}$	ν_{O-H}	$\Delta\nu_{O-H}$
	(cm^{-1})							
0	3592	-	3549	-	3567	-	3475	-
1	3142	-450	3222	327	3208	359	3035	-440
2	2808	-784	3014	535	2999	568	2909	-566
3	2699	-893	3002	547	2982	585	2807	-668
4	2354	-1238	2745	804	2676	891	2869	-606
5	1969	-1623	2815	734	2864	703	2837	-638
6	454	-3138	2962	587	2823	744	2249	-1226
7	214	-3378	2168	1381	2763	804	257	-3218
8	-	-	2619	930	192	3375	-	-

[a]References [117,119,126,127]

Figure 5.2 (c) reports simulated IR spectrum of monohydrated cluster of tfa. The strongest IR band at 3142 cm^{-1} corresponds to O−H stretching of tfa, and IR peak at 1746 cm^{-1} is due to C=O stretching. Thus, on hydration of tfa by a single H$_2$O molecule, a large red shift of 450 cm^{-1} for O−H stretching mode is noted. A very small red shift of 37 cm^{-1} is also seen for C=O stretching mode. It is interesting to observe that while symmetric stretching of H$_2$O gets red-shifted by 90 cm^{-1}, a blue shift of 38 cm^{-1} is seen for the asymmetric stretching mode. A weak band is also observed at 171 cm^{-1} for the H bond between O atom of H$_2$O and transferring H atom of tfa. In di-hydrated cluster, a red shift of 784 cm^{-1} is obtained compared with the isolated tfa molecule for stretching mode of O−H bond. IR bands higher than 3000 cm^{-1} in Figure 5.2 (d) are due to H-bonded and free O−H bond stretching frequencies in solvent H_2O molecules. The peak at 3449 cm^{-1} is due to the stretching mode of H bond between carbonyl O atom and H atom of solvent H_2O, while the same at 3270 cm^{-1} refers to inter water H bonding in the hydrated cluster. A weak band at 3706 cm^{-1} is assigned to stretching of free O−H bond of water molecules. Band due to the formation of H bond between O atom of solvent H_2O and transferring H atom of tfa is predicted at 188cm^{-1} that is blue-shifted by 17 cm^{-1} compared with mono-hydrated cluster. IR band due to C=O stretching mode of tfa in this di-hydrated cluster is observed at 1732cm^{-1}, which is red-shifted by 51 cm^{-1}.

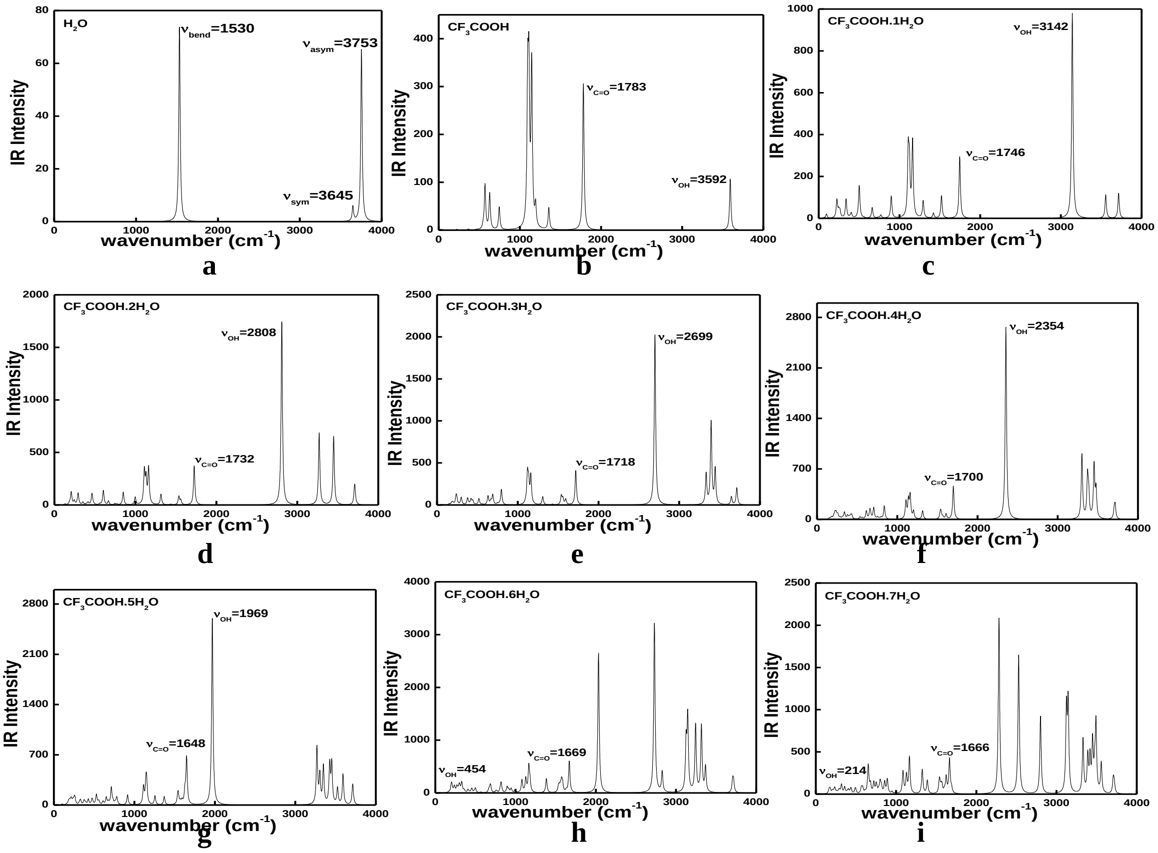

Figure 5.2 Simulated scaled IR spectra of (**a**) H_2O and (**b-i**) $CF_3COOH.nH_2O$, n=0-7, clusters calculated at ωB97X-D/aug-cc-pVDZ level of theory. Calculated scaled O-H (ν_{O-H}) and C=O ($\nu_{C=O}$) stretching frequencies of the acid molecule (in cm^{-1}) are also given.

Calculated IR spectrum of tri-hydrated cluster is depicted in Figure 5.2 (e) showing IR band at 2699 cm^{-1}, which corresponds to O−H stretching of tfa. IR band for this rupturing O−H bond is red-shifted by 893 cm^{-1}, and the IR peak due to formation of hydrogen bond between O atom of solvent H_2O and transferring H atom of tfa is blue-shifted by 130 cm^{-1}. Band for C=O stretching mode of tfa is calculated at 1718 cm^{-1}, suggesting a red shift of 65 cm^{-1}. A strong band predicted at 3395 cm^{-1} refers to stretching mode of H bond between carbonyl O atom and H atom of H_2O. IR peaks observed beyond 3500 cm^{-1} are due to stretching of free O−H bond of H_2O units, and bands in the 3300−3500 cm^{-1} range are assigned to O−H bonds of water that are H-bonded either to tfa or to another H_2O. O−H stretching of tfa (2354 cm^{-1}) is further red-shifted on addition of another solvent watermolecule to tri-hydrated cluster of tfa. IR spectrum of the most stable structure of tfa·4H_2O cluster is displayed in Figure 5.2 (f). A very weak band appearing at 317 cm^{-1} is due to the newly formed hydrogen bond between O atom of solvent H_2O and transferring H atom of tfa. IR peak observed at 1700 cm^{-1} is due to C=O stretching mode of tfa, and this is red-shifted by 83 cm^{-1} compared with free tfa. The band predicted at 3301 cm^{-1} is assigned to stretching mode of the H bond between carbonyl O atom and H atom of water and peak positions beyond this band represents stretching vibrations of inter water hydrogen-bonded O−H bond and free O−H bond of solvent H_2O molecules. In the case of penta-hydrated cluster of tfa, the calculated red shift of the peak position due to O−H stretching of tfa in IR spectrum is 1623 cm^{-1}, as shown in Figure 5.2 (g). Because of shortening of H-bond length between O atom of H_2O and transferring H atom of tfa, the corresponding IR band is blue-shifted by 148 cm^{-1}. The peak due to C=O stretching is also predicted to be red-shifted. Peaks in the region of 3200−3700 cm^{-1} are due to O−H bonds; those are H-bonded either to another solvent molecule or to tfa in this penta-hydrated cluster. One can easily notice that the calculated red shift for O−H stretching mode in tfa is systematically larger from monohydrated to penta-hydrated cluster. However, the calculated red shift for C=O stretching mode in tfa, because of the formation of hydrogen bond between carbonyl O atom and H atom of nearest solvent H_2O molecule, is not as significant. At the same time, because of the formation of new hydrogen bond between transferring H atom and O atom of nearest solvent H_2O, a blue shift in the IR peak position is observed in these hydrated clusters, and the shift is systematically larger from di-hydrated to penta-hydrated cluster. Calculated IR spectrum for the minimum energy structure of hexa-hydrated cluster is shown in Figure 5.2 (h). Note that the proton of tfa is transferred to the solvent water molecule in this structure. IR peaks at 2033 and 2730cm^{-1} are assigned to O−H asymmetric stretching frequencies of H_3O^+. The peak at 2827 cm^{-1} refers to the symmetric stretching of O−H bonds in H_3O^+, indicating a large blue shift in the newly formed O−H bond in this system. Bands past 3600 cm^{-1} refer to water O−H bonds that are not H-bonded. Peaks in the range of 3000−3500 cm^{-1} are because of H-bonded O−H bonds of water. Stretching of C=O and C−O bonds of tfa in this cluster are coupled to bending motions of H_3O^+ unit. A weak band at 454 cm^{-1} assigned to the stretching of the rupturing O−H bond in tfa undergoes a huge red shift of 3138 cm^{-1}.In the case of hepta-hydrated cluster, symmetric stretching of O−H bonds in H_3O^+ is at 2800 cm^{-1}, and bands at 2283 and2528 cm^{-1} in Figure 5.2 (i) are assigned to asymmetric modes of O−H bonds in H_3O^+. Bands beyond 3700 cm^{-1} refer to water O−H bonds that are not H-bonded, and bands due to H-bonded O−H bonds of water are predicted in 3000−3700 cm^{-1} range. A weak band at 214 cm^{-1} is observed that refers to stretching of the rupturing O−H bond in tfa. Similar salient features are noted in the IR spectra of hydrated clusters of acetic acid, benzoic acid and oxalic acid molecules. The prominent aspects of their IR spectra are alone discussed, which has relevance to the dissociation of the acid molecule.

In the case of free acoh, the experimentally reported[132] O−H stretching frequency (ν_{OH}) is 3566 cm^{-1} whereas the calculated value is 3829 cm^{-1}. The average scaling factor for the O−H stretching frequency, considering acoh, acoh.1H_2O, and acoh.2H_2O is 0.93. The scaled O−H stretching (ω_{OH}) in free acetic acid is thus 3549 cm^{-1}.With the addition of a water molecule to the acetic acid molecule, the O-H stretching frequency of the −COOH group, ω_{OH}, in acoh.1H_2O, is observed to be red-shifted to 3222 cm^{-1}. Simulated scaled IR spectra of acetic acid (acoh) and its hydrated clusters, acoh.nH_2O (n = 1−8), are provided in Figure 5.3 (a)-(i).

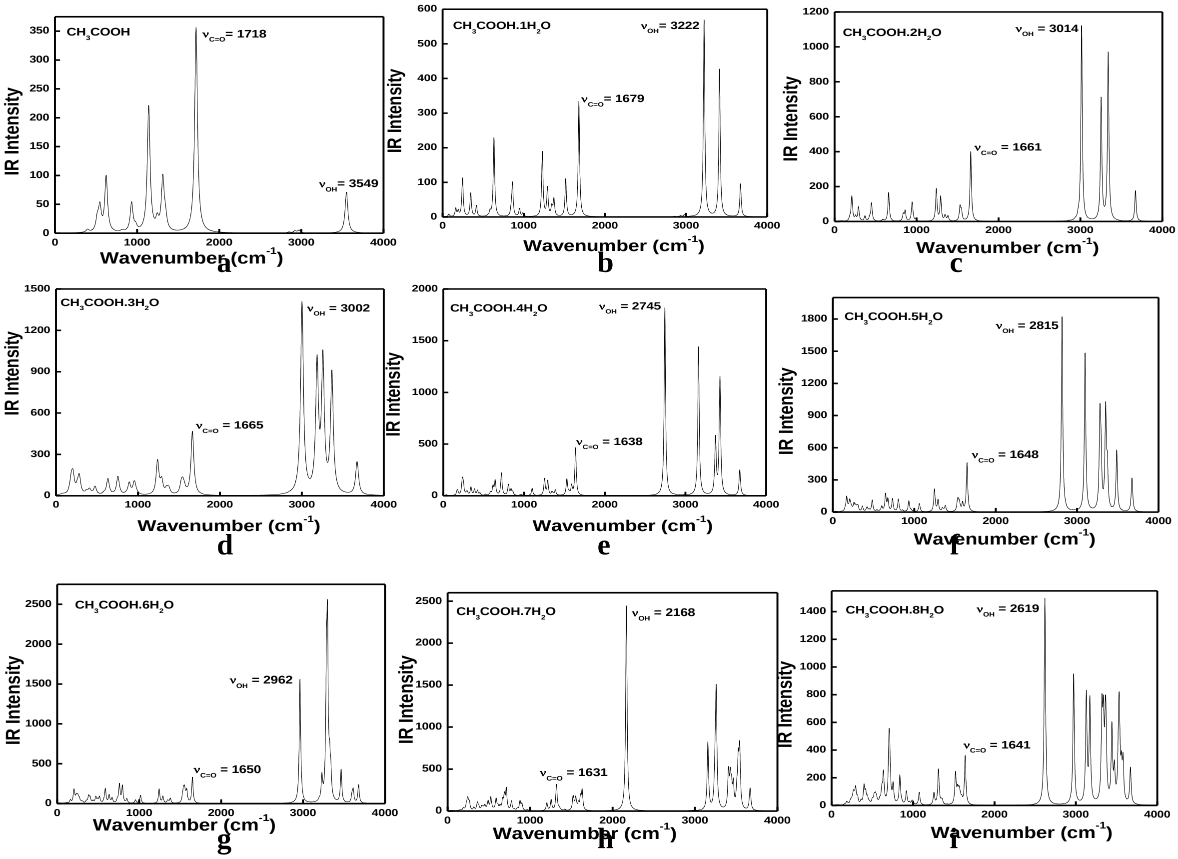

a b c d e f g h i

Figure 5.3 (a-i) Simulated scaled IR spectra of $CH_3COOH.nH_2O$, n=0-8, clusters calculated at ωB97X-D/aug-cc-pVDZ level of theory. Calculated scaled O-H ($\nu_{O\text{-}H}$) and C=O ($\nu_{C=O}$) stretching frequencies of the acid molecule (in cm^{-1}) are also given.

Similarly, for the di-hydrated cluster, the O-H stretching frequency of acetic acid is calculated to be red-shifted to 3014 cm^{-1} compared to the available experimental value of 2992 cm^{-1}. In the case of acoh.3H$_2$O and acoh.4H$_2$O clusters, the calculated ω_{OH} is 3002 and 2745 cm^{-1}, respectively. The O−H stretching frequency of acetic acid in the penta-hydrated cluster, though red-shifted compared to that of the free acid by 734 cm^{-1}, is slightly blue-shifted relative to that for acoh.4H$_2$O ($\Delta\omega_{OH}$ = 804cm^{-1}). The acoh.6H$_2$O also has a slight blue shift compared to acoh.5H$_2$O but is red-shifted by 587 cm^{-1} compared to free acoh. The cage-like hepta-hydrate has a largely red-shifted ω_{OH} of 2168 cm^{-1}. However, the calculated ω_{OH} of acoh.8H$_2$O is 2619 cm^{-1}, showing that the O-H bond is not as weakened as in the case of the hepta-hydrate. The calculated scaled IR stretching frequencies of the O−H bond of the −COOH group of acetic acid hydrated clusters are given in Table 5.3. There is no characteristic change observed in the scaled C=O stretching frequencies ($\omega_{C=O}$) of hydrated acetic acid clusters.

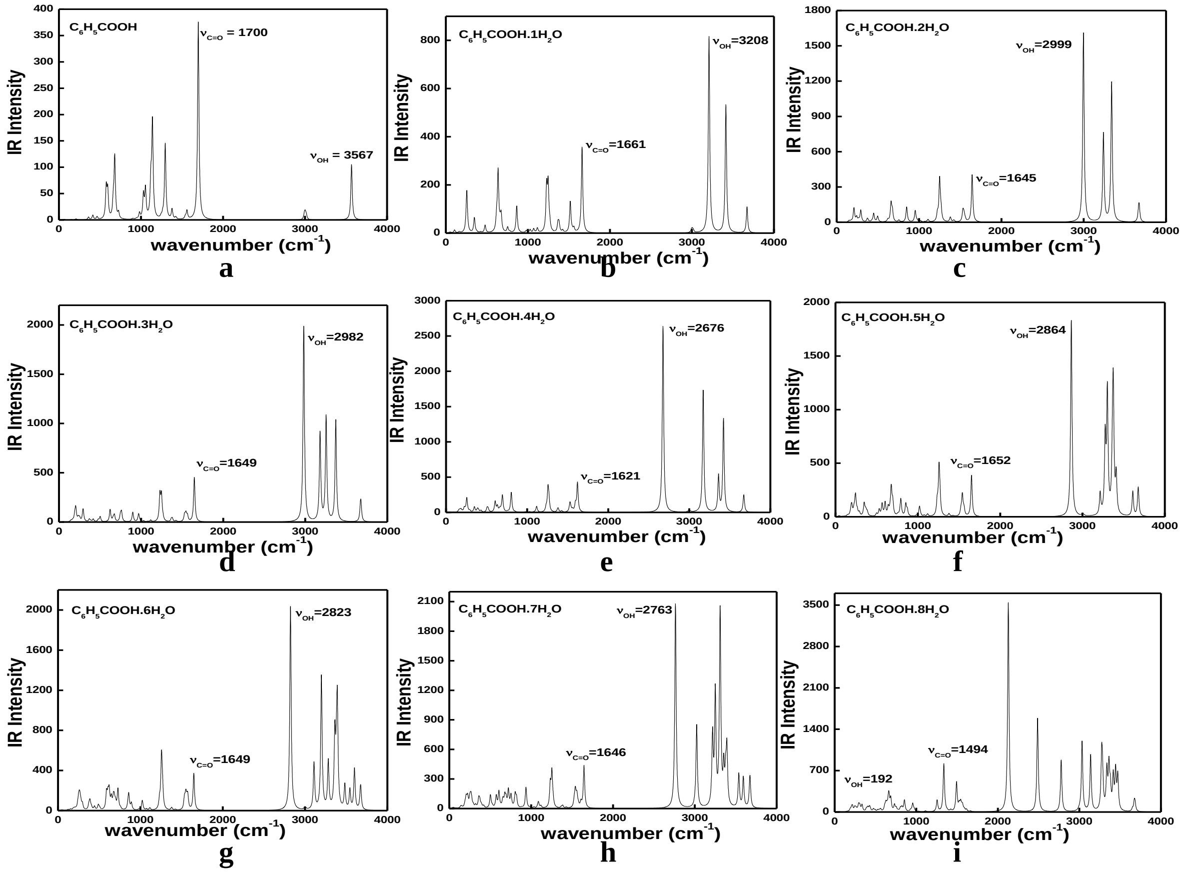

Figure 5.4 (a-i) Simulated scaled IR spectra of C$_6$H$_5$COOH.nH$_2$O, n=0-8, clusters calculated at ωB97X-D/aug-cc-pVDZ level of theory. Calculated scaled O-H (ν_{O-H}) and C=O ($\nu_{C=O}$) stretching frequencies of the acid molecule (in cm^{-1}) are also given.

Simulated scaled IR spectra of hydrated clusters of benzoic acid molecule are given in Figure 5.4 (a)-(i). The harmonic OH stretching frequency for free benzoic acid molecule, calculated at the current level of theory, is 3838 cm^{-1} while that which is experimentally observed is 3567 cm^{-1}.[133] Due to lack of experimental data, for higher hydrates of benzoic acid, O-H stretching frequency of benzoic acid is the taken as the basis for calculating scaling factor. Scaling factor, determined by taking the ratio of experimental to calculated O-H stretching frequency, is 0.93. The scaled O-H stretching frequencies of hydrated clusters of benzoic acid are given in Table 5.3. The red-shift of carboxylic O-H stretching frequency in the hydrated clusters with respect to free benzoic acid molecule is also given. It is seen that moving from the unionized hepta-hydrate to the ionized octa-hydrate, there is a large red-shift of 2571 cm^{-1}. Though red-shift in C=O stretching frequency due to the weakening of carbonyl bonds is also expected, no significant red-shift is observed in the C=O peaks of hydrated benzoic acid clusters. The newly formed peaks corresponding to the hydronium ions are clearly observed in case of bz.8H_2O.

The calculated O-H stretching frequency of free oxalic acid molecule, based on harmonic approximation is 3720 cm^{-1} while the experimentally reported value is 3475 cm^{-1}.[124] The scaling factor, taking the ratio of experimental to calculated O-H stretching frequency of oxalic acid molecule, is determined to be 0.93. The scaled O-H stretching frequencies of the most acidic O-H bond of the hydrated clusters of oxalic acid, as well their shift with respect to isolated oxalic acid molecule, are given in Table 5.3. The symmetric free oxalic acid molecule has a calculated scaled O-H stretching frequency of 3475 cm^{-1}. For hydrated clusters of oxalic acid, the nomenclature given in Chapter 3 is followed. With the addition of a water molecule, the O1-H bond elongates while there is no significant change in O2-H bond length. There is a red shift of 440 cm^{-1} in the calculated O1-H stretching frequency while for O2-H stretching frequency, it is only 83 cm^{-1}. Similarly, for di and tri-hydrate of oxalic acid molecule, where the water molecules form hydrogen bonds with only O1-H bond and not O2-H bond, the red shift in the calculated O1-H stretching frequency are 566 and 668 cm^{-1} respectively. The red shifts in O2-H stretching frequency in both cases are negligible.

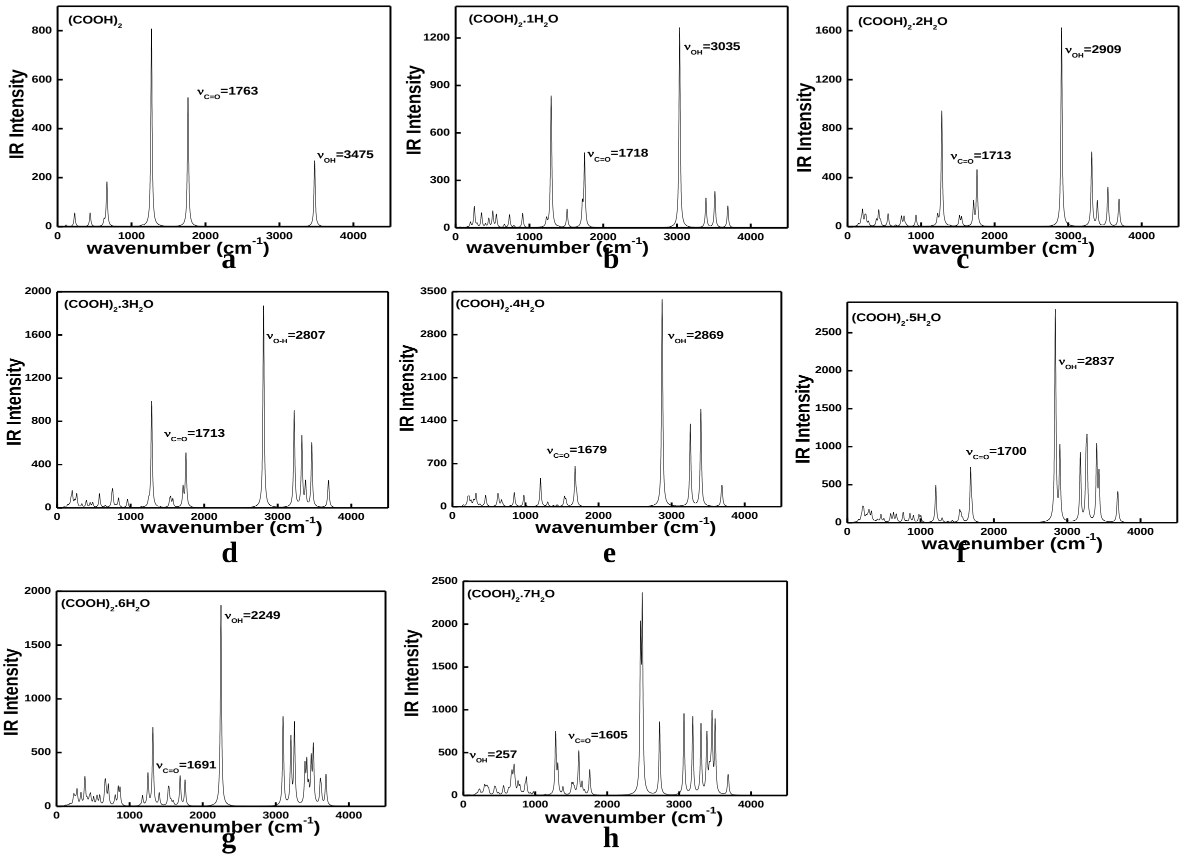

Figure 5.5 (a-h) Simulated scaled IR spectra of (COOH)$_2$.nH$_2$O, n=0-7, clusters calculated at ωB97X-D/aug-cc-pVDZ level of theory. Calculated scaled O-H ($\nu_{O\text{-}H}$) and C=O ($\nu_{C=O}$) stretching frequencies of the acid molecule (in cm^{-1}) are also given.

The symmetric oxa.4H$_2$O has calculated O-H stretching frequency of 2869 cm^{-1}. The penta-hydrate of oxalic acid molecule has three water molecules hydrogen bonded to one hydroxyl bond and two water molecules hydrogen bonded to the other hydroxyl bond of the acid molecule. The calculated red shift in O1-H and O2-H stretching frequencies are 638 and 576 cm^{-1}, respectively. In the hexa-hydrate, the solvent water molecules are concentrated more on one of the hydroxyl bonds. This is reflected in the red shifts of O1-H and O2-H stretching frequencies. The red shift for O1-H is 1226 cm^{-1} while that for O2-H is only 26 cm^{-1}. It is interesting to note that for oxa.7H_2O, upon the dissociation of the oxalic acid molecule, the calculated O1-H stretching frequency has a very large red shift of 3218 cm^{-1}. There is no significant change in O2-H stretching frequency. The very large red shift of the O1-H stretching frequency is an indication of the hydroxyl bond dissociation of the oxalic acid molecule. The IR spectrum of the hepta-hydrate also shows formation of new peaks corresponding to the stretching frequencies of hydrated proton. The simulated, scaled IR spectra of oxalic acid and its hydrated clusters are given in Figure 5.5 (a)-(h). Not much change is observed in the carbonyl stretching frequencies of the hydrated oxalic acid clusters.

5.2.4 Bond dissociation curve

A rigid potential energy scan of the acidic O-H bond can help in understanding the energy barrier for the proton transfer from the acid molecule to the neighboring water molecule in hydrated clusters of carboxylic acid molecules. The relative energy of the system, at each variation of the acidic O-H bond, with respect to the equilibrium geometry of that size cluster, is plotted against the varying O-H bond length to get the O-H bond dissociation curve. O-H bond length of ~1.0 Å implies that the proton is still with the acid molecule while O-H bond distance of 1.4 Å and beyond is a clear indication that the proton has transferred from the acid to water molecule. Depending on the position of the energy minima with respect to the O-H bond length, the process of proton transfer from the acid to water molecule can be explained. In case of $CF_3COOH.nH_2O$, the O-H bond dissociation curve is given in Figure 5.6.

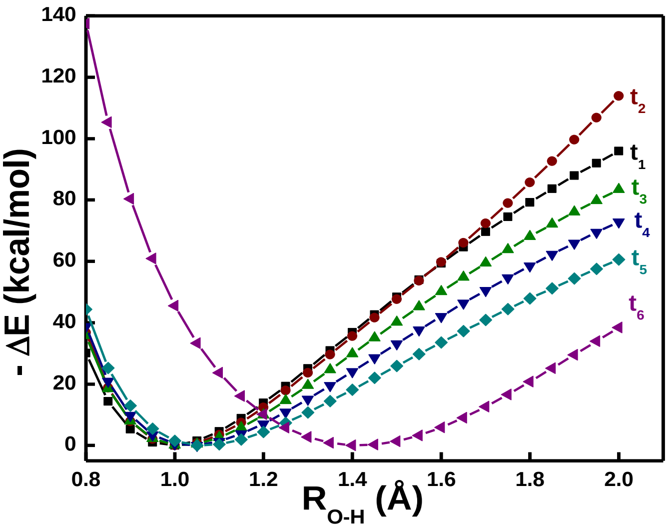

Figure 5.6 Rigid potential energy scan of O-H bond of $CF_3COOH.nH_2O$, n=1-6, calculated at ωB97X-D/aug-cc-pVDZ level of theory. ΔE gives the relative energy of the system at each point of the scan of the dissociating O-H bond, with respect to the energy of the equilibrium geometry. Curves marked as t_n (n=1-6) represents potential energy surface of hydrated cluster having n solvent water molecules upon increasing bond length of dissociating O-H bond of the acid.

Up to penta-hydrated cluster, the energy minima of the dissociation curve is found to be around 1.0 Å. Increasing the O-H bond length further causes an increase in the energy of the system. However, in case of $CF_3COOH.6H_2O$, the minimum in energy for the acidic O-H bond dissociation curve is when the O-H bond length is ~1.4 Å, indicating the transfer of proton from the acid to water molecule. The destabilization of the system due to increase in O-H bond length does not seem to follow any particular order. The degree of destabilization depends on the ability of the geometry of the hydrated cluster to accommodate the increase in O-H bond length. Maximum destabilization is observed for $CF_3COOH.2H_2O$.

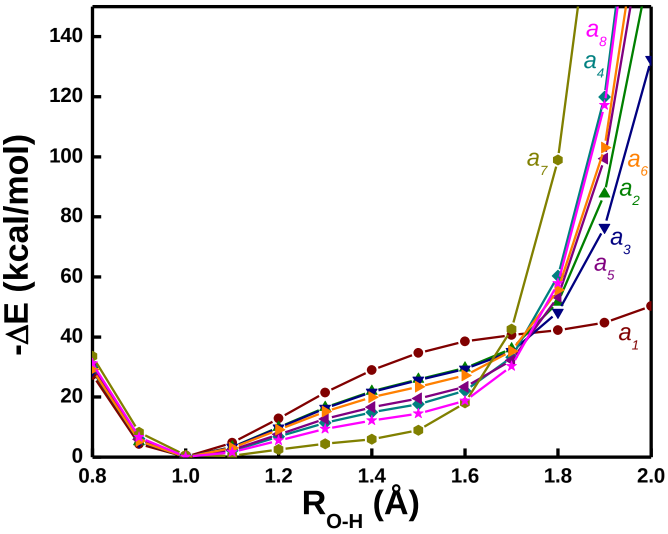

Figure 5.7 Rigid potential energy scan for O-H bond of $CH_3COOH.nH_2O$, n=1-8, calculated at ωB97X-D/aug-cc-pVDZ level of theory. ΔE gives the relative energy of the system at each point of the scan of the dissociating O-H bond, with respect to the energy of the equilibrium geometry. Curves marked as a_n (n=1-8) represents potential energy surface of hydrated cluster having n solvent water molecules upon increasing bond length of dissociating O-H bond of the acid.

For acetic acid hydrated clusters, the dissociation curve for acidic O-H bond has a minimum when O-H bond length is ~1.0 Å. With further elongation of the O-H bond, an increase in energy is observed, indicating that there is a barrier for proton transfer from the acid molecule to the water molecule. Though the energy barrier for proton transfer is observed to decrease with the addition of water molecules, it is seen that even with eight water molecules, a barrier-less transfer of proton is not achieved. The dissociation curve of the O-H bond for hydrated clusters of acetic acid molecule is given in Figure 5.7.

In case of benzoic acid-water clusters, the bond dissociation curve for acidic O-H bond is given in Figure 5.8. As can be seen from the figure, the energy minimum for the dissociation curve of the acidic O-H bond of $C_6H_5COOH.nH_2O$, n=1-7, systems is when O-H bond length is ~1.0 Å. Increasing the O-H bond length further, increases the energy of the system. Thus proton transfer from the acid molecule to water molecule is not observed in these cases.

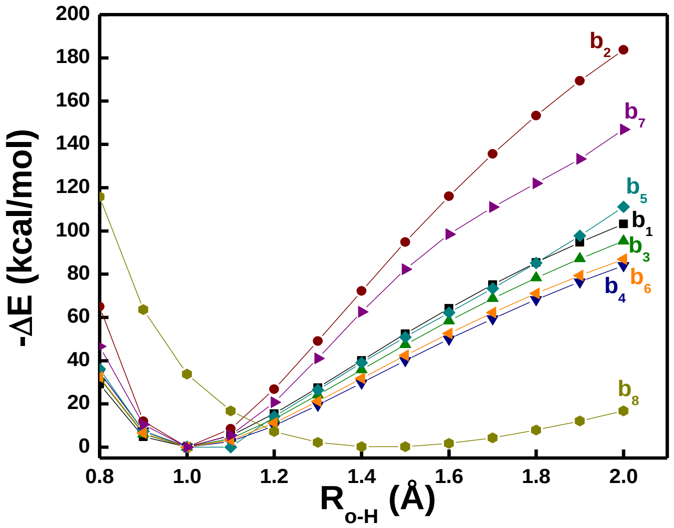

Figure 5.8 Rigid potential energy scan for O-H bond of $C_6H_5COOH.nH_2O$, n=1-8, calculated at ωB97X-D/aug-cc-pVDZ level of theory. ΔE gives the relative energy of the system at each point of the scan of the dissociating O-H bond, with respect to the energy of the equilibrium geometry. Curves marked as b_n (n=1-8) represents potential energy surface of hydrated cluster having n solvent water molecules upon increasing bond length of dissociating O-H bond of the acid.

For $C_6H_5COOH.8H_2O$, the energy is very high when O-H bond length is 1.0 Å. The energy decreases with increase in O-H bond length and equilibrium O-H bond length is seen to lie between 1.4 and 1.6 Å. This implies that the most stable conformer of octa-hydrated benzoic acid will show proton transfer from the acid molecule to the water molecule. The degree of destabilization, due to elongation of the acidic O-H bond is observed to be highest in $C_6H_5COOH.2H_2O$. The destabilization of the hydrated system depends on the inability of the cluster to accommodate the increase in O-H bond length, and does not follow any order, as can be seen from Figure 5.8. The dissociation curve of one of the hydroxyl bonds of oxalic acid molecule shows that except for hepta-hydrated oxalic acid cluster, there is a barrier for proton transfer from the acid molecule to solvent water molecules, as shown in Figure 5.9.

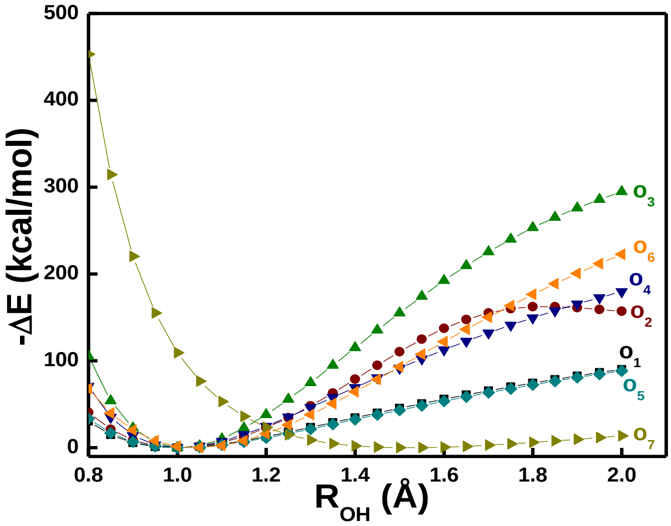

Figure 5.9 Rigid potential energy scan for O-H bond of $(COOH)_2.nH_2O$, n=1-7, calculated at ωB97X-D/aug-cc-pVDZ level of theory. ΔE gives the relative energy of the system at each point of the scan of the dissociating O-H bond, with respect to the energy of the equilibrium geometry. Curves marked as O_n (n=1-7) represents potential energy surface of hydrated cluster having n solvent water molecules upon increasing bond length of dissociating O-H bond of the acid.

A rigid potential energy scan, keeping all but the length of dissociating O-H bond of the acid-water cluster constant shows an energy minimum when the acidic O-H bond length is around 1.0 Å for oxa.nH_2O, n=1-6. There is an increase in energy with further elongation of the O-H bond length implying that there is barrier for the process of proton transfer from the acid molecule to solvent water molecule. In the hepta-hydrated oxalic acid cluster, however, the energy is high when O-H bond length is 1.0 to 1.2 Å. It is observed to decrease beyond O-H bond length of 1.4 Å. This implies that the proton is already transferred to the solvent water molecule in this size of hydrated cluster. The bond dissociation curve provides further confirmation that first dissociation of oxalic acid occurs in presence seven solvent water molecules. It also signifies that in presence of seven water molecules, barrier for the transfer of proton from oxalic acid to solvent water molecule becomes zero. The degree of destabilization of the hydrated clusters of oxalic acid (excluding hepta-hydrate) with increase in O-H bond distance does not follow any particular order as this depends on the geometry of the hydrated acid cluster and its ability to accommodate the elongated hydroxyl bond. It is noted that the destabilization of oxa.1H_2O and oxa.5H_2O are relatively low when compared to other hydrated acid clusters while the highest destabilization is observed in case of oxa.3H_2O.

5.2.5 Hydrogen Bond Energy

The dissociation of the acidic O-H bond as well as the strengthening of the H bond between the acidic H atom and the O atom of the nearest water molecule,

Table 5.4 Hydrogen bond energy of acidic O-H bond (E_{O-H}) and H..O(H_2) bond ($E_{H..O(H2)}$) in the most stable conformers of hydrated carboxylic acid, RCOOH.nH_2O, n=0-8 systems.

n	$CF_3COOH.nH_2O$		$CH_3COOH.nH_2O$		$C_6H_5COOH.nH_2O$		$(COOH)_2.nH_2O$	
	E_{O-H}	$E_{H..O(H2)}$	E_{O-H}	$E_{H..O(H2)}$	E_{O-H}	$E_{H..O(H2)}$	E_{O-H}	$E_{H..O(H2)}$
	in kcal/mol							
0	211.4	-	210.9	-	211.5	-	210.5	--
1	196.4	10.9	201.7	8.6	201.1	8.9	193.2	13.0
2	179.5	17.1	192.2	12.4	191.1	12.9	186.4	14.9
3	172.6	19.7	191.4	13.2	190.3	13.8	181.1	17.1
4	153.7	27.4	178.1	18.1	173.9	19.8	184.2	15.0
5	130.7	35.8	182.1	16.8	184.4	15.0	182.1	16.5
6	35.9	136.4	189.6	14.1	182.2	16.1	146.9	29.8
7	19.1	177.9	143.8	30.5	179.8	17.0	23.2	169.7
8	-	-	169.9	20.2	31.7	144.8	-	-

H..O(H_2), can be tracked to study the proton transfer in the hydrated carboxylic acid clusters. Table 5.4 gives the hydrogen bond energy of the acidic O-H bond and the forming H..O(H_2) bond. Hydrogen bond energy for acidic O-H and H..O(H_2) bonds shows that the former decreases and the latter increases, as the size of the cluster increases. It is seen that the hydrogen bond energy value for acidic O-H bond is higher than that of H..O(H_2), when the proton resides with acid molecule while the reverse is observed when proton transfer occurs. This is expected as before ionization, the acidic O-H bond is stronger while after ionization, the H..O(H_2) bond is stronger.

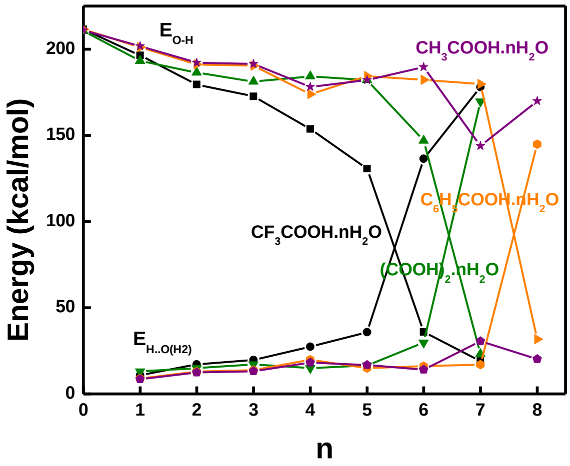

Figure 5.10 Variation of hydrogen bond energy of most acidic O-H bond ($E_{O\text{-}H}$) and H..O(H_2) bond ($E_{H..O(H2)}$) of hydrated clusters of carboxylic acids with increase in size of the hydrated cluster (n). The violet, green, black and orange line shows the hydrogen bond energy of $CH_3COOH.nH_2O$, $(COOH)_2.nH_2O$, $CF_3COOH.nH_2O$ and $C_6H_5COOH.nH_2O$, n=1-8, clusters respectively, calculated at ωB97X-D/aug-cc-pVDZ level of theory.

The H..O(H_2) bond increases in strength with addition of more water molecules, and finally when the proton transfer occurs from the acid molecule to solvent water molecules, the H..O(H_2) bond becomes stronger than the O-H bond of the acid. The variation of hydrogen bond energy of acidic O-H and H..O(H_2) bonds of hydrated clusters of the carboxylic acids are given in Figure 5.10. The cross over in the hydrogen bond energy profiles of the two bonds can be taken as an indication for bond dissociation of the acid molecule. It is seen that cross-over occurs at n=6, n=7 and n=8 for $CF_3COOH.nH_2O$, $(COOH)_2.nH_2O$ and $C_6H_5COOH.nH_2O$ respectively. No such cross-over is observed in case of $CH_3COOH.nH_2O$, implying that even eight water molecules are not sufficient to break the acidic O-H bond in acetic acid molecule.

5.3 Conclusion

The dissociation of hydrated carboxylic acid molecules, to form contact ion pairs, will be reflected in some of its properties. Analyzing some of the properties reveal that while static polarizability and net dipole moment show no characteristic features corresponding to proton transfer, the acidic O-H bond dipole, IR spectra, O-H bond dissociation curve and hydrogen bond energy give indication about the formation of contact ion pair.

Static polarizability of the acid-water clusters is observed to vary linearly with the size of the clusters (n). Hence, though prediction of static polarizability of higher hydrates of the acid clusters can be done very reliably (regression value > 0.99), it does not give an indication about the formation of contact ion pair.

The net dipole moment of hydrated acid clusters depend on the geometry of the system. The direction of the dipole moment vector is not always aligned with the breaking O-H bond of the acid molecule and thus cannot indicate the formation of contact ion pair. The bond dipole moment of the dissociating O−H bond does show a characteristic feature of acid dissociation in case of hydrated clusters of trifluoroacetic acid, benzoic acid and oxalic acid. A sharp dip is seen in the acidic O-H bond dipole moment, in case of the ionized acid clusters when compared to unionized clusters. Such a dip is absent in case of acetic acid hydrated clusters, where even with eight water molecules, proton transfer does not occur.

To compare with experimental data, IR spectral properties of the acid hydrates are simulated. A strong correlation is found between the reported values and the present calculated data. The formation of a charge-separated ion pair is manifested in simulated IR spectra. IR spectra for the most stable structures of each size hydrated acid clusters are simulated, and the variation in acidic O-H peak positions is in accordance with the extent of elongation of the O−H bond in the acid molecule. In the case of tfa, a minimum of six water molecules are needed for ionization, which is characterized by formation of new peaks in the hexa-hydrated cluster corresponding to stretching frequencies of hydrated proton. Similarly huge red shift; with respect to isolated acid molecule, is observed in the hydroxyl bond stretching frequency of $C_6H_5COOH.8H_2O$ and $(COOH)_2.7H_2O$, along with formation of new IR peaks. This indicates the dissociation of the O-H bond of the acid molecule and proton transfer from the acid molecule to solvent water molecules. $CH_3COOH.nH_2O$ systems provide no such observations.

A rigid potential energy scan, altering the dissociating hydroxyl bond, shows that there is a barrier in proton transfer from the acid to water molecules in case of mono to penta-hydrate of trifluoroacetic acid, mono to hepta-hydrate of benzoic acid, mono to octa-hydrate of acetic acid and mono to hexa-hydrate of oxalic acid. In the case of hexa, octa and hepta-hydrates of trifluoroacetic acid, benzoic acid and oxalic acid, the transfer is barrier-less.

The hydrogen bond energy profiles of the dissociating hydroxyl bond of the acid molecule and the hydrogen bond between the acidic H atom of the acid molecule and the O atom of the nearest water molecule shows characteristic features upon dissociation of the acid molecule. For trifluoroacetic acid-water clusters, hydrogen bond energy of the dissociating O-H bond is greater than the hydrogen bond energy of the forming H..O bond between the acidic H atom and the O atom of the nearest water molecule, for all except hexa and hepta-hydrates. In case of hexa and hepta-hydrates clusters the reverse is true. For benzoic acid-water clusters, the breaking O-H hydrogen bond energy is greater than that of forming H..O bond till hepta hydrated cluster but in case of octa hydrate, the same for forming H..O bond is stronger. Similarly for oxalic acid-water clusters, the hydrogen bond energy of the most acidic O-H bond of the acid molecule is greater than the forming H..O bond for $(COOH)_2.nH_2O$, n=1-6, while reverse is true for hepta-hydrate. No such cross-over in the energy profiles of the two bonds is observed in case of acetic acid molecule. These properties can be used as indicators to study microhydration in acid molecules to track proton transfer and formation of contact ion pairs.

Chapter 6

Microhydration of 2-Naphthol at Ground, First Excited Triplet and First Excited Singlet states: A Case Study on Photo Acids

---

The only existing things are atoms and empty space;
all else is mere opinion.

\- Democritus of Abdera d. 370B.C.

Photo acids undergo significant enhancement in their acidity upon electronic excitation. This leads to excited state proton transfer to the solvent. The change in electron density distribution of a photo acid can be determined from its excited state acidity constant. This information is of much interest to both photo chemists, who can study the differences in reactivity of molecules in ground and excited state, and theoretical chemists, who can calculate the excited state electronic structure and the nature of the transitions involved. The significant change in acidity of these molecules makes them an ideal system to probe solute-solvent interactions and solvent polarities.[134] Photo acids can be used as molecular probes for determining the structural transitions of proteins under various conditions.[135] Water accessibility in biological surfaces can also be probed using photo acids.[136,137] The excited state pKa of a photo acid is generally determined from the Förster cycle, based on absorption and emission data.[138] It can also be determined using photo-potentiometry.[139]

In aqueous solution, aromatic compounds like phenol and 2-naphthol have ground state pKa values of 10.0 and 9.2 respectively, while their excited state pKa values are just 3.6 and 2.8 respectively.[140] Theoretical calculations to explain excited state proton transfer in phenols has been reported.[141] Two different explanations have been proposed for the increase in acidity in the first excited singlet state. One proposition attributes the increase in acidity to a charge transfer in the photo acid.[142,143] According to the other proposition, the enhanced excited state acidity is largely determined by the deprotonated photo acid.[141]

Jackson and Porter reported that the acidity constants of ground and first excited triplet states of 2-naphthol are comparable while that of the first excited singlet state differ by a factor of ~10^6.[15] The studies were based on flash photolysis, fluorescence and phosphorescence measurements. They provide a qualitative explanation for this observation based on electron density. The difference in the pKa value of ground state and excited states of 2-naphthol could be reflected in the number (n) of water molecules needed for their ionization. This chapter explores the microhydration of 2-naphthol (nap) at ground (nap_{S0}), first excited triplet (nap_{T1}) and first excited singlet (nap_{S1}) states, to understand the correlation between n and pKa at different electronic states.

6.1 Theoretical Methods

The ground state geometries are optimized at ωB97X-D/aug-cc-pVDZ level of theory. The first excited singlet and first excited triplet states are optimized at CAM-B3LYP/ aug-cc-pVDZ level of theory. CAM-B3LYP is a long-range corrected hybrid exchange-correlation functional designed to better describe electronic excitations and charge-transfer processes.[144–147] The excited state calculations are done using Time-Dependent DFT (TD-DFT). The input geometries are chosen such that minimum number of water molecules is needed to ionize the O-H bond of nap. The water molecules are placed in such a way so as to increase the number of hydrogen bonds formed between the solvent water molecules and nap, facilitating the easy dissociation of the O-H bond of nap. The minimum energy equilibrium structure of each size cluster at ground, first excited triplet and first excited singlet state is selected to determine the minimum number of water molecules needed to dissociate nap. A rigid potential energy scan, at CAM-B3LYP/aug-cc-pVDZ level of theory, of the most stable conformer of each size cluster, at S_0, T_1 and S_1 states, is carried out by keeping all but the dissociating O-H bond of nap constant. The potential energy profile of the hydrated nap system is obtained by plotting the relative energy, with respect to most stable structure, at each O-H bond distance against the O-H bond distance. All calculations are carried out using the general ab initio quantum package, Gaussian.[148]

6.2 Results and Discussion

6.2.1 Microhydration at ground state

At ground state, two conformers are possible for nap_{S0}. Structures of both the conformers, along with their relative energy, are given in Figure 6.1. The two structures differ in the relative position of the O-H bond with respect to the naphthalene ring. In the most stable conformer (see Figure 6.1 (i)), the O-H bond faces the ring while in the higher energy conformer, the O-H bond faces away from the ring. This is consistent with the results obtained from MP2/aug-cc-pVDZ level of theory reported recently.[149] The O-H bond length is 0.961 Å and the C-O bond length is 1.364 Å in the most stable conformer at the present level of theory.

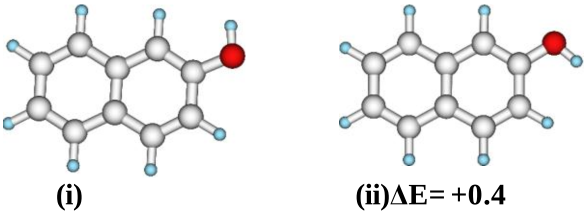

Figure 6.1 Equilibrium structures of 2-naphthol, at ground state, calculated at ωB97X-D/aug-cc-pVDZ level of theory. Zero point energy corrected relative energy (in kcal/mol) of the higher energy conformer with respect to minimum energy conformer is also given. Red balls represent oxygen, grey balls represent carbon and blue balls represent hydrogen atoms.

With the addition of a single water molecule, the most stable conformer has the H atom of the nap forming hydrogen bond with the O atom of the water molecule. The O-H bond length of the naphthol molecule increases to 0.972 Å and the C-O bond length decreases to 1.356 Å. the hydrogen bond distance between the acidic hydrogen atom of nap and the O atom of the water molecule is calculated to be 1.853 Å. Another structure is also observed for the mono-hydrate of nap ($nap_{S0}.1H_2O$), which is higher in energy than the most stable conformer by just 0.3 kcal/mol, as shown in Figure 6.2 (ii). The difference between this conformer and the most stable conformer is in the relative position of the O-

H bond of the nap with respect to the naphthalene ring. All the equilibrium conformers obtained for nap$_{S0}$.1H_2O along with their zero point corrected relative energy are given in Figure 6.2.

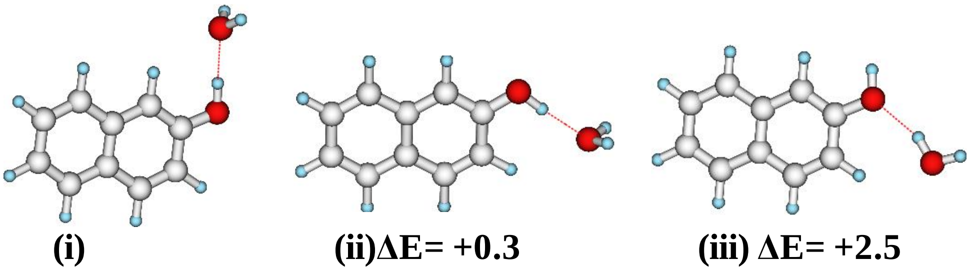

Figure 6.2 Equilibrium structures of mono-hydrate of 2-naphthol, at ground state, calculated at ωB97X-D/aug-cc-pVDZ level of theory. Zero point energy corrected relative energy (in kcal/mol) of the higher energy conformer with respect to minimum energy conformer is also given. Red balls represent oxygen, grey balls represent carbon and blue balls represent hydrogen atoms.

With two water molecules, the most stable conformer has the O-H bond of nap hydrogen bonded to the oxygen atom of one of the water molecules. The other water molecule is hydrogen bonded to the first water molecule, without direct bonding with the nap. The four equilibrium geometries obtained for the di-hydrate of nap (nap$_{S0}$.2H_2O) along with their zero point corrected relative energy is given in Figure 6.3. Unlike as observed in carboxylic acids, a closed ring motif is absent in case of the di-hydrates, possibly due to the steric strain involved in such a ring formation. The O-H and C-O bond lengths of nap in the most stable conformer are 0.994 and 1.326 Å respectively.

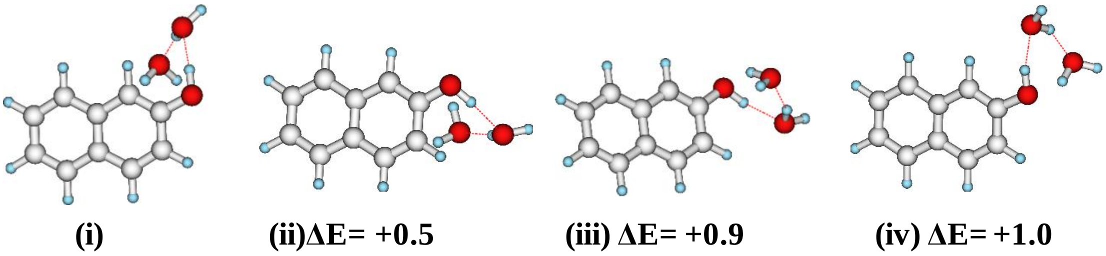

Figure 6.3 Equilibrium structures of di-hydrate of 2-naphthol, at ground state, calculated at ωB97X-D/aug-cc-pVDZ level of theory. Zero point energy corrected relative energy (in kcal/mol) of the higher energy conformer with respect to minimum energy conformer is also

given. Red balls represent oxygen, grey balls represent carbon and blue balls represent hydrogen atoms.

Six equilibrium structures are obtained for the tri-hydrate of nap ($nap_{S0}.3H_2O$), as shown in Figure 6.4. The most stable conformer has the three water molecules and the O-H bond of the nap forming hydrogen bonded close-ring motif. Open chain structures are found to be higher in energy than the closed ring conformers. The O-H and C-O bond length of nap are 0.985 and 1.362 Å respectively, for the most stable conformer of $nap_{S0}.3H_2O$, while the hydrogen bond distance between the acidic O-H of nap and the O atom of the nearest water molecule is 1.627 Å.

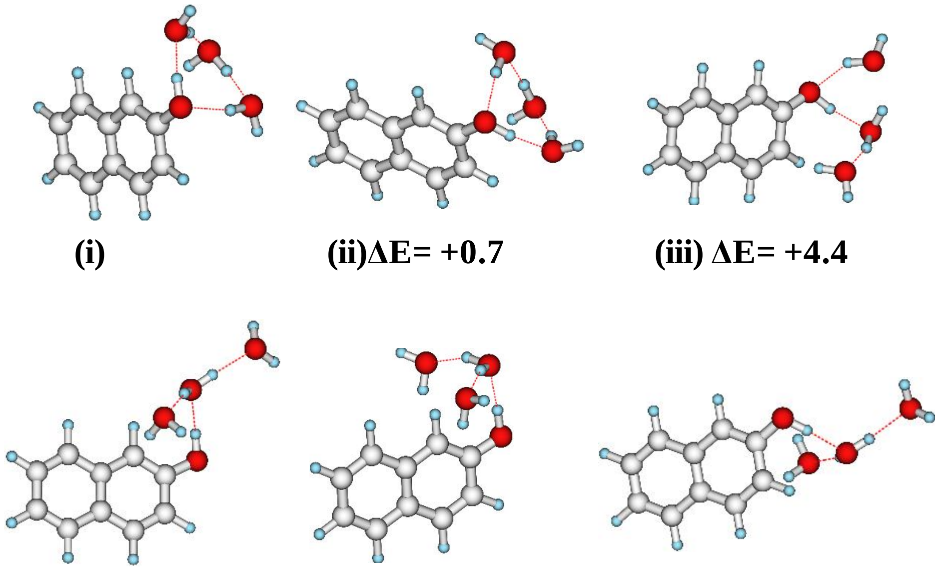

(i) **(ii)ΔE= +0.7** **(iii) ΔE= +4.4**

(iv) ΔE= +4.7 **(v)ΔE= +4.7** **(vi) ΔE= +5.3**

Figure 6.4 Equilibrium structures of tri-hydrate of 2-naphthol, at ground state, calculated at ωB97X-D/aug-cc-pVDZ level of theory. Zero point energy corrected relative energy (in kcal/mol) of the higher energy conformer with respect to minimum energy conformer is also given. Red balls represent oxygen, grey balls represent carbon and blue balls represent hydrogen atoms.

A closed ring conformer is the most stable geometry obtained for the tetra-hydrate of nap ($nap_{S0}.4H_2O$). All the six equilibrium conformers obtained for $nap.4H_2O$ are given in Figure 6.5 along with the relative energy of each conformer with respect to the most stable conformer. The O-H and C-O bond lengths of nap in the most stable conformer are 0.987 and 1.360 Å respectively.

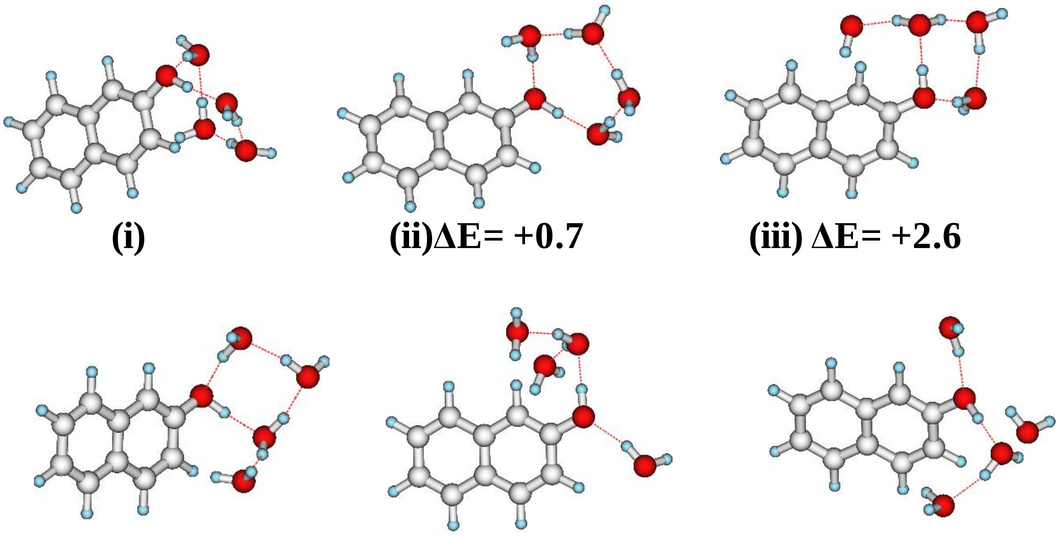

(i) **(ii)ΔE= +0.7** **(iii) ΔE= +2.6**

(iv)ΔE= +3.3 **(v) ΔE= +8.8** **(vi) ΔE= +9.0**

Figure 6.5 Equilibrium structures of tetra-hydrate of 2-naphthol, at ground state, calculated at ωB97X-D/aug-cc-pVDZ level of theory. Zero point energy corrected relative energy (in kcal/mol) of the higher energy conformer with respect to minimum energy conformer is also given. Red balls represent oxygen, grey balls represent carbon and blue balls represent hydrogen atoms.

It can be seen that none of the conformers show proton transfer from nap to the solvent water molecules at the ground state.

6.2.2 Microhydration at first excited triplet state

Of the two equilibrium conformers obtained for nap at the first excited triplet state (T1), the most stable conformer has the O-H bond facing away from the naphthalene ring. The other conformer, with O-H bond facing towards the ring, is 16.8 kcal/mol higher in energy than the most stable conformer. The O-H and C-O bond lengths of the most stable conformer are 0.961 and 1.364 Å respectively. Both the conformers are shown in Figure 6.6.

(i) **(ii) ΔE= +16.8**

Figure 6.6 Equilibrium structures of 2-naphthol, at first excited triplet state, calculated at CAM-B3LYP/aug-cc-pVDZ level of theory. Zero point energy corrected relative energy (in kcal/mol) of the higher energy conformer with respect to minimum energy conformer is also given. Red balls represent oxygen, grey balls represent carbon and blue balls represent hydrogen atoms.

With the addition of a single water molecule, the most stable conformation at first excited triplet state has the O-H bond facing away from the ring and the O atom of the water molecule forming hydrogen bond with H atom of nap. All conformations obtained for the first excited triplet state of mono-hydrate of nap ($nap_{T1}.H_2O$) are given in Figure 6.7. The O-H and C-O bond length of nap are respectively, 0.975 and 1.358 Å. The hydrogen bond distance between the hydroxyl H atom of nap and O atom of water molecule is 1.840 Å.

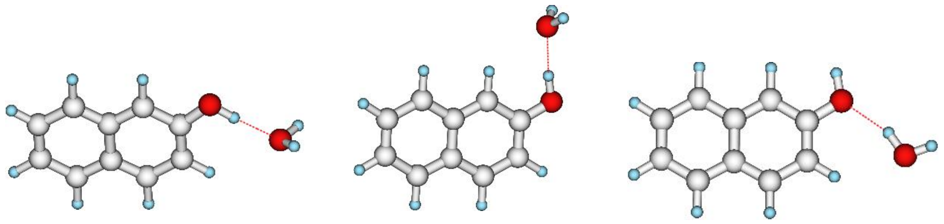

(i) **(ii) ΔE= + 16.3** **(ii) ΔE= +18.5**

Figure 6.7 Equilibrium structures of 2-naphthol.1H_2O, at first excited triplet state, calculated at CAM-B3LYP/aug-cc-pVDZ level of theory. Zero point energy corrected relative energy (in kcal/mol) of the higher energy conformer with respect to minimum energy conformer is also given. Red balls represent oxygen, grey balls represent carbon and blue balls represent hydrogen atoms.

The most stable conformation of the first excited triplet state of di-hydrate of nap ($nap_{T1}.2H_2O$) has an open chain conformation with the O-H bond facing way from the naphthalene ring as shown in Figure 6.8 (i). The O-H and C-O bond lengths are 0.979 and 1.353 Å respectively. Higher energy conformations of $nap_{T1}.2H_2O$ are also given in Figure 6.8.

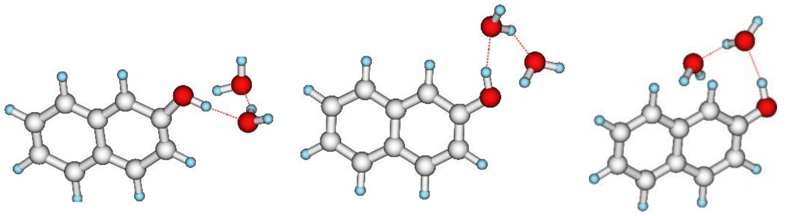
(i) **(ii) ΔE= + 14.8** **(ii) ΔE= +16.6**

Figure 6.8 Equilibrium structures of 2-naphthol.$2H_2O$, at first excited triplet state, calculated at CAM-B3LYP/aug-cc-pVDZ level of theory. Zero point energy corrected relative energy (in kcal/mol) of the higher energy conformer with respect to minimum energy conformer is also given. Red balls represent oxygen, grey balls represent carbon and blue balls represent hydrogen atoms.

For the tri-hydrate of nap ($nap_{T1}.3H_2O$), the most stable conformation in the first excited triplet state also has an open chain motif, with one water molecule forming direct hydrogen bond with nap and the other two water molecules forming hydrogen bonds with the first water molecule. This conformation is more stable than the next stable conformation by 9.6 kcal/mol, which has a closed ring geometry. All the conformers of $nap_{T1}.3H_2O$ are given in Figure 6.9. The O-H and C-O bond lengths of nap in the tri-hydrate are 0.994 and 1.354 Å respectively.

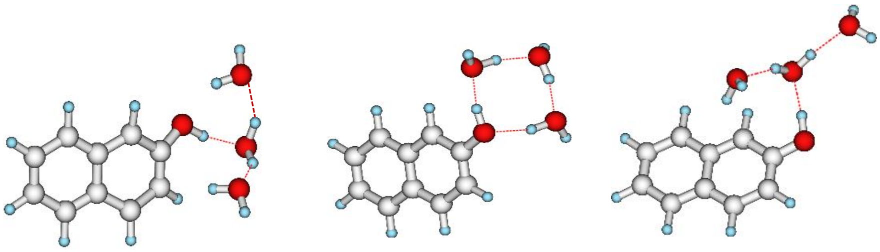
(i) **(ii) ΔE= + 9.6** **(ii) ΔE= +17.3**

Figure 6.9 Equilibrium structures of 2-naphthol.$3H_2O$, at first excited triplet state, calculated at CAM-B3LYP/aug-cc-pVDZ level of theory. Zero point energy corrected relative energy (in kcal/mol) of the higher energy conformer with respect to minimum energy conformer is also given. Red balls represent oxygen, grey balls represent carbon and blue balls represent hydrogen atoms.

It is observed that even with four water molecules, proton transfer does not take place in case of first excited triplet state of tetra-hydrate of nap ($nap_{T1}.4H_2O$). The most stable conformation has a closed ring conformation which is more stable than the other conformations obtained, by 19.2 kcal/mol (see Figure 6.10). The O-H and C-O bond length of nap are 0.993 and 1.370 Å respectively.

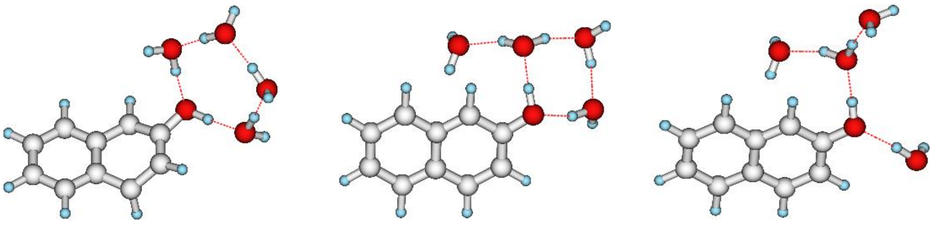

(i) **(ii) ΔE= + 19.2** **(ii) ΔE= +26.6**

Figure 6.10 Equilibrium structures of 2-naphthol.4H_2O, at first excited triplet state, calculated at CAM-B3LYP/aug-cc-pVDZ level of theory. Zero point energy corrected relative energy (in kcal/mol) of the higher energy conformer with respect to minimum energy conformer is also given. Red balls represent oxygen, grey balls represent carbon and blue balls represent hydrogen atoms.

6.2.3 Microhydration at first excited singlet state

The most stable conformer of nap, at the first excited singlet state (S_1), has the O-H bond facing away from the naphthalene ring. The O-H and C-O bond lengths of nap are 0.966 and 1.346 Å respectively. This structure is more stable than the structure in which the O-H bond is facing towards the naphthalene ring, by 0.7 kcal/mol. Both the structures are given in Figure 6.11.

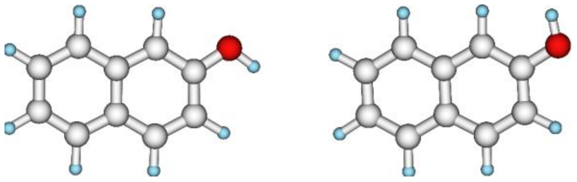

(i) **(ii)ΔE= +0.7**

Figure 6.11 Equilibrium structures of 2-naphthol, at first excited singlet state, calculated at CAM-B3LYP/aug-cc-pVDZ level of theory. Zero point energy corrected relative energy (in kcal/mol) of the higher energy conformer with respect to minimum energy conformer is also given. Red balls represent oxygen, grey balls represent carbon and blue balls represent hydrogen atoms.

Three equilibrium conformers are obtained for the first excited singlet state of mono-hydrate of 2-naphthol (nap$_{S1}$.1H_2O), as shown in Figure 6.12. The most stable conformation of nap$_{S1}$.1H_2O, at first excited singlet state has the O-H bond of the nap facing towards the naphthalene ring. The H atom of the water molecule forms hydrogen bonding with the oxygen atom of the nap. The O-H and C-O bond lengths of nap are 0.965 and 1.356 Å respectively.

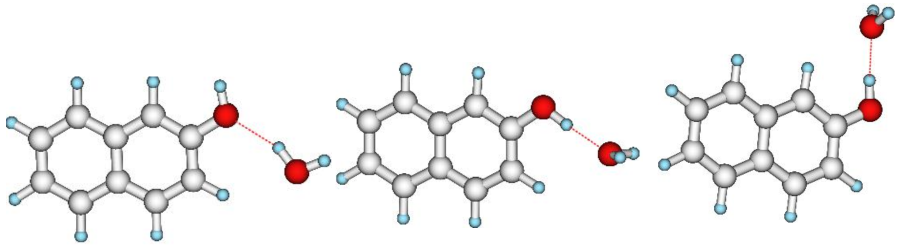

(i) **(ii)ΔE= +31.6** **(iii) ΔE= +32.2**

Figure 6.12 Equilibrium structures of 2-naphthol.1H_2O, at first excited singlet state, calculated at CAM-B3LYP/aug-cc-pVDZ level of theory. Zero point energy corrected relative energy (in kcal/mol) of the higher energy conformer with respect to minimum energy conformer is also given. Red balls represent oxygen, grey balls represent carbon and blue balls represent hydrogen atoms.

With two water molecules, five conformers are observed for the first excited singlet state of di-hydrate of nap (nap$_{S1}$.2H_2O) as shown in Figure 6.13. The most stable conformer has the O-H bond of nap facing away from the ring and forming open chain hydrogen bonds with the water molecules. The O-H and C-O bond lengths of nap are 0.994 and 1.326 Å respectively.

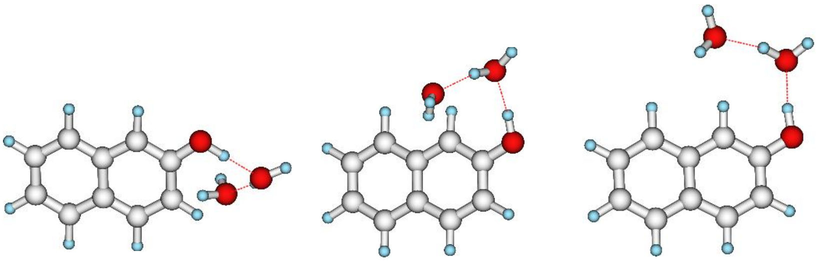

(i) **(ii)ΔE= +1.3** **(iii) ΔE= +1.3**

Figure 6.13 Equilibrium structures of 2-naphthol.2H_2O, at first excited singlet state, calculated at CAM-B3LYP/aug-cc-pVDZ level of theory. Zero point energy corrected relative energy (in kcal/mol) of the higher energy conformer with respect to minimum energy conformer is also given. Red balls represent oxygen, grey balls represent carbon and blue balls represent hydrogen atoms.

The most stable conformation at the first excited singlet state of tri-hydrate of nap ($nap_{S1}.3H_2O$) has a hydrogen bonded closed ring conformation (see Figure 6.14 (i)). The O-H and C-O bond length of nap are 1.001 and 1.341 Å respectively. A slightly higher energy structure is also obtained, differing only in the relative position of the O-H bond of nap (see Figure 6.14 (ii)). Higher energy equilibrium conformers of $nap_{S1}.3H_2O$ at the first excited singlet state are also given in Figure 6.14. It must be noted that closed ring conformation are more stable than the open chain ones.

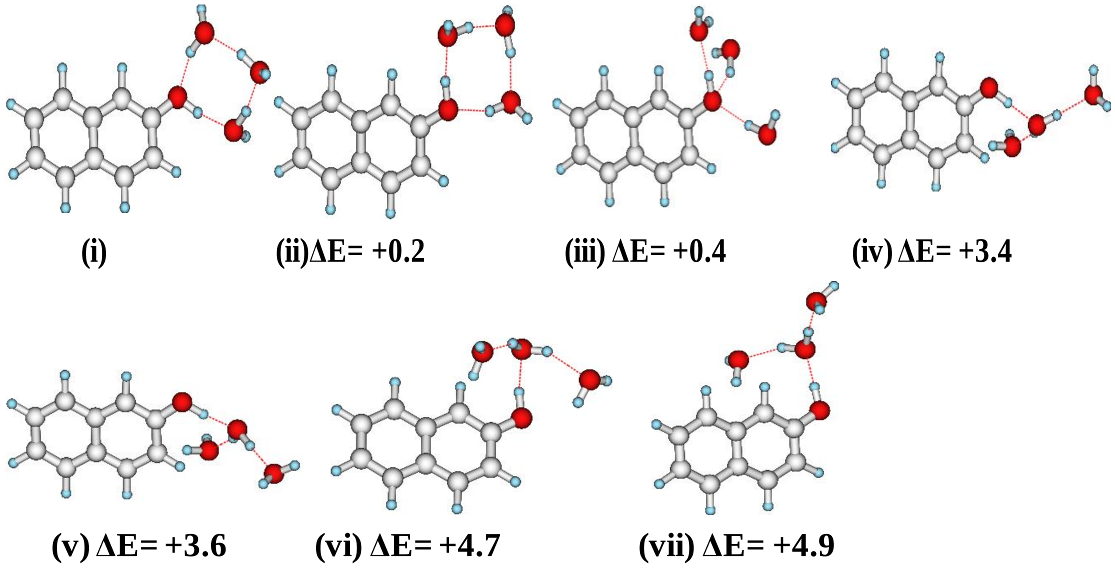

(i) **(ii)ΔE= +0.2** **(iii) ΔE= +0.4** **(iv) ΔE= +3.4**

(v) ΔE= +3.6 **(vi) ΔE= +4.7** **(vii) ΔE= +4.9**

Figure 6.14 Equilibrium structures of 2-naphthol.$3H_2O$, at first excited singlet state, calculated at CAM-B3LYP/aug-cc-pVDZ level of theory. Zero point energy corrected relative energy (in kcal/mol) of the higher energy conformer with respect to minimum energy conformer is also given. Red balls represent oxygen, grey balls represent carbon and blue balls represent hydrogen atoms.

Interestingly, the most stable conformer of tetra-hydrate of nap ($nap_{S1}.4H_2O$), at the first excited singlet state, shows proton transfer from nap to the neighboring water molecule. This conformer is more stable than the next stable conformer by 1.0 kcal/mol. The most stable conformer has an open chain conformation with two water molecules stabilizing the first water molecule through hydrogen bonding and the H atom of the fourth water molecule forming hydrogen bond with the oxygen atom of nap (see Figure 6.15 (i)). The

O..H hydrogen bond distance between O atom of nap and nearest H atom of the hydrated proton is 1.598 Å. Four other higher energy equilibrium conformers of $nap_{S1}.4H_2O$ are also obtained, as shown in Figure 6.15.

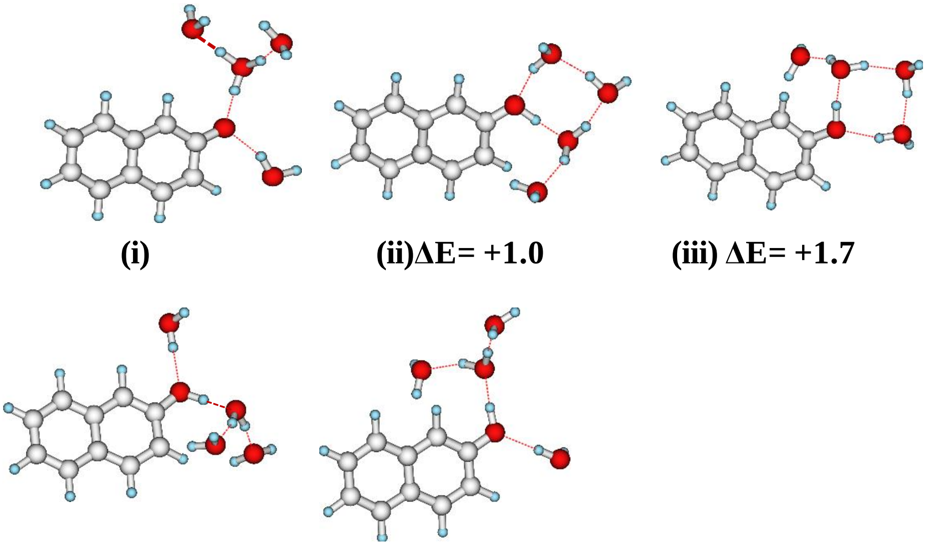

(i) **(ii)ΔE= +1.0** **(iii) ΔE= +1.7**

(iv)ΔE= +7.4 **(v) ΔE= +8.7**

Figure 6.15 Equilibrium structures of 2-naphthol.$4H_2O$, at first excited singlet state, calculated at CAM-B3LYP/aug-cc-pVDZ level of theory. Zero point energy corrected relative energy (in kcal/mol) of the higher energy conformer with respect to minimum energy conformer is also given. Red balls represent oxygen, grey balls represent carbon and blue balls represent hydrogen atoms.

6.2.4 O-H Potential Energy Profile of nap

The dissociating O-H bond potential energy profile of the hydrated clusters of nap gives the barrier for proton transfer from nap to the neighboring solvent water molecule. The potential energy profiles for the dissociating O-H bond of tetra-hydrate of nap, at the ground, first excited triplet and first excited singlet state are given in Figure 6.16. The equilibrium bond length of O-H in nap is ~1 Å for mono, di, tri and tertra-hydrates of nap in the ground and first excited triplet state. In these cases, it is seen that when the O-H bond distance is increased, the energy increases and the system becomes less stable. The potential energy profile of the dissociating O-H bond of nap at the first excited singlet state of mono, di and tri-hydrates also show a minimum at O-H bond distance ~1 Å. Further increase in O-H bond length leads to destabilization of the system.

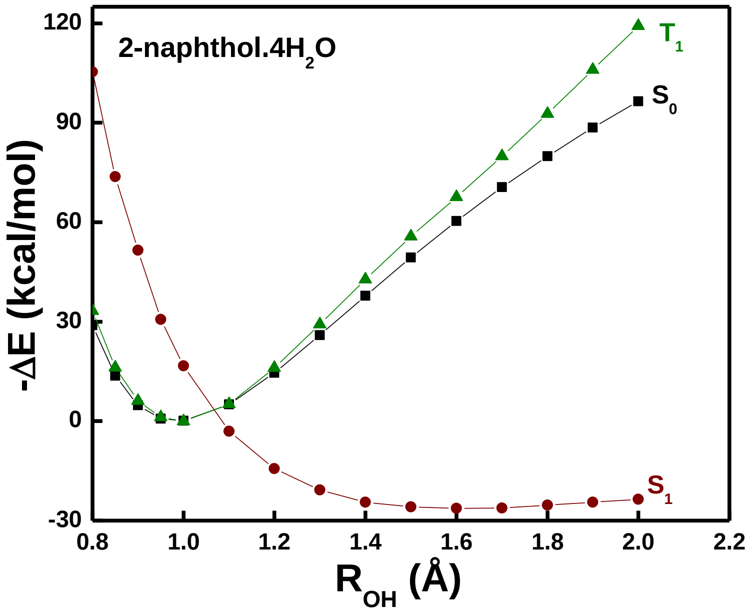

Figure 6.16 Rigid potential energy scan of O-H bond of 2-naphthol.4H_2O, at ground, first excited triplet and singlet state. ΔE gives the relative energy of the system at each point of the scan of the dissociating O-H bond, with respect to the energy of the equilibrium geometry. Curves marked as S_0, T_1 and S_1 represent potential energy surfaces of ground, first excited triplet and singlet states respectively of 2-naphthol.4H_2O, upon increasing the bond distance of dissociating O-H bond of the acid.

However, a rigid potential energy scan of the acidic O-H bond of nap.4H_2O at the first excited singlet state reveals that in the presence of four water molecules, the acidic proton transfer from nap to the neighboring water molecule becomes a barrier-less process, as shown in Figure 6.16. In fact, in the first excited singlet state, the tetra-hydrate becomes unstable at O-H bond distances less than 1.4 Å. The potential energy profiles show that a barrier exists for proton transfer from nap to solvent water molecules in all cases except the tetra-hydrate of nap at the first excited singlet state. In case of nap_{S1}.4H_2O, spontaneous dissociation of the O-H bond is observed. This is in line with the experimentally observed fact that first excited singlet state is more acidic than the ground and first excited triplet state.

6.3 Conclusion

Microhydration studies of 2-naphthol at ground, first excited triplet and singlet states are carried out using TD-DFT. It is seen that even in the presence of four water molecules, proton transfer from naphthol to water molecules is not observed for either ground or first excited triplet state. However, proton transfer becomes a barrier-less process for first excited singlet state of tetra-hydrate of naphthol.

Single determinant methods are not enough to accurately describe the excited states of a system. To completely define the excited state chemistry, multi-reference calculations are required. Hence excited state calculations are complicated and time-consuming. Although TD-DFT is a powerful and widely used procedure, higher multi-reference methods have to be employed to get a better picture of the photo-chemistry of hydrated-naphthol systems. The present chapter deals with the structures and the potential energy profiles of hydrated clusters of 2-naphthol, at different energy states. To get a comprehensive understanding of the microhydration of photo acids, the following actions are planned to be undertaken in the future. A multi-reference method, like CASSCF, can be used to verify the present results. Further studies to understand the reason behind the difference in pKa of S_0, T_1 and S_1 states of 2-naphthol could be carried out. A wider range of systems will be studied so that a general expression can be derived to predict the pKa of photo acids, if n is known.

Chapter 7

Prediction of pKa:
From Molecule to Bulk

Truth, in science, can be defined as the working hypothesis best fitted to open the way to the next better one.

- Konrad Lorenz

Proton transfer reactions are widely studied because of their fundamental importance in biological systems, atmospheric phenomena and synthetic applications. Understanding of the effect of chemical environment on the acidity of a system and vice-versa are important in comprehending the mechanism of several processes like enzyme-catalysis. The acidity of a system is defined by its pKa. Spectrophotometry, pH titrations etc are some of the methods for determining pKa of a system experimentally. But accurate experimental pKa determination becomes complicated in many cases like very strong acids and very weak acids, due to leveling effect of the solvent etc. The experimental pKa value for H_2SO_4 ranges from -3 to -9 while that for CF_3SO_3H range from -6 to -14.[150,151] Accurate pKa values for some very weak acids have been reported from kinetic measurements employing sensitive techniques such as NMR.[152–157] However, accurate pKa determination from experiment remains difficult for many systems.

Quantum chemical methods have been used to obtain pKa values. The pKa can be determined indirectly from free energies calculations in solution. An excellent review by Ho and Coote and the references given therein, as well as a few recent reports are a few among the numerous publications that discuss the strategies applied to determine pKa values using quantum chemical calculations in a thermodynamic route.[158–162]

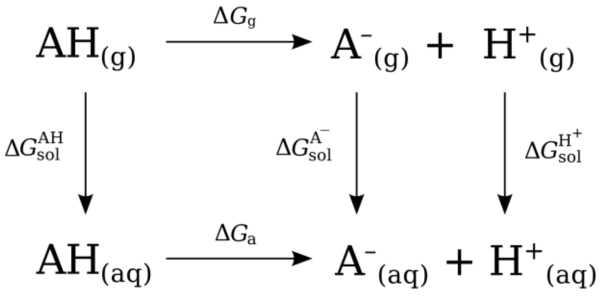

Figure 7.1 Thermodynamic cycle for determining pKa indirectly from free energy. AH refers to the acid. Subscript (g) and (aq) denote the species in gas and aqueous phase respectively.

The free energy of acid (AH) dissociation calculated following the simplest thermodynamic cycle is as shown in Figure 7.1. Here, first the acid is desolvated, then it is deprotonated in the gas phase and finally the conjugate base and the separated proton are solvated. This is the most commonly used thermodynamic cycle due to its simplicity. The free energy of acid dissociation can then be defined as:

$$\Delta G_a = \Delta G_g + \Delta G_{sol}^{A-} + \Delta G_{sol}^{H+} - \Delta G_{sol}^{AH} \qquad 7.1$$

where ΔG_a and ΔG_g refers to the free energy change of the system in the aqueous solution and gas phase respectively. ΔG_{sol}^{A-}, ΔG_{sol}^{H+} and ΔG_{sol}^{AH} represent free energy of solvation of A^-, H^+ and the acid, AH respectively. The free energy change of the system in gas phase is given by:

$$\Delta G_g = G_g^{A-} + G_g^{H+} - G_g^{AH} \qquad 7.2$$

where G_g^{A-}, G_g^{H+} and G_g^{AH} are the gas phase free energies of the anion, proton and acid, respectively. All these free energy values can be obtained from computational calculations except G_g^{H+} and ΔG_{sol}^{H+}. Since properties of systems without electron cannot be studied using quantum chemical methods, these values have to be determined experimentally or from thermodynamic theory. The ΔG_{sol}^{H+} value has been under debate for some time, but generally accepted value is -265.9 kcal/mol.[163–165] pKa is then calculated as:

$$pK_a = \frac{\Delta G_a}{2.303RT} \qquad 7.3$$

Though accurate gas phase reaction energies can now be calculated using high level computational methods available, free energy calculations in solution remains difficult. For neutral solutes, the dielectric continuum models like PCM and SMD give solvation free energies with an accuracy of 1 kcal/mol.[166,167] However, ionic species are involved in pKa calculations which have much lower accuracy. Accurate prediction of pKa of an acid is very difficult as a small error in free energy calculations will cause a large deviation of the pKa from the true value. The main source of error in thermodynamic determination of pKa arises from the uncertainty in free energy of hydration of proton and neglect of the solute-solvent molecular interactions, which are not considered in continuum solvation models, as discussed in Chapter 3 of this thesis.

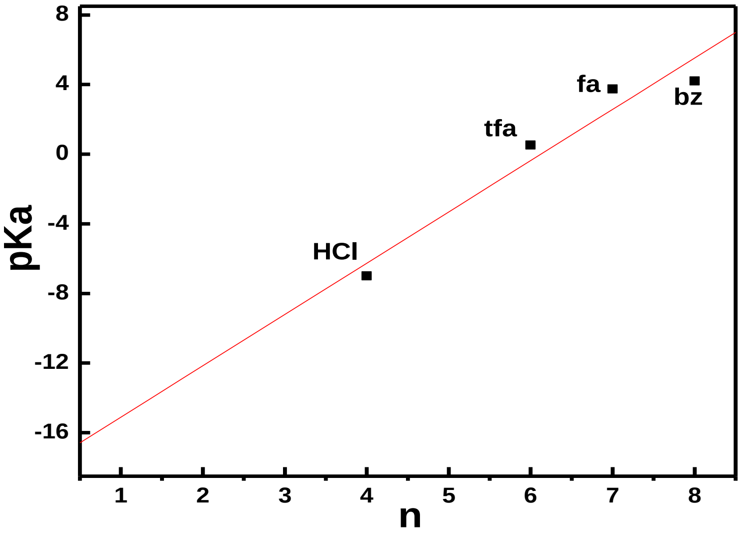

Figure 7.2 Plot of pKa v/s number of water molecules needed for dissociation (n), for HCl, trifluoroacetic acid (tfa), formic acid (fa) and benzoic acid (bz), calculated at ωB97X-D/aug-cc-pVDZ level of theory.

A novel non-thermodynamic route for calculating pKa value is presented here. A linear correlation is observed between the pKa of acid and the number of water molecules (n) needed for its dissociation, in case of acids studied at present applying the same level of theory, as depicted in Figure 7.2. Number of solvent water molecules needed to dissociate strong acid molecule, HCl has been a point of debate. Recent computational studies explained the difference in results on the basis of temperature dependence of relative stability of the structures.[9] Based on our own independent study, at the present level of theory, it is predicted that dissociation of HCl molecule and formation of ion-pair occurs with four water molecules. Linear fitting produces the relation: pKa = 2.9n-18.0, with R^2 = 0.94. This relation can be exploited to qualitatively predict unknown pKa values based on electron structure theory, where experimental measurement is rather difficult.[127]

A more generalized relation, including acids previously reported in literature, also shows linear dependence of pKa and n, as shown in Figure 7.3. It may be noted that the calculations reported for other acids are not at the same level of theory.

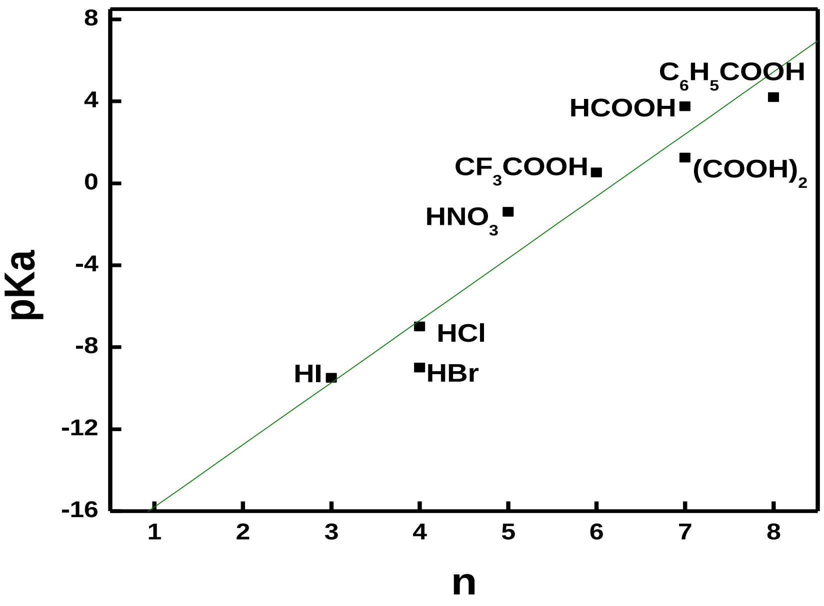

Figure 7.3 Plot of pKa v/s number of water molecules needed for dissociation (n), for HI, HBr, HCl, HNO3, trifluoroacetic acid, formic acid, oxalic acid and benzoic acid.

It has been previously reported that HI, HBr and HNO_3, having pKa values -9.5, -9 and -1.4 respectively, require 3, 4 and 5 water molecules for acid dissociation.[13,67] Including these data points to our study, the correlation between pKa and n can be best fitted as: pKa=3.1n-19.2, with an R^2 value of 0.93.[126] Thus, the pKa of an acid can be predicted if n is known. This provides a non-thermodynamic route for determining pKa of an acid, connecting a molecular level property of the acid molecule, to macroscopic property, the pKa of the acid, in the ground state. To obtain a more reliable relation, a larger set of data is required, with all the calculations carried out at the same level of theory.

In the case of excited state, microhydration leading to dissociation is studied considering 2-naphthol as a case study (see chapter 6). The pKa of the first excited singlet state of 2-naphthol is very small compared to its ground and first excited triplet state. This is reflected in its ‘n’. In the first excited singlet state, the presence of just four water molecules leads to proton transfer from 2-naphthol to the solvent water molecules. This is not observed in case of ground or first excited triplet state. However, the correlation between pKa and ‘n’ of a system that exists for the ground state acids, may not be applicable in the excited state, as is suggested by the case study on 2-naphthol. Further excited state studies need to be carried out to obtain a better correlation between pKa and ‘n’.

Summary and Future Perspectives

Salient features of theoretical results presented in the previous chapters may be summarized as follows. The structure of the hydrated acid cluster depends on the H-bonded network between the acid molecule and water molecules. On successive addition of each water molecule to isolated carboxylic acid molecule, O−H bond of −COOH group becomes longer and weaker. The distance between H atom of the acid and O atom of the neighboring water molecule decreases. As is expected, it is seen that electronic effect affects the strength of the acidic O-H bond. Trifluoroacetic acid, oxalic acid and benzoic acid molecules require 6, 7 and 8 water molecules respectively, for their dissociation, while even in the presence of eight water molecules, acetic acid molecule remains undissociated. The geometry of the ionized hydrated acid cluster resembles that of Eigen cation interacting with the corresponding carboxylate anion surrounded by the remaining water molecules. The weakening of the O-H bond of the acid molecule, with the addition of water molecules, and subsequent formation of contact ion pair are reflected in the bond dipole moment, H bond energy, IR spectra and bond dissociation energy profiles of the O-H bond of the acid molecule in the hydrated acid clusters. On successive addition of solvent water molecules, the barrier for proton transfer from the acid molecule to the neighboring solvent water molecule reduces. Microhydration of photo acid is also considered by taking 2-naphthol as a case study. It is seen that fewer number of water molecules are required to dissociate 2-naphthol in the first excited singlet state when compared to its ground and first excited triplet state (pKa of S_1 state is much lower compared to S_0 and T_1 state).

One of the major challenges of studying microhydration of acids is the increase in structural complexity with increase in size of the hydrated acid clusters. A large conformational variety within a small relative energy range is obtained. This indicates a shallow potential energy surface. The number of H bond donors and acceptors increases with increase in number of water molecules in the hydrated acid clusters. Converging to a local minimum is an inherent defect of Newton-Raphson based algorithm which is used for geometry optimization. Thus selection of input geometries is crucial in determining the geometry of the cluster. As the increase in size of the hydrated clusters increases the number of possible input geometries, only clusters up to octa-hydrates are studied here to avoid missing out an important conformation.

The main motive of the thesis was to understand microhydration of acids at the molecular level and obtain a correlation between molecular and bulk level acid strength. As was discussed in the previous chapters, number of water molecules needed to dissociate an acid molecule depends on the strength of the acid. A weak acid molecule needs more number of solvent water molecules whereas a strong acid needs less number of water molecules. Bulk property like pKa value of an acid also indicates the strength of an acid. It is interesting to investigate if any correlation exists between these two parameters, bulk parameter: pKa and molecular parameter: number (n) of solvent water molecules needed to form contact ion-pair. A linear relation is observed between the number of water molecules needed to dissociate an acid molecule and its pKa.

For obtaining a valid equation connecting the pKa of the acid and the number of water molecules needed to dissociate the acid molecule, a larger set of data is required, with all the calculations done at a same level of theory. Microhydration studies of a larger group of chemical systems, like amines, alcohols etc. can help in establishing a reliable equation to calculate the pKa of an acid from n. Also from the case study on 2-naphthol it is inferred that the linear correlation between pKa and n, that exists in the ground state, may not be applicable in the excited states. Further, observed linear correlation between n and pKa is to be explained. The author aspires to pursue these studies to obtain logical conclusions.

References

[1] J. Tomasi, B. Mennucci, R. Cammi, *Chem. Rev.* **2005**, *105*, 2999–3093.

[2] A. V. Marenich, C. J. Cramer, D. G. Truhlar, *J. Phys. Chem. B* **2009**, *113*, 6378–6396.

[3] N. Agmon, H. J. Bakker, R. K. Campen, R. H. Henchman, P. Pohl, S. Roke, M. Thämer, A. Hassanali, *Chem. Rev.* **2016**, *116*, 7642–7672.

[4] S. Pylaeva, C. Allolio, B. Koeppe, G. S. Denisov, H. Limbach, D. Sebastiani, P. M. Tolstoy, *Phys. Chem. Chem. Phys.* **2015**, *17*, 4634–4644.

[5] J. A. Fournier, C. J. Johnson, C. T. Wolke, G. H. Weddle, A. B. Wolk, M. A. Johnson, *Science (80-.).* **2014**, *344*, 1009–1012.

[6] C. Lao-ngam, P. Asawakun, S. Wannarat, K. Sagarik, *Phys. Chem. Chem. Phys.* **2011**, *13*, 4562–4575.

[7] S. Woutersen, H. J. Bakker, *Phys. Rev. Lett.* **2006**, *96*, 138305-1–4.

[8] J. M. Headrick, E. G. Diken, R. S. Walters, N. I. Hammer, R. A. Christie, J. Cui, E. M. Myshakin, M. A. Duncan, M. A. Johnson, K. D. Jordan, *Science (80-.).* **2005**, *308*, 1765–1769.

[9] A. Vargas-Caamal, J. L. Cabellos, F. Ortiz-Chi, H. S. Rzepa, A. Restrepo, G. Merino, *Chem. - A Eur. J.* **2016**, *22*, 2812–2818.

[10] S. Sugawara, T. Yoshikawa, T. Takayanagi, M. Tachikawa, *Chem. Phys. Lett.* **2011**, *501*, 238–244.

[11] H. Forbert, M. Masia, A. Kaczmarek-kedziera, N. N. Nair, D. Marx, *J. Am. Chem. Soc.* **2011**, *133*, 4062–4072.

[12] S. Li, F. Tao, R. Gu, *Chem. Phys. Lett.* **2006**, *426*, 1–7.

[13] S. Odde, B. J. Mhin, S. Lee, H. M. Lee, K. S. Kim, *J. Chem. Phys* **2004**, *120*,

9524–9535.

[14] K. H. Weber, F.-M. Tao, *J. Phys. Chem. A* **2001**, *105*, 1208–1213.

[15] G. Jackson, G. Porter, *Proc. R. Soc. A Math. Phys. Eng. Sci.* **1961**, *260*, 13–30.

[16] R. L. Johnston, *Atomic and Molecular Clusters*, Taylor And Francis, **2002**.

[17] M. Moskovits, *Annu. Rev. Phys. Chem.* **1999**, *42*, 465–499.

[18] A. W. Castleman, R. G. Keesee, *Chem. Rev.* **1986**, *86*, 589–618.

[19] A. Kumar, S. R. Gadre, X. Chenxia, X. Tianlv, S. R. Kirk, S. Jenkins, *Phys. Chem. Chem. Phys.* **2015**, *17*, 15258–15273.

[20] M. Becucci, S. Melandri, *Chem. Rev.* **2016**, *116*, 5014–5037.

[21] S. R. Gadre, S. D. Yeole, N. Sahu, *Chem. Rev.* **2014**, *114*, 12132–12173.

[22] T. C. Cheng, B. Bandyopadhyay, J. D. Mosley, M. A. Duncan, *J. Am. Chem. Soc.* **2012**, *134*, 13046–13055.

[23] C. Desfrancois, S. Carles, J. P. Schermann, *Chem. Rev.* **2000**, *100*, 3943–3962.

[24] T. A. Miller, *Science (80-.).* **1984**, *223*, 545–553.

[25] F. Sylla, M. Veltcheva, S. Kahaly, A. Flacco, V. Malka, *Rev. Sci. Instrum.* **2012**, *83*, 33507-1–7.

[26] L. M. Goss, S. W. Sharpe, T. A. Blake, V. Vaida, J. W. Brault, *J. Phys. Chem. A* **1999**, *103*, 8620–8624.

[27] V. Chandrasekaran, L. Biennier, E. Arunan, D. Talbi, R. Georges, *J. Phys. Chem. A* **2011**, *115*, 11263–11268.

[28] F. N. Keutsch, R. J. Saykally, *Proc. Natl. Acad. Sci. U. S. A.* **2001**, *98*, 10533–10540.

[29] K. Liu, R. S. Fellers, M. R. Viant, R. P. McLaughlin, M. G. Brown, R. J. Saykally, *Rev. Sci. Instrum.* **1996**, *67*, 410–416.

[30] J. B. Paul, C. P. Collier, R. J. Saykally, J. J. Scherer, A. O'Keefe, *J. Phys. Chem.*

A **1997**, *101*, 5211–5214.

[31] V. E. Bondybey, A. M. Smith, J. Agreiter, *Chem. Rev.* **1996**, *96*, 2113–2134.

[32] R. E. Smalley, L. Wharton, D. H. Levy, *Acc. Chem. Res.* **1977**, *10*, 139–145.

[33] T. J. Balle, W. H. Flygare, *Rev. Sci. Instrum.* **1981**, *52*, 33–45.

[34] J. M. Weber, E. Leber, M. W. Ruf, H. Hotop, *Phys. Rev. Lett.* **1999**, *82*, 516–519.

[35] A. Grubisic, Y. J. Ko, H. Wang, K. H. Bowen, *J. Am. Chem. Soc.* **2009**, *131*, 10783–10790.

[36] J. Harnes, M. Winkler, A. Lindblad, L. J. Sæthre, K. J. Børve, *J. Phys. Chem. A* **2011**, *115*, 10408–10415.

[37] H. Kistenmacher, G. C. Lie, H. Popkie, E. Clementi, *J. Chem. Phys.* **1974**, *61*, 546–561.

[38] P. Hobza, H. L. Selzle, E. W. Schlag, *J. Phys. Chem.* **1996**, *100*, 18790–18794.

[39] S. Tsuzuki, T. Uchimaru, K. Matsumura, M. Mikami, K. Tanabe, *Chem. Phys. Lett.* **2000**, *319*, 547–554.

[40] S. S. Xantheas, *J. Chem. Phys.* **1995**, *102*, 4505–4517.

[41] S. Yoo, E. Aprà, X. C. Zeng, S. S. Xantheas, *J. Phys. Chem. Lett.* **2010**, *1*, 3122–3127.

[42] L.-J. Guo, X. Liu, G.-F. Zhao, Y.-H. Luo, *J. Chem. Phys.* **2007**, *126*, 234704-1–7.

[43] D. R. Kauffman, D. Alfonso, C. Matranga, H. Qian, R. Jin, *J. Am. Chem. Soc.* **2012**, *134*, 10237–10243.

[44] S. S. Xantheas, T. H. Dunning, *J. Chem. Phys.* **1993**, *99*, 8774–8792.

[45] S. Grimme, *J. Comput. Chem.* **2006**, *27*, 1787–1799.

[46] T. Schwabe, S. Grimme, *Phys. Chem. Chem. Phys.* **2007**, *9*, 3397–3406.

[47] S. Grimme, J. Antony, S. Ehrlich, H. Krieg, *J. Chem. Phys.* **2010**, *132*, 154104-1–19.

[48] S. Gohr, S. Grimme, T. Söhnel, B. Paulus, P. Schwerdtfeger, *J. Chem. Phys.* **2013**, *139*, 174501-1–8.

[49] S. Grimme, *Wiley Interdiscip. Rev. Comput. Mol. Sci.* **2011**, *1*, 211–228.

[50] L. Goerigk, S. Grimme, *J. Chem. Theory Comput.* **2011**, *7*, 291–309.

[51] A. Abo-Riziq, B. Crews, L. Grace, M. S. De Vries, *J. Am. Chem. Soc.* **2005**, *127*, 2374–2375.

[52] A. Luchow, D. Spangenberg, C. Janzen, A. Jansen, M. Gerhards, K. Kleinermanns, *Phys. Chem. Chem. Phys.* **2001**, *3*, 2771–2780.

[53] U. Buck, F. Huisken, *Chem. Rev.* **2000**, *100*, 3863–3890.

[54] V. B. Pacheco, P. Chaudhuri, *J. Phys. Chem. A* **2013**, *117*, 5675–5684.

[55] H. Ohtaki, T. Radnai, *Chem. Rev.* **1993**, *93*, 1157–1204.

[56] R. B. Sunoj, M. Anand, *Phys. Chem. Chem. Phys.* **2012**, *14*, 12715–12736.

[57] J. S. Mancini, J. M. Bowman, *J. Phys. Chem. Lett.* **2014**, *5*, 2247–2253.

[58] M. B. Craddock, C. S. Brauer, K. R. Leopold, *J. Phys. Chem. A* **2008**, *112*, 488–96.

[59] A. A. Hassanali, J. Cuny, M. Ceriotti, C. J. Pickard, M. Parrinello, *J. Am. Chem. Soc.* **2012**, *134*, 8557–8569.

[60] M. Rozenberg, A. Loewenschuss, *J. Phys. Chem. A* **2009**, *113*, 4963–4971.

[61] S. Re, Y. Osamura, K. Morokuma, *J. Phys. Chem. A* **1999**, *103*, 3535–3547.

[62] A. Gutberlet, G. Schwaab, Ö. Birer, M. Masia, A. Kaczmarek, H. Forbert, M. Havenith, D. Marx, *Science (80-.).* **2009**, *324*, 1545–1548.

[63] J. S. Mancini, J. M. Bowman, *Phys. Chem. Chem. Phys.* **2015**, *17*, 6222–6226.

[64] P. Ayotte, M. Hébert, P. Marchand, *J. Chem. Phys* **2005**, *123*, 184501-1–8.

[65] R. Iftimie, V. Thomas, S. Plessis, P. Marchand, P. Ayotte, *J. Am. Chem. Soc.* **2008**, *130*, 5901–5907.

[66] S. Odde, B. J. Mhin, K. H. Lee, H. M. Lee, P. Tarakeshwar, K. S. Kim, *J. Phys. Chem. A* **2006**, *110*, 7918–7924.

[67] J. R. Scott, J. B. Wright, *J. Phys. Chem. A* **2004**, *108*, 10578–10585.

[68] A. Smith, M. A. Vincent, I. H. Hillier, *J. phys. chem A* **1999**, *103*, 1132–1139.

[69] R. Biswas, W. Carpenter, J. A. Fournier, G. A. Voth, A. Tokmakoff, *J. Chem. Phys.* **2017**, *146*, 154507-1–11.

[70] F. Dahms, R. Costard, E. Pines, B. P. Fingerhut, E. T. J. Nibbering, T. Elsaesser, *Angew. Chemie - Int. Ed.* **2016**, *55*, 10600–10605.

[71] D. Marx, M. E. Tuckerman, J. Hutter, M. Parrinello, *Nature* **1999**, *397*, 601–604.

[72] F. Ito, *Chem. Phys.* **2011**, *382*, 52–57.

[73] B. Ouyang, T. G. Starkey, B. J. Howard, *J. Phys. Chem. A* **2007**, *111*, 6165–6175.

[74] B. Ouyang, B. J. Howard, *Phys. Chem. Chem. Phys.* **2009**, *11*, 366–373.

[75] K. Haupa, A. Bil, A. Barnes, Z. Mielke, *J. phys. chem A* **2015**, *119*, 2522–2531.

[76] G. Ritzhaupt, J. P. Devlin, *J. Phys. Chem.* **1991**, *95*, 90–95.

[77] S. M. Hurley, T. E. Dermota, D. P. Hydutsky, A. W. Castleman, *J. Chem. Phys.* **2003**, *118*, 9272–9277.

[78] P. A. Giguère, S. Turrell, *J. Am. Chem. Soc.* **1980**, *102*, 5473–5477.

[79] G. M. Chaban, R. B. Gerber, K. C. Janda, *J. Phys. Chem. A* **2001**, *105*, 8323–8332.

[80] Y. Miller, G. M. Chaban, R. B. Gerber, *Chem. Phys.* **2005**, *313*, 213–224.

[81] S. S. Xantheas, *Int. Rev. Phys. Chem.* **2006**, *25*, 719–733.

[82] V. Vaida, H. G. Kjaergaard, K. J. Feierabend, *Int. Rev. Phys. Chem.* **2003**, *22*, 203–219.

[83] V. Vaida, *J. Phys. Chem. A* **2009**, *113*, 5–18.

[84] K. R. Leopold, *Annu. Rev. Phys. Chem.* **2011**, *62*, 327–349.

[85] G. G. Abad, P. F. Bernath, C. D. Boone, S. D. McLeod, G. L. Manney, G. C.

Toon, *Atmos. Chem. Phys.* **2009**, *9*, 8039–8047.

[86] S. Yu, *Atmos. Res.* **2000**, *53*, 185–217.

[87] Y. I. Tsai, S. Kuo, *Atmos. Environ.* **2013**, *81*, 270–279.

[88] F. Ito, *Vib. Spectrosc.* **2014**, *71*, 57–61.

[89] F. Ito, *Comput. Theor. Chem.* **2013**, *1016*, 48–53.

[90] F. D’Amico, F. Bencivenga, A. Gessini, E. Principi, R. Cucini, C. Masciovecchio, *J. Phys. Chem. B* **2012**, *116*, 13219–13227.

[91] L. Pu, Y. Sun, Z. Zhang, *J. Phys. Chem. A* **2010**, *114*, 10842–10849.

[92] S. Lopes, R. Fausto, L. Khriachtchev, *J. Chem. Phys.* **2016**, *144*, 84308-1–11.

[93] Q. Gao, K. T. Leung, *J. Chem. Phys.* **2005**, *123*, 74325-1–11.

[94] M. V Fedotova, S. E. Kruchinin, *J. Mol. Liq.* **2011**, *164*, 201–206.

[95] K. Kawamura, N. Lai-Ling, I. R. Kaplan, *Environ. Sci. Technol.* **1985**, *19*, 1082–1086.

[96] M. Jang, R. M. Kamens, *Environ. Sci. Technol.* **2001**, *35*, 3626–3639.

[97] S. Berne, L. Kovacic, M. Sova, N. Krasevec, S. Gobec, I. Krizaj, R. Komel, *Bioorg. Med. Chem.* **2015**, *23*, 4264–4276.

[98] A. K. Tummanapelli, S. Vasudevan, *Phys. Chem. Chem. Phys.* **2015**, *17*, 6383–6388.

[99] E. G. Schnitzler, W. Jäger, *Phys. Chem. Chem. Phys.* **2014**, *16*, 2305–2314.

[100] K. H. Weber, F. J. Morales, F.-M. Tao, *J. Phys. Chem. A* **2012**, *116*, 11601–11617.

[101] M. Darvas, S. Picaud, P. Jedlovszky, *Phys. Chem. Chem. Phys.* **2011**, *13*, 19830–19839.

[102] J. M. Hermida-Ramón, E. M. Cabaleiro-Lago, J. Rodríguez-Otero, *Chem. Phys.* **2004**, *302*, 53–60.

[103] Y. Xu, A. B. Nadykto, F. Yu, L. Jiang, W. Wang, *J. Mol. Struct. THEOCHEM*

2010, *951*, 28–33.

[104] J. A. Pople, *Rev. Mod. Phys.* **1999**, *71*, 1267–1274.

[105] F. Jensen, *Introduction to Computational Chemistry*, **2007**.

[106] H. B. Schlegel, *J. Comput. Chem.* **1982**, *3*, 214–218.

[107] D. K. Maity, *J. Phys. Chem. A* **2013**, *117*, 8660–8670.

[108] J. Da Chai, M. Head-Gordon, *Phys. Chem. Chem. Phys.* **2008**, *10*, 6615–6620.

[109] P. Giannozzi, S. Baroni, N. Bonini, M. Calandra, R. Car, C. Cavazzoni, D. Ceresoli, G. L. Chiarotti, M. Cococcioni, I. Dabo, et al., *J. Phys. Cond. Mat.* **2009**, *21*, 395502-1–19.

[110] J. P. Perdew, K. Burke, M. Ernzerhof, *Phys. Rev. Lett.* **1996**, *77*, 3865–3868.

[111] P. E. Blöchl, *Phys. Rev. B* **1994**, *50*, 17953–17979.

[112] M. W. Schmidt, K. K. Baldridge, J. A. Boatz, S. T. Elbert, M. S. Gordon, J. H. Jensen, S. Koseki, N. Matsunaga, K. A. Nguyen, S. Su, et al., *J. Comput. Chem.* **1993**, *14*, 1347–1363.

[113] G. Schaftenaar, J. H. Noordik, *J. Comput. Aided. Mol. Des.* **2000**, *14*, 123–134.

[114] R. E. Kagarise, *J. Chem. Phys.* **1957**, *27*, 519–522.

[115] D. R. Lide, *CRC Handbook of Chemistry and Physics*, CRC Press Taylor And Francis: Boca Raton, FL, **2005**.

[116] P. Krishnakumar, D. K. Maity, *Comput. Theor. Chem.* **2017**, *1099*, 185–194.

[117] P. Krishnakumar, D. K. Maity, *J. Phys. Chem. A* **2014**, *118*, 5443–5453.

[118] J. L. Derissen, *J. Mol. Struct.* **1971**, *7*, 67–80.

[119] P. Krishnakumar, D. K. Maity, *J Phys. Chem. A* **2017**, *121*, 493–504.

[120] B. P. van Eijck, Van Opheusden J., van Schaik M. M. M, van Zoeren E., *J. Mol. Spectrosc.* **1981**, *86*, 465–479.

[121] K. Aarset, E. M. Page, D. A. Rice, *J. Phys. Chem. A* **2006**, *110*, 9014–9019.

[122] P. D. Godfrey, D. Mcnaughton, *J. Chem. Phys.* **2013**, *138*, 24303-1–8.

[123] P. Krishnakumar, D. K. Maity, *New J. Chem.* **2017**, *41*, 7195–7202.

[124] Z. Nahlovska, B. Nahlovsky, T. G. Strand, *acta Chem. Scand.* **1970**, *24*, 2617–2628.

[125] R. L. Redington, T. E. Redington, *J. Mol. Struct.* **1978**, *48*, 165–176.

[126] P. Krishnakumar, D. K. Maity, *Mol. Phys.* **2017**, DOI 10.1080/00268976.2017.1359346.

[127] P. Krishnakumar, D. K. Maity, *New J. Chem.* **2017**, *41*, 7195–7202.

[128] T. Lu, F. Chen, *J. Comput. Chem.* **2012**, *33*, 580–592.

[129] E. Espinosa, E. Molins, C. Lecomte, *Chem. Phys. Lett.* **1998**, *285*, 170–173.

[130] C. Conley, F. Tao, *Chem. Phys. Lett.* **1999**, *301*, 29–36.

[131] E. M. Cabaleiro-Lago, J. M. Hermida-Ramon, J. Rodriguez-Otero, *J. Chem. Phys.* **2002**, *117*, 3160–3168.

[132] C. V Berney, R. L. Redington, K. C. Lin, *J. Chem. Phys.* **1970**, *53*, 1713–1721.

[133] S. G. Stepanian, I. D. Reva, E. D. Radchenko, G. G. Sheina, *Vib. Spectrosc.* **1996**, *11*, 123–133.

[134] C. Reichardt, *Solvents and Solvent Effects in Organic Chemistry*, **2003**.

[135] N. Amdursky, *Phys. Chem. Chem. Phys.* **2015**, *17*, 32023–32032.

[136] R. Simkovitch, D. Huppert, *J. Phys. Chem. A* **2015**, *119*, 1973–1982.

[137] R. Simkovitch, D. Huppert, *J. Phys. Chem. A* **2015**, *119*, 641–651.

[138] T. Förster, *Pure Appl. Chem* **1973**, *34*, 225–234.

[139] D. D. Rosebrook, W. W. Brandt, *J. Phys. Chem.* **1966**, *70*, 3857–3862.

[140] J. Gao, N. Li, M. Freindorf, *J. Am. Chem. Soc.* **1996**, *118*, 4912–4913.

[141] G. Granucci, J. T. Hynes, P. Millié, T. H. Tran-Thi, *J. Am. Chem. Soc.* **2000**, *122*, 12243–12253.

[142] E. Vander Donckt, *Progress in Reaction Kinetics*, Pergamon Press: London, **1970**.

[143] L. Salem, *Electrons in Chemical Reactions: First Principles*, Wiley: Newyork, **1982**.

[144] E. Rudberg, P. Sałek, H. Ågren, *J. Chem. Phys.* **2005**, *123*, 184108-1–7.

[145] M. J. G. Peach, T. Helgaker, P. Salek, T. W. Keal, O. B. Lutnaes, D. J. Tozer, N. C. Handy, *Phys. Chem. Chem. Phys.* **2006**, *8*, 558–562.

[146] T. Yanai, D. P. Tew, N. C. Handy, *Chem. Phys. Lett.* **2004**, *393*, 51–57.

[147] R. Kobayashi, R. D. Amos, *Chem. Phys. Lett.* **2006**, *420*, 106–109.

[148] M. J. Frisch, G. W. Trucks, H. B. Schlegel, G. E. Scuseria, M. A. Robb, J. R. Cheeseman, G. Scalmani, V. Barone, **2016**, *Revision A.*

[149] J. Novak, A. Prlj, N. Basaric, C. Corminboeuf, N. Doslic, *Chem. - A Eur. J.* **2017**, *23*, 8244–8251.

[150] K. E. Gutowski, D. A. Dixon, *J. Phys. Chem. A* **2006**, *110*, 12044–12054.

[151] J. P. Guthrie, *Can. J. Chem.* **1978**, *56*, 2342–2354.

[152] F. M. Wong, C. C. Capule, D. X. Chen, S. Gronert, W. Wu, *Org. Lett.* **2008**, *10*, 2757–2760.

[153] T. Amyes, J. Richard, *J. Am. Chem. Soc.* **1996**, *118*, 3129–3141.

[154] J. P. Richard, G. Williams, J. Gao, *J. Am. Chem. Soc.* **1999**, *121*, 715–726.

[155] A. Rios, J. P. Richard, T. L. Amyest, *J. Am. Chem. Soc.* **2002**, *124*, 8251–8259.

[156] A. Sievers, R. Wolfenden, *J. Am. Chem. Soc.* **2002**, *124*, 13986–13987.

[157] F. M. Wong, C. C. Capule, W. Wu, *Org. Lett.* **2006**, *8*, 6019–6022.

[158] P. G. Seybold, G. C. Shields, *Wiley Interdiscip. Rev. Comput. Mol. Sci.* **2015**, *5*, 290–297.

[159] A. D. Bochevarov, M. A. Watson, J. R. Greenwood, D. M. Philipp, *J. Chem. Theory Comput.* **2016**, *12*, 6001–6019.

[160] J. Ho, M. L. Coote, *J. Chem. Theory Comput.* **2009**, *5*, 295–306.

[161] J. Ho, M. L. Coote, *Theor. Chem. Acc.* **2010**, *125*, 3–21.

[162] J. T. Muckerman, J. H. Skone, M. Ning, Y. Wasada-Tsutsui, *Biochim. Biophys. Acta - Bioenerg.* **2013**, *1827*, 882–891.

[163] M. D. Tissandier, K. A. Cowen, W. Y. Feng, E. Gundlach, M. H. Cohen, A. D. Earhart, J. V. Coe, T. R. Tuttle, *J. Phys. Chem. A* **1998**, *102*, 7787–7794.

[164] C. Lim, D. Bashford, M. Karplus, *J. Phys. Chem.* **1991**, *95*, 5610–5620.

[165] C. P. Kelly, C. J. Cramer, D. G. Truhlar, *J. Phys. Chem. B* **2006**, *110*, 16066–16081.

[166] Y. Takano, K. N. Houk, *J. Chem. Theory Comput.* **2005**, *1*, 70–77.

[167] C. J. Cramer, D. G. Truhlar, *Acc. Chem. Res.* **2008**, *41*, 760–768.